SELF-ASSEMBLED PEPTIDE TEMPLATE DIRECTED SYNTHESIS OF ONE-DIMENSIONAL INORGANIC NANOSTRUCTURES and THEIR APPLICATIONS

A DISSERTATION SUBMITTED TO
MATERIALS SCIENCE AND NANOTECHNOLOGY PROGRAM
OF THE GRADUATE SCHOOL OF ENGINEERING AND SCIENCE
OF BILKENT UNIVERSITY
IN PARTIAL FULFILLMENT OF THE REQUIREMENTS
FOR THE DEGREE OF
DOCTOR OF PHILOSOPHY

by

HANDAN ACAR

December, 2012

I certify that I have read this thesis and that in my opinion it is fully fully adquate, in scope and quality, as a dissertation for the degree of doctor in philosophy.

_____

Assist. Prof. Dr. Mustafa Özgür Güler (Advisor)

I certify that I have read this thesis and that in my opinion it is fully fully adquate, in scope and quality, as a dissertation for the degree of doctor in philosophy.

_____

Prof. Dr. Engin Umut Akkaya

I certify that I have read this thesis and that in my opinion it is fully fully adquate, in scope and quality, as a dissertation for the degree of doctor in philosophy.

_____

Assist. Prof. Dr. Emrah Özensoy

I certify that I have read this thesis and that in my opinion it is fully fully adquate, in scope and quality, as a dissertation for the degree of doctor in philosophy.

Prof. Dr. Baki Emir Denkbaş

I certify that I have read this thesis and that in my opinion it is fully fully adquate, in scope and quality, as a dissertation for the degree of doctor in philosophy.

Assist. Prof. Dr. Necmi Bıyıklı

Approved for the Institute of Engineering and Science

Prof. Dr. Levent Onural

Diresctor of the Graduate School

ABSTRACT

SELF-ASSEMBLED PEPTIDE TEMPLATE DIRECTED SYNTHESIS OF ONE-DIMENSIONAL INORGANIC NANOSTRUCTURES and THEIR APPLICATIONS

Handan Acar

Ph.D. in Materials Science and Nanotechnology

Supervisor: Assist. Prof. Dr. Mustafa Özgür Güler

December, 2012

Engineering at the nano scale has been an active area of science and technology over the last decade. Inspired by nature, synthesis of functional inorganic materials using synthetic organic templates constitutes the theme of this thesis. Developing organic template directed synthesis approach for inorganic nanomaterial synthesis was aimed. For this purpose, an amyloid like peptide sequence which is capable of self-assembling into nanofibers in convenient conditions was designed and decorated with functional groups showing relatively high affinity to special inorganic ions, which are presented at the periphery of the one-dimensional peptide nanofiber. These chemical groups facilitated the deposition of targeted inorganic monomers onto the nanofibers yielding one-dimensional organic-inorganic core-shell nanostructures.

The physical and chemical properties of the synthesized peptide nanofibers and inorganic nanostructures were characterized using both qualitative and quantitative methods.

First, silica nanotubes were obtained by silica mineralization around these peptide nanofiber templates for the construction of sensors for explosives. The fluorescence dye was used to coat the silica nanotubes to detect explosive vapor. The surface of the silica nanotubes were porous enough to adsorb more dye compared to the silica nanoparticles and silica film, and causes faster fluorescence quenching in the presence of explosives like trinitrotoluene and dinitrotoluene. The silica nanotubes which synthesized with this peptide nanofiber templates can be used in catalysis and sensors in which high surface area is advantageous. In the second part of the thesis, titanium dioxide nanotubes were obtained from titania mineralization. They are well-known with their fascinating properties as a result of the one-dimensional nanostructure, such as more efficient electron transfer and less electron-hole recombination. The sufficient photoactivity of titanium dioxide makes them suitable materials for Dye-Sensitized Solar-Cell construction. It is demonstrated that the peptide nanofiber templated titanium dioxide nanotubes have more than two times more efficiency compared to template-free synthesized titanium dioxide particles. Finally, designed peptide sequence was conducted to a multi-step seeding mediated growth method for gold mineralization around peptide nanofibers. The gold-peptide hybrid nanostructures with different packing characteristics and sizes were synthesized and fully characterized. Further, it was demonstrated that the dry film of these nanostructures showed a resistive switching dominant conductivity, due to the

nanogaps in between gold nanoparticles as a result of particle alignment driven by the peptide nanofiber.

The results obtained in this thesis encourage use of a new “bottom-up” synthesis approach. Specially designed peptides with desired properties and functional groups were synthesized and peptide nanofibers formed were further used as templates for inorganic mineralization. Not only it is possible to synthesis high amount of nanostructure with this approach, but also formed one-dimensional nanostructures show advance functionalities used in several applications as a part of the thesis scope. This methodology is suitable for many metals and metal oxide based applications.

Keywords: Biomimetic mineralization, Nanomaterials, Peptide, Self-assembly, One-Dimensional Nanostructures, Template Directed Synthesis.

ÖZET

KENDİLİĞİNDEN DÜZENLENEN PEPTİT KALIPLAR YARDIMIYLA İNORGANİK TEK-BOYUTLU NANOYAPILARIN SENTEZİ ve UYGULAMA ALANLARI

Handan Acar

Malzeme Bilimi ve Nanoteknoloji Programı, Doktora

Tez Yöneticisi: Yar. Doç. Dr. Mustafa Özgür Güler

Aralık, 2012

Son yıllarda, bilim ve teknoloji alanında nano düzeyde mühendislik oldukça yoğun çalışılan bir alan olmuştur. Bu tez; işlevsel inorganik malzemelerin, doğadan ilham alınarak, yapay organik kalıplar yardımıyla sentezlenmesi üzerine yeni bir yöntem sunmaktadır. Organik kalıp ile inorganik nanomalzeme sentezlenmesi yönteminin geliştirilmesi amaçlanmıştır. Bu amaçla, uygun koşullarda nanofiber haline gelebilmesi için programlanmış amiloyid benzeri peptit sekansı tasarlanmıştır. Bu tasarım sırasında, oluşan nanofiberin dış kısmında kalan ve ortamdaki belli inorganik iyonlarla bağlanma eğilimi gösteren işlevsel gruplarla döşenmiştir. Bu işlevsel kimyasal gruplar, hedeflenen inorganik monomerlerin peptit nanofiberlerin üzerlerinde birikerek, tek-boyutlu organik içerikli- inorganik kabuklu nanomalzeme oluşması için görevlidir. Sentezlenen peptit nanofiberlerin ve inoganik

nanomalzemelerin fiziksel ve kimyasal özellikleri, kalitatif ve kantitatif metotlarla karakterize edilmiştir.

İlk olarak, Silisyum ile peptit nanofiber kalıpların etrafında yapılan mineralizasyon işleminden elde edilen silika nanotüpler, patlayıcı sensörü geliştirilesinde kullanılmıştır. Silika nanotüpler patlayıcıların varlığını algılaması için, floresan boya ile kaplanmıştır. Nanotüplerin yüzeylerinin bir hayli gözenekli olmaları, nanoparçacıklara ve film yüzeye göre floresan boyayı daha fazla tutmasını ve dolayısıyla trinitrotoluen ve dinitrotoluen gibi patlayıcıların olduğu ortamlarda daha hızlı floresan sönümlemesi göstermesini sağlamıştır. Bu şekilde peptit nanofiber kalıp kullanılarak sentezlenen tek boyutlu silika nanotüpler, yüksek yüzey alanları sayesinde katalizör ve sensör gibi malzemelerin hazırlanmasında kullanılabilirler. İkinci kısımda, titanyum mineralizasyonu ile titanyum dioksit nanotüpler elde edilmiştir. Tek-boyutlu yapı, elektron transferini daha verimli gerçekleşrirebilmesi ve elektron-boşluk yeniden birleşmesinin daha az meydana gelmesi gibi üstün özellikler göstermektedir. Bu özellikler ile elde edilmiş titanyum dioksit tek-boyutlu nanoyapıların gelen ışığa gösterdiği tepki artar ve bunlar boyayla uyarılan güneş pili yapımında kullanılmaya uygun hale gelir. Peptit nanofiberlerin kalıp olarak kullanılmasıyla elde edilen titanyum dioksit nanotüpler ile yapılan güneş pillerinin herhangi bir kalıp kullanılmadan sentezlenen titanyum dioksit parçacıklar ile yapılanlara göre iki katından daha fazla verimle çalıştığı gösterilmiştir. Son olarak, altın mineralizasyonu çalışmasında, çok basamaklı, tek noktadan büyütme metodu geliştirilmiştir. Bu yöntemle farklı uzunluklarda ve şekillerde birçok altın-peptit hibrit nanoyapıları elde edilmiştir. Özellikle, büyüklükleri birbirine benzer altın nanoparçacıkların peptit nanofiberler etrafında tutunması ile oluşan tek-boyutlu

nanoyapılar, kontrollu bir şekilde elde edilmiştir. Tek-boyutlu altın-peptit hibrit nanoyapılarındaki altın nanoparçacıkların arasındaki boşluklardan dolayı, nanoyapıların oldukça iletken olduğu gözlemlenmiştir. Bu yapıların kuru filmlerinde ise, tünellemenin baskın olduğu direnç değişimi gösteren ile bir iletkenlik gözlemlenmiştir.

Bu tezde elde edilen sonuçlarla yeni bir temelden yukarı yaklaşımı gösterilmiştir. İstenilen özelliklerde ve işlevsel gruplarla tasarlanmış peptitler sentezlenmiş ve bunlardan inorganik mineralizasyonlarda kalıp olarak kullanılabilen nanofiberler oluşması sağlanmıştır. Bu yaklaşımla, yüksek miktarda nanaomalzeme sentezi yapılması mümkün olabileceği gibi, oluşan tek-boyutlu nanoyapıların oldukça gelişmiş özellikleri ile birçok uygulama alnında kullanmak mümkün olabilir. Bu sentez yöntemi, birçok metal ve metal oksit temelli uygulamada yer bulabilir.

Anahtar Kelimeler: Biyomimetik mineralizasyon, Nanomalzemeler, Peptit, Kendiliğinden Düzenlenme, Tek-Boyutlu Nanoyapılar, Kalıp Kullanarak Sentez.

To mom…

Acknowledgement

Dr. Mustafa Özgür Güler; you thought me to be a well-disciplined, conscientious and self-motivated researcher, and the moral values of being a fair scientist. The most valuable thing that you taught to me is the esteem that I profess to science. When I got lost, you enlightened my path with your guidance and support. I owe this thesis to your advice with your words: “I do not recommend you to do another job”. I will be always proud of being your student. The scientific advance you brought to me and the ecole of BML group will always be with me through my academic life. You sculptured me into a fair scientist.

Dr. Ayşe Begüm Tekinay; thank you for your encouragement to be curious about everything in science. You are a role model for me to be a successful female scientist. I was always welcome whenever I visited you and asked for your advice. Thank you for being so kind to me.

Dr. Aykutlu Dâna, your intelligence and your curiosity in all branches of science always evoked my admiration. I learnt a lot from you while working with you. It will be always honor for me to have worked with you. You were always very tactful to me, and I will always remember you with admiration.

I would like to thank Prof. Dr. Engin Umut Akkaya, Ass. Prof. Dr. Ali Osmay Güre and Ass. Prof. Dr. Emrah Özensoy for their fruitful discussions and guidance during my Ph.D.

Sıla Toksöz; it is a honor for me to be your friend and lab mate. I gained different aspects to science from you. You are also a sister for me. I am very lucky that you made me feel like a part of your noble and generous family. I will always remain

grateful to you and your family. I wish always the best for you which you deserve very much. I am sure I will be proud of your triumphs in the future. Ruslan Garifullin, you were with me almost from the beginning. We worked together in the lab. You have a huge work on this thesis and I owe a big thank to you. Adem Yıldırım, I learnt a lot from your sincere helps and patience. You are a very special and valuable scientist, and I will always be proud of having the chance of working with you.

Mustafa Güler, you put up my whims so much. You helped me whenever I needed you, thank you very much. Your observations always guided my research. Since we worked for hours together in a dark TEM room, you have become very close friend of mine. I will always remember you and your style in my life.

Okan Öner Ekiz, we started together in the same office. I wish I can say that we grown up together here, but we mostly got older. I am sure that, any objective aspect can see your successes and appreciate them. Hakan Ceylan, you always inspired me. Although I got some troubles in Boston, I am very grateful to that travel, since I earned a brother like you. I always appreciate your optimism (which is scientifically proved) and your excitement. Melis Şardan, Oya Ustahüseyin, Göksu Çınar; I am very lucky to be so close with you. Your friendship and intelligence helped me to get over the bad times. Being in the same research group with you will always be a honor for me. Being close friends with you will always warm my heart. I will always feel your support with me. Dr. Rükan Genç, thank you very much for enlightening my way with your not only scientific point of view, but also friendship. I learnt a lot from your optimism.

Oğuz Hanoğlu, how can I describe your place in my life; squirrels! Your determination of following your dreams always inspired me. I learnt a lot from you and your view of life, and I am sure I will continue to learn. You are very valuable and special friend of mine.

Can Ataca, talking with you always made me very self-confident. What is your secret about this feeling? I hope it is just being realistic. I feel your support with me whether you are on the other side of the world! Your sense of humor, sympathy and intelligence evoke my admiration. And Hasan Şahin, you both were very close and special friends for me. I will always remember the times with you. I owe a thank to both of you, because you colorized my life in UNAM. I always appreciate your friendship and feel very lucky to have you. I am sure that I will always be proud of your successes wherever you are.

Nilay Arkün, you are like a sister for me. I had many troubles and you were always there. The rational thoughts of you always evoked my admiration. I learnt to say “I love you” without hesitation from you. I always felt myself very comfortable with you and your big genuine family. Onurcan Özçelik, my brother, you accept me as I am. I have never listened someone else for that much long time with a full focus. The intelligence, honesty and politeness of your thoughts always amazed me. I know that, where ever you both will be in future, we will always be close. Yıldıray Kabak, you were there when I needed you most! We like each other very much, which makes it easier for me to understand your badly desire to find a passion. I am sure that you will have whatever you want in your life, with the help of your talent and ambitions. As I talked with you, we are both lucky in different points of view. As

you said, sometimes leaving and starting from zero is the best. I will not start from zero, I will always have you, my very precious friends.

Kavaklıdere Rotaract Club, you are my family in Ankara. As I say from the beginning, being a part of you is a great prestige for me. It is a fortune to me to have that much big, wonderful family. I always feel very comfortable, cheerful and excited when I am with you. I always know that, I am a member of not only a club, but also a huge and warm family.

Yelloz and Tomtiş, you thought me something that I could never learn from a human but you two lovely cats. I learnt to love and be loved. I really appreciate you both because of the feeling of peace you gave to me when I needed it most.

One of the most important things in life is feeling of belonging to a home. Whatever happens to me, I know that I have a family which I belong to. Mom, Hande and Aydan, you are the most important people in my life. Where you are is home to me. We have been through a lot of things during my Ph.D., and we got over all of them together. We will always do it together, whatever it comes in life. I love you all.

My mom, although you never told us anything what you have experienced, I can understand it very deeply. You did it for us, for our future. And, I did it, for you…

Table of Contents

Table of Figures

Table of Schemes

Chapter 1

Introduction

1. Introduction

Organic materials and polymers are strongly integrated into modern technology; nevertheless, inorganic materials still preserve their status as the basic elements in engineering. However, there is an increasing awareness that the conventional methods of “heat and beat” have several limitations in fulfilling the requirements for future advanced materials. In particular the limitations are generally in the construction of complex architectures from nanoscale to macroscale. This knowledge creates a vital need for novel synthesis methods.

Among nanoscale assembly techniques, top-down approaches have attracted attention for many years. Neverthless, researchers in areas such as lithography and etching have faced difficulties related to the cost, process speed and diffraction limit of top-down devices. On the other hand, “bottom-up” approaches can offer large-scale, rapid, and low-cost production of nanostructures with a diverse range of starting materials. Self-assembly is a bottom-up approach, the spontaneous aggregation of many different subunits into larger, well-defined, functional objects with different properties.

In the self-assembly processes; atoms, molecules, particles, and other building blocks organize themselves into functional structures as driven by the energetic of the system. Molecular self-assembly is also a useful technique for material designing. It involvs non-covalent supramoleculer interactions, such as hydrogen bonding, hydrophobic, electrostatic, metal-ligand, π-π and van der Waals interactions. Althpugh these interactions are relatively weak interactions with compare to covalent bonds, sufficient number of them can yield a stable assembly. Many new self-

assembling material can be design to organize into ordered coplex structures by understanding the mechanism of these assembly processes [1]. Self-assembly is controlled by many factors including temperature, pH, and electrolyte concentration. Novel self-assembled materials for both biological and nonbiological applications are being developed for regenerative medicine [1-5], electronics [6-9], optics [10], and as pH detection [11]. There is no doubt that new approaches using conceptually new solutions, such as “biomimetic design” and self-assembly, should be developed and used to expand the frontiers of possibility in this field. The ability of biomimetic materials to organize inorganic “bricks” into nanoscale, microscale and macroscale materials has great potential for electronics [12, 13], catalysis [14, 15], sensors[16], molecular recognition [17], magnetism [18-20], optics [21], photonics [22] and biomedical applications [23].

One-dimensional nanostructures have found widespread use in the fabrication of nanoscale electronic, mechanic, magnetic, optical, and combinatorial devices owing to their high ratio of surface area to volume and quantum-confinement effects [24-26]. By studying one-dimensional nanostructures, the effects of reduction of size and dimensionality on mechanical, thermal and electrical properties can be investigated. An example of mechanical one-dimensional supramolecular nanostructures in nature can be seen in cytoskeletons. Actin filaments, intermediate filaments and microtubules are the three main classes of protein filaments that form the cytoskeleton; actin and microtubules act in concert during cell movement and morphogenesis [27]. Although nanoscience is still far away from being able to mimic such intricacy, biology continues to inspire the design of nanodevices. Amyloid plaques are another natural example of one-dimensional nanostructures formed by

very stable self-assembling peptides, and are known to play a role in Alzheimer's disease [28]. As a result of the biological relevance of one-dimensional aggregates in neurodegenerative diseases, the self-assembly mechanisms of such one-dimensional nanostructures are of interest to researchers.

Amino acids are the building blocks of proteins, and of the living organisms. They are also utterly important for the formation of inorganic structure of the living organism. Synthesis of peptide in desired sequences attracts the scientists for many years, due to the such importance of proteins. The first peptide synthesis published by Emil Fischer (9 October 1852 – 15 July 1919) and Fourneau [29]. Fischer won Nobel Prize in Chemistry in 1902 by the synthesis of Diketopiperazine hydrolysis glycoglycin (Figure 1.1). This reaction opened tremendous fields in many branches of science and although it has been more than 100 years, synthesis of an artificial peptide with desired properties is still a hot topic.

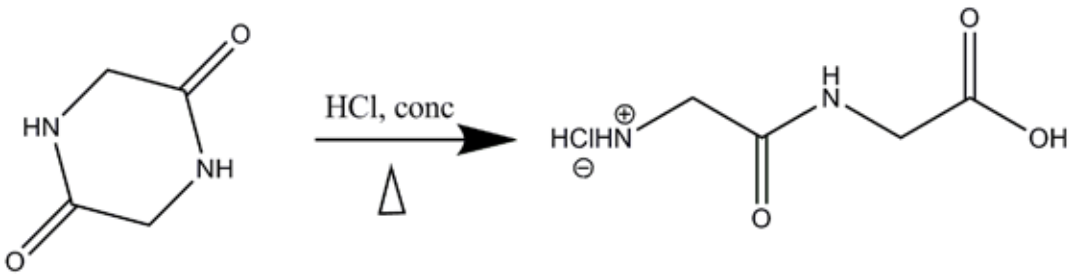

Figure 1.1. Fischer's synthesis of glycoglycin.

After Fischer's innovation, longer sequences intended to synthesis by wet chemistry. Solid Phase Peptide Synthesis (SPPS) pioneered by Robert Bruce Merrifield (July 15, 1921 – May 14, 2006), who won the Nobel prize in 1984 [30]. SPPS allows the synthesis of both natural and unnatural peptides with many functional groups. In this method, amino acids bind each other via amide (peptide)

bonds. The peptide synthesis occurs by coupling the C-terminus of one amino acid to the N-terminus of another. To prevent unintended reactions, protecting groups are used.

As can be seen in scheme 1.1 this synthesis strategy is based on the usage of solid insoluble beads modified with linkers. The coupling reaction starts on this linkers. The free N-terminal amine of a solid-phase attached amino acid is coupled to a single C-terminus activated and N-terminus protected amino acid unit. The N-terminus of the amino acid is protected due to avoid unintended reactions, with Fluorenylmethyloxycarbonyl (Fmoc) group. After deprotection of N-terminus of the new attached amino acid, it coupled to the other amino acid. This strategy is based on repeated cycles of coupling- washing- deprotection- washing processes. At the end of coupling of all predetermined sequence of amino acids, the linker between solid-phase and peptide cleaved by a trifluoroacetic acid (TFA). After the filtration of remained solid-phase, synthesized peptide-TFA solution would be separated.

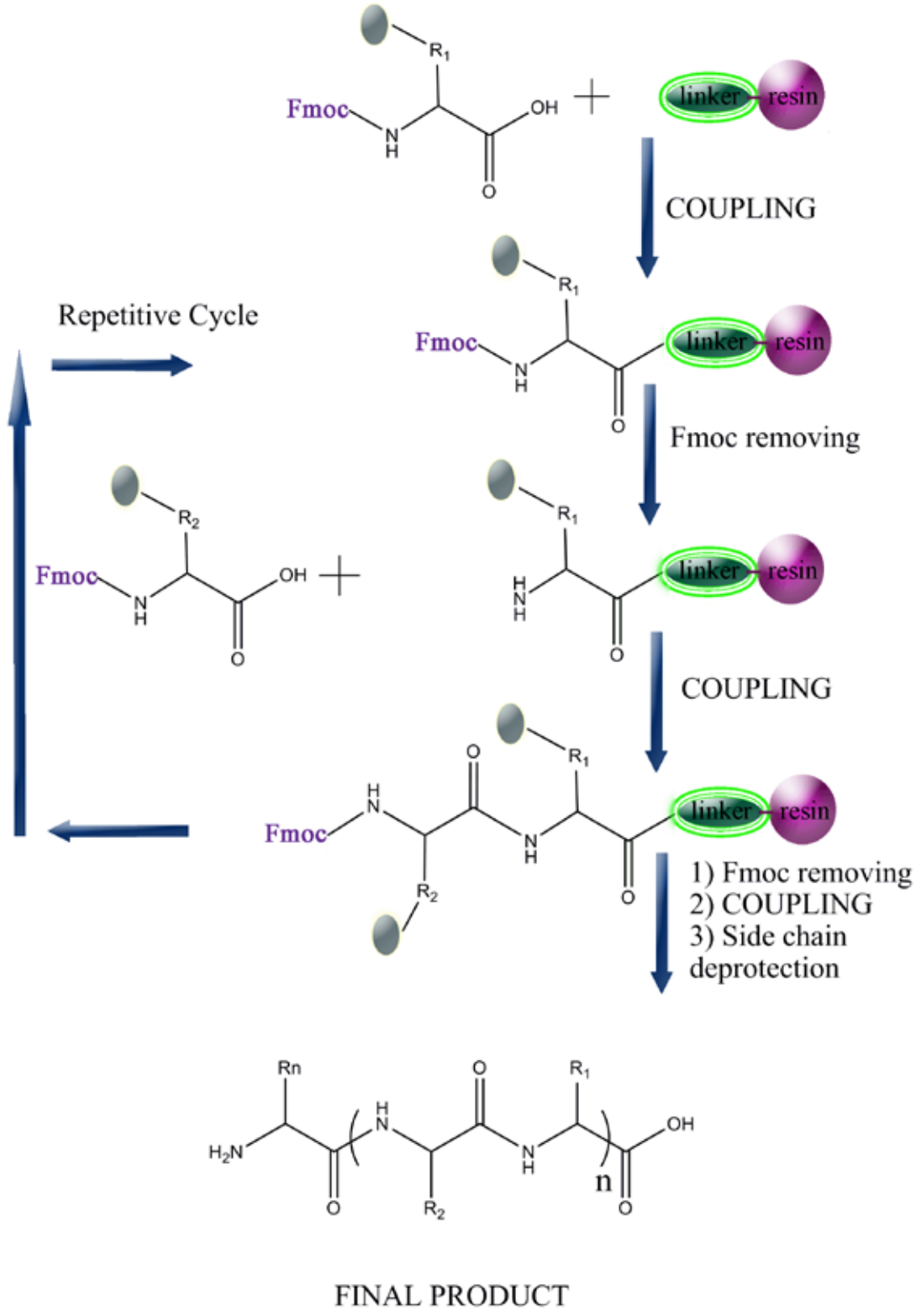

Scheme 1.1. Schematic description of Solid-Phase Peptide Synthesis

Proteins and peptides can assist forward the synthesis of inorganic materials in an environmental-friendly strategy via a process known as biomineralization. Nature inspired synthetic peptide networks have wide applications including bioactive tissue scaffolds [31, 32], carrier agents [33, 34], and templated synthesis of inorganic materials [35, 36]. Recently, the high mechanical stability of peptide nanofiber networks was shown [37, 38].

The design of the amino acid sequence could be chosen to implement any functionality to the peptide. To determine the functional groups of a peptide, the affinity of binding with intended mineral ions in the medium should be considered. The ions of different minerals have some particular properties such as being Lewis acid or base.

The design of the peptide used in this thesis was achieved with the consideration of properties of functional groups. The electrostatic interactions between functional groups and mineral ions in the medium designed by taking the Ralph Pearson's Hard Soft Acid Base (HSAB) Theory [39]. According to this theory; *soft* acids react faster and form stronger bonds with *soft* bases, whereas *hard* acids react faster and form stronger bonds with *hard* bases. Here *'hard'* implies to species which are small, have high charge states and *'soft'* implies to species which are big, have low charge states.

In this thesis, we described the design and synthesis of a peptide molecule with special functional groups. The peptide molecule is able to self-assemble into one-dimensional nanostructure under appropriate conditions. The functional groups have affinity to bind particular mineral ions in the medium, by which these peptide nanofibers act as templates. The structures formed by accumulation of minerals

around these peptide nanofibers are uniformed and well-defined nanostructures and have many application areas such as sensors, dye-sensitized solar cells and electronics as described in this thesis.

In Chapter 4, the synthesis of fluorescent silica nanotubes forming a porous network by using biomineralization process through self-assembled peptidic nanostructures are described. Fluorescent porous organic-inorganic thin films are interest of explosive detection because of their vapor phase fluorescence quenching property. The amine groups on the peptide nanofibrous scaffold were used for silicon ions seeding and accumulation. Silica nanotubes were used to prepare highly porous surfaces and they were doped with a florescent dye by physical adsorption for explosive sensing. These porous surfaces exhibited fast, sensitive and highly selective fluorescence quenching against nitro-explosive vapors. The materials developed in this work have a vast potential in sensing applications benefiting from the elevated surface area.

The synthesis of one-dimensional anatase titanium (IV) oxide nanostructures was explained in Chapter 5 by using amine functionalized self-assembled amyloid-like peptide nanofibers as templates. Mineralization of peptide templates leads to hybrid organic-inorganic material, where surface of nanofibers is coated with a titanium oxide precursor. Further formulation of this material as a paste and its direct application to transparent conductive oxide (TCO) glass surface, followed by calcination, leads to a fully functional electrode with a nanostructured anatase TiO_2 layer. Photovoltaic performance of the obtained layer is assessed in dye sensitized solar cell efficiency measurements.

The amyloid like peptide molecule self-assembling into one-dimensional nanofibers has affinity to gold ions. These molecules were used as templates for growth of one-dimensional gold nanostructures as described in Chapter 6 in the presence of ethanol as a seeding agent and ascorbic acid as a reducing agent. We performed multi-step seed mediated synthesis of gold nanowires by evaluating several parameters including the molar ratios of peptide/ gold precursor, peptide and ascorbic acid concentration as well as the effect of the reduction kinetics of the ascorbic acid. Gold nanostructures with wide range of morphologies (e.g. smooth nanowires, noodle-like one-dimensional nanostructures and also this homogenous aggregates of spherical nanoparticles) were synthesized by use of green chemistry method and they have potential use in several applications including electronics and optics.

Chapter 2

Background

This work is partially described in the following publication:

Toksoz, S., H. Acar, and M.O. Guler, "Self-assembled one-dimensional soft nanostructures", *Soft Matter*, 6(23),p.,5839-5849, 2010.

2. Background

Supramolecular interactions are driving forces of self-assembly in simple systems. Understanding interactions in the assembly mechanisms of biological molecules has become a crucial factor in designing nanoscale materials. It is important for appreciate the high complexity of self-assembly process of nature.

The interactions that coordinate the amino acids in natural one-dimensional systems are highly dynamic and often delicate, due to their relatively weak nature in comparison to that of covalent bonds [40]. However, the sufficient number of these weak interactions can yield strong and stable aggregations. Biological one-dimensional entities including viruses [41] and fungi [42] have been found to be used as templates for nanostructure synthesis, such as wires [43, 44].

In order to understand and control the self-assembly of supramolecular structures, the non-covalent interactions taking part in this process must be studied in detail [45, 46]. This background informaiton focuses on one-dimensional self-assembled organic nanostructures classified according to the forces acting on their formation ranked, in order from the strongest interaction to the weakest. (Table 2.1).

Type of Interaction	Strength (kJ/mol)	Properties
Electrostatic	50-300	Non-selective
Coordination binding	50-200	Directional
Hydrogen Bonding	5-120	Selective, directional
π-π Stacking	0-50	Directional
Solvophobic	Depends on solvent type	Little directional constraint
van der Waals	< 5	Non-directional, non-selective
Covalent	350	Irreversible

Table 2.1. Strength and properties of non-covalent interactions. Adapted from [40, 47].

2.1. Electrostatic Interactions

Electrostatic interactions are based on Coulombic attraction between opposite charges. In host/guest chemistry, many receptors for anions and cations use electrostatic interactions to hold the guest in place [48]. The principles of formation of nanostructures through electrostatic interactions can be read in Faul and Antonietti's review [47].

Zhang *et al.* developed ionic self-complementary peptides, one of which is named RADA16, a peptide which forms nanofibers in aqueous solutions by using β-sheet structures [49]. RADA16 contains negatively charged aspartic acids and positively charged arginines. Forming hydrogels in physiological media, the gels promoted the growth of neural cells in an integrated network that showed synaptic activity [50]. In this case, the charged properties of the peptide nanostructures served not only for their self-assembly but also for guidance of the cells. These hydrogels have actually been shown to improve the attachment and

differentiation of a variety of cell types, including stem [51] and endothelial cells [52].

Peptide amphiphile molecules [53] exploit a number of non-covalent interactions to self-assemble [54]. Two oppositely charged peptide amphiphiles have been shown to self-assemble into one-dimensional nanofibers by electrostatic interactions in aqueous solution at neutral pH [55]. The use of oppositely charged biomacromolecules to induce self-assembly has also been demonstrated, where heparin molecules screened the positive charge of a peptide sequence [56]. Size of the macromolecules plays an important role in formation of nanofibers as well [57], as larger molecules including DNA and chondrotin sulfate result in gelation of positively-charged peptides, whereas bovine serum albumin, a smaller molecule, cannot induce self-assembly.

Tetrapyrroles are large macrocyclic molecules containing four pyrrole rings. They self-assemble into light-harvesting and energy-transferring nanostructures in biological systems. Porphyrins from tetrapyrrole family are attractive building blocks to synthesize photocatalytic and light-responsive nanotubes; two oppositely charged porphyrins were employed to self-assemble through electrostatic interactions [58]. It is possible to change the function and the structure of the nanotubes by modifying the porphyrin building blocks, suggesting a high degree of control over the nanotubes.

2.2. Metal coordination

Over the past few decades, many studies have been carried out regarding coordination polymers and crystal engineering of metal complexes; selective

metal ion binding has been found to be a promising approach to control the fabrication of nanoscale self-assembled structures. In metal coordinated structures, metal ion functioning had been used along with some other non-covalent interactions [59-62] including hydrogen bonding, π–π stacking interactions and van der Waals forces. Potential applications of these nanostructures lie in the development of new materials, including metal-organic frameworks [63, 64], with magnetic, non-linear optical and photoluminescent properties.

Metal centers interact with ligands via medium strength directional metal-ligand bonding. A broad knowledge of coordination chemistry contributes to the selection of appropriate metal-ligand pairs and binding modes for the assembly of supramolecular structures with differing shapes. A coordination system consists of a central metal atom, called the coordination center, ligated to other atoms, called ligands, where the coordination bonds are delocalized over the ligands, thus reducing the Coulomb repulsion between the electrons. The *d*-orbital occupation changes the symmetry of the metal coordination sites, thereby changing the supramolecular shape. To obtain the desired structure, the metal coordination environment and binding mode of the linkers must be carefully designed, where the shape is encoded both in the ligands and the metal ions. For the metal center, transition metal ions can be useful as they not only stabilize the structures but also interact with other elements, allowing construction of more complex structures. To form complex structures, the metal centers should be available for further coordination; bulky ligands can be used to hinder the attachment of same or other ligands to the metal centers, thereby preventing

saturation of the metal centers.

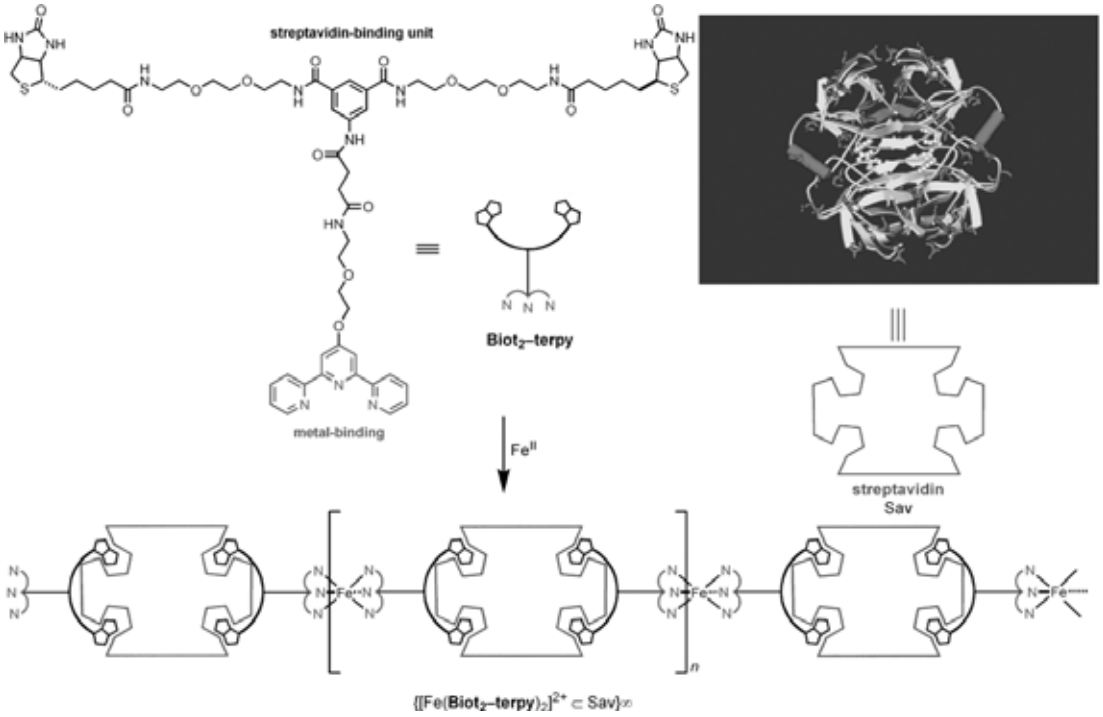

Figure 2.1. Bis-biotinylated terpyridine forms a linear tetrabiotinylated connector, the [Fe(Biot2-terpy)2]2+ complex, upon reaction with ferrous ion. The presence of streptavidin results in formation of linear coordination polymers [65].

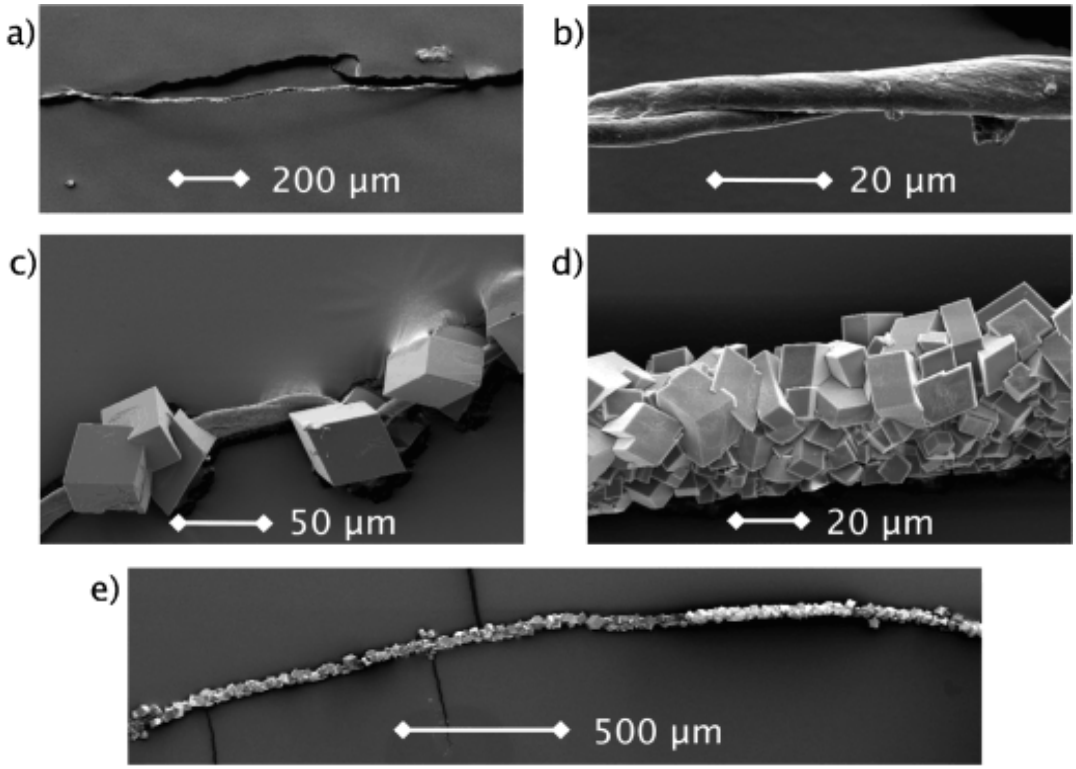

Figure 2.2. SEM images of MOPF bundles containing $CaCl_2$. (a) $8x10^{-7}$ M Fe solution containing 0.05 M $CaCl_2$, 5 min at RT; and (b) a zoom into it. (c-e) Biomineralized bundles of 8 x 10^{-6} M Fe solution, 12 hours: (c) 0.01 M $CaCl_2$; (d-e) 0.05 M $CaCl_2$ [65].

The transition-metal connectors in conjunction with proteins are used to create one-dimensional metal-organic protein frameworks [63]. It was demonstrated that streptavidin, a homotetrameric protein with four biotin binding sites, combined with a linear tetrabiotinylated connector, the $[Fe(Biot_2\text{-terpy})_2]^{2+}$ complex bearing four biotin groups, with the aim of producing a collagen mimetic material for calcite biomineralization. Self-assembly took place through non-covalent interactions of coordination polymers and protein aggregates into a one-dimensional metal–organic protein framework (MOPF) to yield millimeter-sized one-dimensional matrices. Ferrous ions were used in the synthesis of $[Fe(Biot_2\text{-terpy})_2]^{2+}$, as terpyridine readily interacts with those ions in a cooperative fashion (Figure 2.1). To induce the

biomineralization of calcite, carbondioxide vapor was streamed over MOPF bundles for nucleation, growth and assembly of calcite microcrystals on the bundles (Figure 2.2). The negatively charged glutamic acid and aspartic acid side chains are thought to have favored chelation of calcium [65].

Self-assembly of *de novo* designed peptides into well-designed structures can be achieved through an appropriately chosen metal ion [66-68]. Selective recognition and binding of the metal ion to the peptide might induce a conformational change. Self-assembly of a fibril forming peptide, a structural variant of a three-stranded helical bundle forming a trimeric leucine zipper, was triggered by silver(I) ion binding to proximal histidine residues [66]. The trigonal planar geometry in the metal ion binding site favored binding of silver(I) ions, which in the presence of soft-donor nitrogen ligands can adopt a trigonal planar coordination in the presence of soft-donor nitrogen ligands. Alternative coordination geometry using ions like copper, zinc and nickel failed to induce self-assembly. In an earlier study, same peptide was shown to self-assemble via a pH-dependent route [69]. Although, the final fiber morphologies were similar for two assembly routes, the lateral association between fibrils to form fibers larger in diameter was less extensive for silver ion induced fibrils. This might be related to the Columbic repulsion due to the partial co-localization of positive charges by counter ions: metal ion induced fibers were positively charged due to the presence of metal ions, in this case one silver(I) ion per peptide; whereas pH-induced fibers have a negative charge at neutral pH.

Cd(II) centers are known for their use as metal coordination, because the d^{10} configuration of cadmium complexes results in formation of various coordination

geometries. Kong *et al.* reported that an imidazole-containing tripodal ligand reacted with Cd(II) complexes of bromide, tetrafluoroborate, and nitrate, and three new coordination polymers were obtained [70]. In the presence of $[CdCl_4]^{2-}$ as a counter anion, one of the complexes adopted a one-dimensional zigzag chain structure. The other two complexes adopted branched chain structures. The Cd(II) centers of the three complexes had different geometries such as distorted square pyramide, tetrahedron, and distorted octahedron. Tetrafluoroborate and nitrate anions were not found in the distorted geometries, but they had an impact on the self-assembly process so that on the final framework. The obtained coordination polymers demonstrated photoluminescence, as all complexes exhibited a blue fluorescence at room temperature in the solid state and could serve as a good candidate for photoactive materials.

Dendron-rod-coils, having unique triblock architecture, self-assemble into one dimensional nanoribbons which have found use as a template for the synthesis of cadmium sulfide nanohelices [71, 72]. Cadmium sulfide semiconductors have potential photovoltaic applications. Cadmium ions have an affinity towards the hydroxy containing dendron region of the ribbons over the organic solvent, which was tetrahydrofuran in this study [71]. After exposure to hydrogen sulfide gas, the localized cadmium ions started to nucleate and grow as cadmium sulfide on one face of the twisted ribbon to form nanohelices with a pitch of 40-50 nm, nearly twice that of ribbons. Nucleation happened in many points at the same time, as revealed by transmission electron microscopy image (Figure 2.3) [73]. In some cases, double coils were encountered, possibly due to the mineralization occured at both faces of the ribbon.

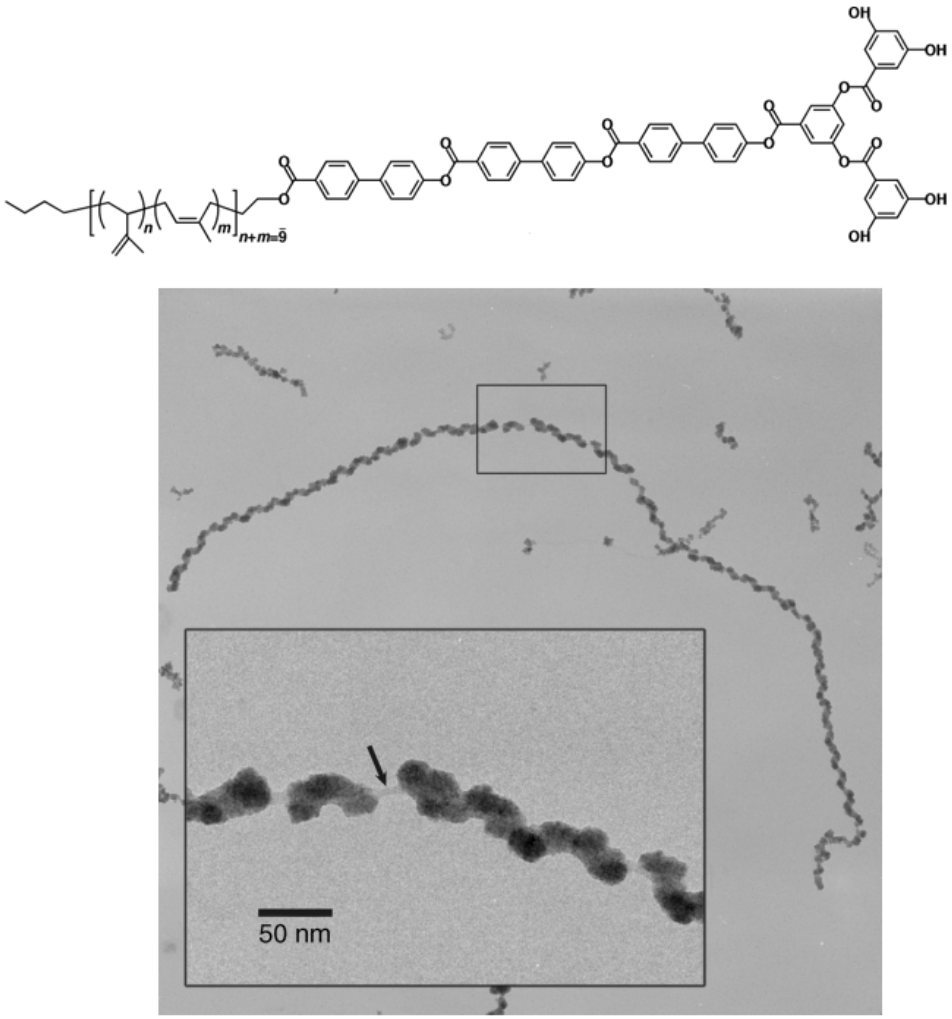

Figure 2.3. Chemical structure of the dendron-rod-coil molecules and TEM image of cadmium sulfide precipitated in a suspension of DRC nanoribbons, at an early stage growth. The inset shows the start of nucleation at different points and the organic ribbon under CdS as indicated by the arrow [71].

2.3. Hydrogen bonding

Arguably the most important noncovalent interaction in the self-assembly process is hydrogen bonding, due to its directionality and strength. The hydrogen atoms act as a bridge between two electronegative atoms; the hydrogen bond donor group consists of an electronegative atom bound to a hydrogen atom that

has a small positive charge due to dipole formation, and the hydrogen bond acceptor group consists of a dipole where the interacting atom of the acceptor group has a source of electrons.

The enthalpy of the hydrogen bond-based self-assembled systems must be balanced in consideration of the enthalpic loss and entropic gains due to hydrogen bonding and stacking interactions/hydrophobic effects, respectively [74]. Generally, hydrogen bonding is not the sole interaction in the self-assembly process; it is usually accompanied by other non-covalent interactions which have lower energies. Although hydrogen bonds are mostly used for constructing 2-D and 3-D nanostructures due to their selectivity and high directionality [75], there are also one-dimensional nanostructures which are self-assembled through hydrogen bonding interactions [76].

Macrocycles containing an even number of alternating D- and L-amino acids, developed by Ghadiri and co-workers, are assembled into nanotubes by orthogonal hydrogen bonding, with the hydrogen bonds of the tubular structures perpendicular to the plane of the individual molecules (Figure 2.4) [77]. In the design of the four cyclic peptides, four non-polar amino acids and one polar amino acid were employed. Non-polar residues were chosen to study the effects of increasing hydrophobic surface contact; the polar residue, glutamine, was selected because of its hydrogen-bonding donor/acceptor capability and its possible participation in intra- and intertubular hydrogen bonding interactions, thus contributing to the structural stability of the system. Similar designs have been shown to form trans-membrane channels for ion transport [78].

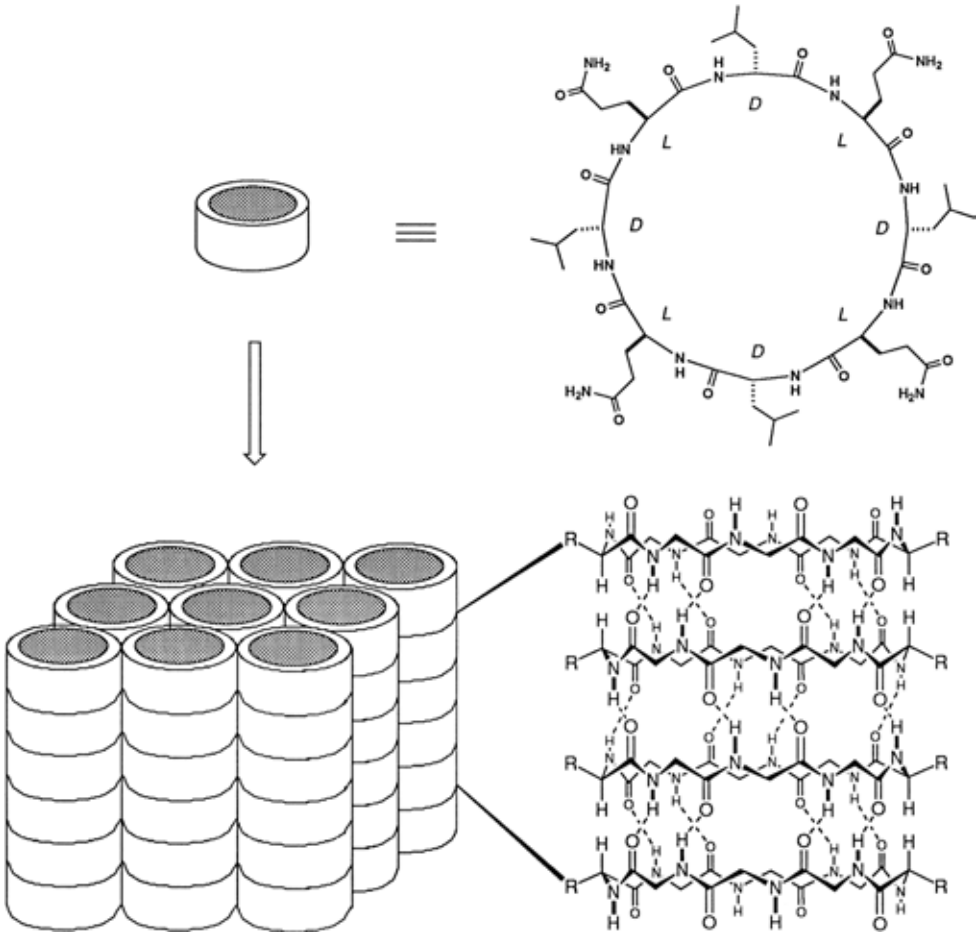

Figure 2.4. Alternating D- and L-amino acids assembling into cyclic peptide nanotubes via the antiparallel ring stacking. Extensive intersubunit hydrogen bonding can be seen in the sketches. Reproduced with permission from [77].

Peptide amphiphile design of Hartgerink *et al.* was first presented in a biomineralization study [53], where the amphiphilic molecule consisted of a hydrophilic peptide headgroup, consecutive cysteine residues for formation of disulfide bonds, a flexible linker region, a phosphorylated serine residue for inducing biomineralization and a hydrophobic alkyl tail. A recent study of the self-assembly mechanism of peptide amphiphiles by Velichko *et al.* revealed that hydrogen bonding is the main interaction contributing to the final one-dimensional shape [79]. In their model, the head groups were designed as

electroneutral in order not to calculate the effects of electrostatics in the self-assembly process. This design enabled them to perform the Monte Carlo-stochastic dynamics simulations in a reasonable time and still capture various aspects of the process. Their coarse-grained model states that transitions from random molecules in solution to different micellar structures are based on the interaction between hydrophobic interactions and hydrogen bonding. Paramonov *et al.* designed 26 different peptide amphiphiles to study a number of parameters in self-assembly such as amino acid choice, directionality of hydrogen bonding and the reasons that the nanofiber structure is favored over other structures [80]. They found that the amino acids near the alkyl tail of the peptide amphiphiles were the main contributors to the β-sheet structure, formed along the Z-axis of the fiber. There, the disruption of the hydrogen bonds, which occurred by methylating the glycine amino acids forming the hydrogen bonds, resulted in a transition from nanofiber structure to nanovesicle structure after a specific number of methylations, due to the fact that the remaining energy was not enough to hold the supramolecular structure of a nanofiber together (Figure 2.5). Guler *et al.* developed peptide amphiphile molecules conjugated to nucleic acids, resulting in thermally more stable duplexes of the conjugate molecule-DNA/RNA in comparison to nucleic acid-nucleic acid duplexes [81]. Such a molecule could be useful in RNA interference studies.

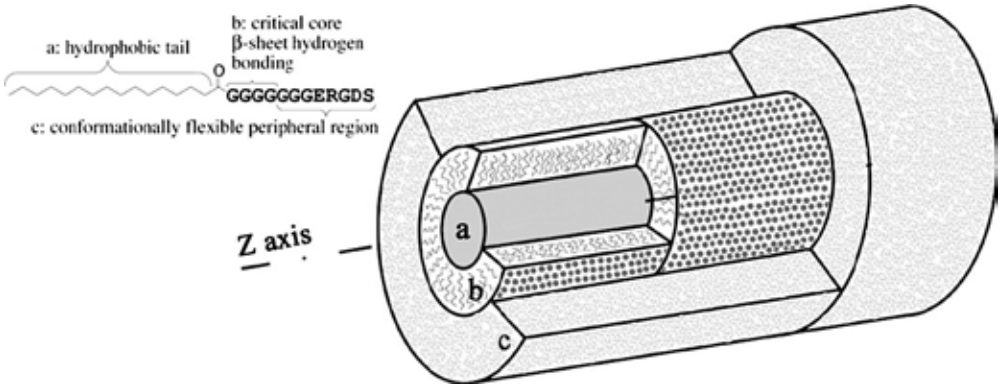

Figure 2.5. The chemical structure and the cartoon of the peptide amphiphile nanofiber: The inner most region, (a), is the hydrophobic core composed of aliphatic tails. (b) is the critical β-sheet hydrogen bonding portion of the peptide. (c), the peripheral peptide region, constitutes the interface between the fiber and the environment [80].

While studying the ability of very short aromatic peptides to form well-ordered amyloid fibrils, Reches *et al.* observed β-amyloid diphenyalanine structural motif of Alzheimer's disease self-assembling into one-dimensional nanotubes [82]. The nanotubes worked well as a mold for casting silver metal nanowires, first by metal ion reduction and then enzymatic degradation of the mold. By using diphenylalanine structural motif of Alzheimer's disease self-assembling into one-dimensional nanotubes [82]. The nanotubes worked well as a mold for casting silver metal nanowires, first by metal ion reduction and then enzymatic degradation of the mold. By using D-phenylalanine in the core structure of the peptide, the researchers achieved the construction of proteolitically stable nanotubes, which might have applications as nanotube-based biosensors. In another study, "teslian" (metal-insulator-metal) coaxial nanocables were developed by using the diphenyalanine peptide nanotubes as templates [83]. Silver ions were reduced in the nanotubes which were then chemically modified

with linker peptides consisting of a diphenylalanine motif and cysteine amino acid. The diphenylalanine motif was devised for interaction with the nanotube surface and cysteine in order to facilitate the imaging process of the structures, aided by gold ions that interact with the thiol group of the amino acid.

Hong *et al.* produced silver nanowires [84] by reducing the silver ions in their organic nanotubes, which consisted of a reduced form of calix[4]quinone with four hydroquinone moieties [85]. Of the eight hydroxyl groups, four outer groups led to self-assembled structures with intermolecular hydrogen bonding in the presence of water molecules. Repeating tubular calix[4]hydroquinone octamers formed short hydrogen bonds between themselves to stabilize a linear tubular polymeric structure, where intertubular π-π stacking interactions contributed to the stability as well.

Hydrogen bonding is a powerful strategy in the self-assembly of one-dimensional structures formed by dendrimeric molecules [86]. Some dendritic dipeptides were shown to self-assemble into helical porous one-dimensional nanostructures [87]. The characterization of the helical nanostructures indicated that the controlled design of periodic non-biological porous structures in bulk and in solution was achieved by dendrimer chemistry. The molecular recognition and self-assembly process are strong enough to tolerate a range of modifications to the amphiphilic structure.

Dendron-rod-coils, which assemble into one dimensional ribbons, form gels in certain solvents and at certain concentrations via hydrogen bonding in the hydroxyl rich regions and π-π stacking of the conjugated segments [88-90]. Zubarev *et al.* designed dendron rod-coil molecules as additives to modify the

properties of polystyrene [90]. The molecules were dissolved in organic solvents to form one-dimensional birefringent ribbon-like nanostructures with a width of 10 nm and a thickness of 2 nm, even at an extremely dilute concentration (Figure 2.6). When the gels were heated to a temperature above the boiling point of the organic solvent (e.g. styrene, dichloromethane, or acrylate derivatives), the gels did not melt revealing the irreversibility of gel structure by temperature. To disassemble the gels, hydrogen bonding must have been disrupted by polar solvents. At 1 wt% concentration, ribbons aggregated into bundles of 5 to 10 flat ribbons, where excess organic solvent use made the relatively isolated ribbons twist and gain a 20 nm pitch. The twisting probably protects the hydroxyl groups in the center of the ribbon from the organic solvent.

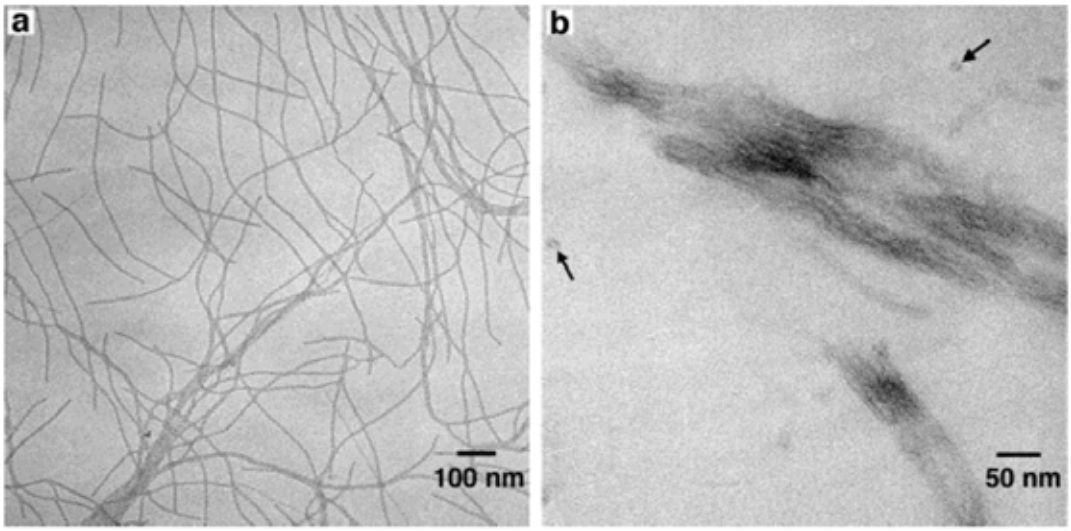

Figure 2.6. Chemical structure of the dendron-rod-coil molecule. (a) Bright field TEM image of unstained 0.004 wt% DRC molecules, dissolved in styrene. (b) High magnification TEM image of a thin slice of the scaffold material, containing 1 wt% DRC molecules. Arrows represent perpendicularly placed individual bimolecular ribbons [89].

Lipid nanotubes are promising templates for producing one-dimensional nanostructures that provide organic, discrete, tubular structures composed of a very high number of identical lipid molecules, as Young's modulus of a single lipid nanotube has been determined to be around 700 MPa [91]. Various nanotube architectures are available with reference to the type of building block, as can be seen in Figure 2.7 [92, 93].

Helices can intertwine and produce aggregated helices; when they reduce into rings, face-to-face non-covalent interactions result in the formation of tubes; instead of rings, rosettes can arrange into stacked rosettes; amphiphilic molecules might roll into sheets to produce nanotubes [93].

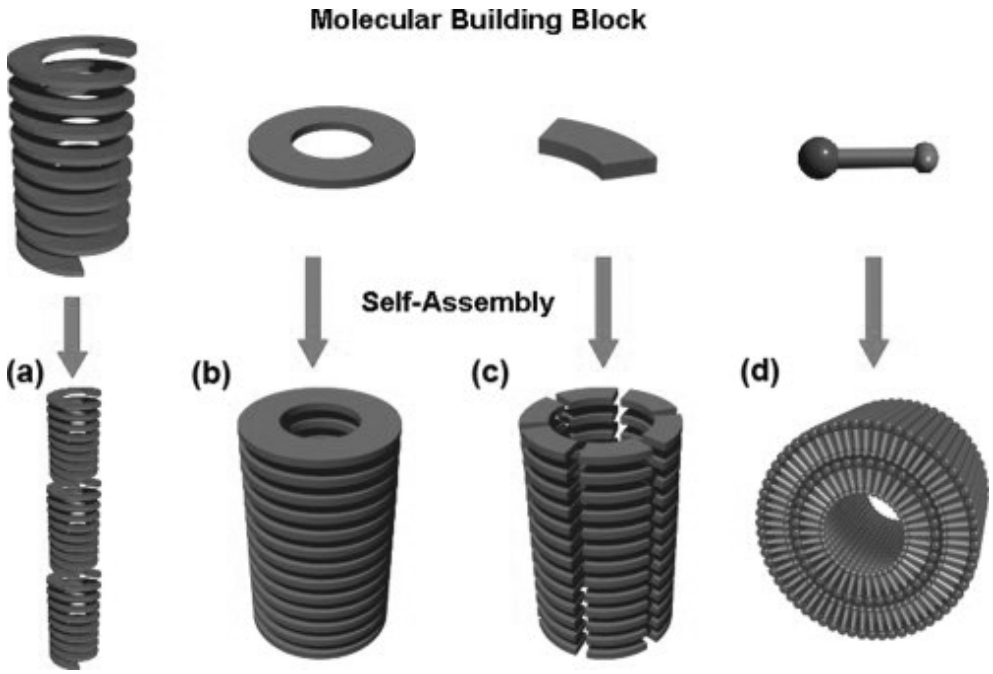

Figure 2.7. Open-ended tubular architectures: (a) aggregated helices from a hollow helix, (b) stacked rings from a ring, (c) stacked rosettes from a rosette, (d) monolayer-based lipid nanotubes from an unsymmetrical bolaamphiphile [92, 93].

Controlling the inner and outer dimensions of nanotubes and the charges and

functionalization of both sides are important in order to obtain well-defined and tailor-made architectures for many different purposes. Kameta *et al.* self-assembled fluorescent lipid nanotubes from an unsymmetrical bolaamphiphile to encapsulate and track the passage of guest molecules through the hollow nanotubes, in order to better understand how the molecules act while entering and exiting the cell through the channels of the lipid bilayer [94]. The same group also developed cardanyl-β-D-glucopyranoside lipid nanotubes to reveal the role of water confined in a lipid nanotube by incorporating 8-anilinonaphthalene-1-sulfonate as a probe, with the ultimate aim of guest encapsulation [92]. Hydroxyl groups of glucopyranoside covering the inner surfaces interacted with water molecules, lowering the solvent polarity to a value similar to that of propanol rather than bulk water.

2.4. π-π interactions

Even though much weaker and less directional when compared to hydrogen bonds, π-π stacking interactions also drive the self-assembly process for π-conjugated systems. The nature of π-π interactions is not very clear, but it is suggested that the geometrical arrangement of the fragments, as well as π electrons, contribute to these interactions [95]. In order to obtain one-dimensional structures as end products, it is necessary to favor growth along the stacking direction rather than lateral growth alongside chains. With the progression of efficient and high yield synthesis methodologies of bulk molecules [96] like dendritic molecules and macrocycles, it has become possible to build nanoscale architectures. Arylene ethynylene macrocycles [97, 98], molecules with large planar surfaces, minimal ring

strain and highly tunable ring sizes of 0.5–5 nm, have been employed mainly for the synthesis of 2-D and 3-D structures [99, 100], as simple self-assembly methods [101] resulted in the formation of agglomerates, aided by solvophobic interactions between the alkyl side chains. Balakrishnan *et al.* achieved the self-assembly of arylene ethylene macrocycles into one-dimensional nanofibers by implementing the sol-gel process [102]. Cooling a homogenous solution results in the gelation of the molecules, which decreases molecular mobility, thus minimizing the lateral growth due to side chain association.

Another type of macrocycles, constituted from oligoamides, is known to form fibrillar structures [103]. The self-assembly mechanism is suggested to rely on face-to-face stacking, aligning the macrocycles into nanotubes containing a large channel (Figure 2.8) [104]. Such nanotubes are proposed to be used as transmembrane channels by modifying the side groups to tune the solubility and membrane compatibility of the macrocycles. Employing different functional groups resulted in differing pore diameters, thus affecting the conductance of the transmembrane channels, showing that it is possible to mimic the ionic channels in biological membranes.

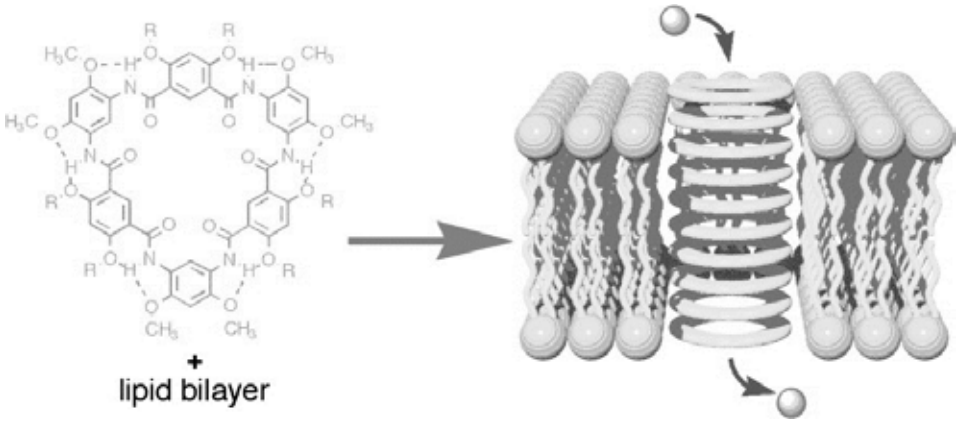

Figure 2.8. Oligoamide macrocycles self-assembling into transmembrane channels through face-to-face stacking [104].

Engelkamp *et al.* demonstrated that the tuning of the supramolecular chirality of one-dimensional objects can be done in a controlled way by simply controlling the strength and directionality of non-covalent interactions [105]. Disk molecules, derived from a phthalocyanine ring and covered with crown ether moieties, formed fibers with right-handed helicity through π-π stacking, which eventually yielded superhelices with left-handed helicity. The advantages of using π-π stacking in the design of nanostructures are its relatively less complex method,and high electron mobility through the nanostructure. High mobility is generally attributed to strong overlapping in a stack of neighboring molecules' electronic wave functions [106] which increases bandwidth and consequently electrical conductivity [107].

In the molecular electronics field, nanowires and nanocables self-assembled via π-π stacking are drawing attention [108-110]. This type of stacking is commonly observed in aromatic compounds with extended π systems. To give an example, hexabenzocoronene is a PAH (Polycyclic Aromatic Hydrocarbon) compound consisting of 13 fused benzene rings, and it was shown to self-assemble into nanocables; researchers also devised a method for putting the cables into organic

field effect transistors by use of elastomer stamps [111]. In another study, a derivative of hexabenzocoronene self-assembled into nanotubes in tetrahydrofuran, where the walls of the tubes consist of helical arrays of π-stacked coronenes covered by hydrophilic glycol chains (Figure 2.9) [112]. The final structures have been found to be electroconductive and have a resistivity comparable to that of gallium nitride semiconductors.

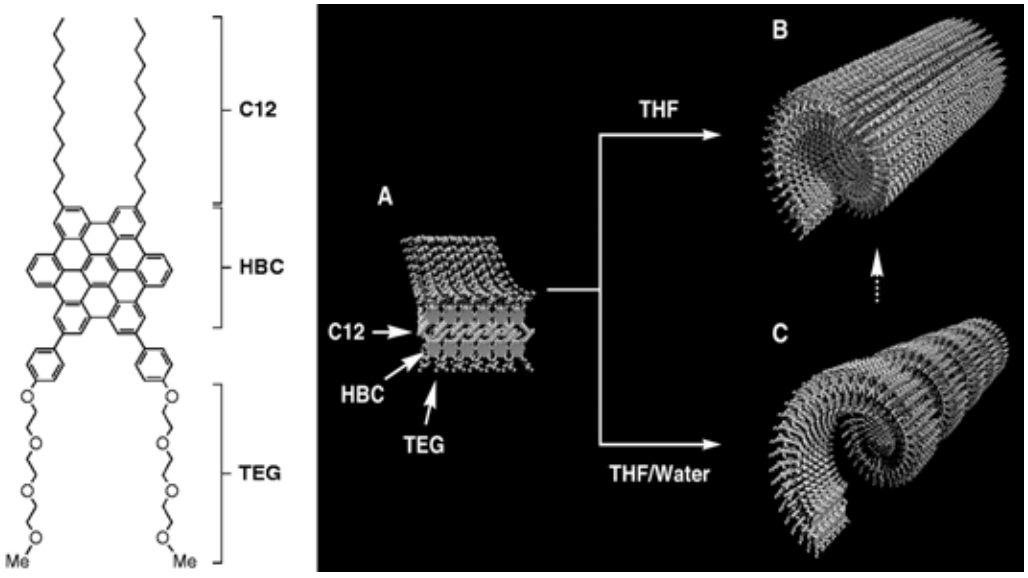

Figure 2.9. The chemical structure of hexa-*peri*-hexabenzocoronene and the self-assembly mechanism into nanotubes and helical coils: (A) A graphitic bilayer tape; each layer consists of one dimensional columns of π-stacked hexabenzocoronene units. (B) A nanotube formed by tight rolling-up of the bilayer tape. (C) A helical coil formed by loose rolling-up of the bilayer tape [111].

Hexabenzocoronene had also been used for producing discotic liquid crystals, called mesogens, by chemically modifying the periphery of hexabenzocoronene, whose liquid crystalline phase showed a rapid switching process within the applied electrical field [113]. π- π stacking and hydrogen bonding are the two

synergistic intermolecular forces controlling the assembly of the central aromatic subunits of the liquid crystals.

As a very well established study to understand the driving forces of self-assembly, Wang et al study on supra-amphiphiles can be given as an example [114]. In this study, many interactions introduced to the peptide structure to achieve rigid self-assembled nanostructures. They used mesogenic groups, strong π-π stacking groups, hydrophobic interactions in water, electrostatic interactions, and so on, to self-assembly of building blocks.

2.5. Solvophobic interactions

Solvophobic interactions, which have little directional constraint, differ from the other non-covalent interactions in terms of inducing self-assembly that hydrophobic interactions are stabilized due to favorable entropy rather than favorable enthalpy, which might even be unfavorable as long as entropy is favored. The solvophobic parts of the molecules tend to associate to minimize their surface area contacting the solvent, whereas the solvophilic parts try to remain in contact with the solvent. The two opposing forces compete with each other, one tending to decrease the interfacial area per molecule, the other tending to increase.

Solvophobic interaction is observed in solvents with a spatial hydrogen-bond network. It is thought to consist of two stages, namely solvation and interaction. According to Rodnikova *et al.*, the solvation is related to the lability of the hydrogen-bond network, whereas elasticity of the network determines the interaction part [115].

The importance of solvophobic interactions in the self-assembled nanostructures has been demonstrated in various studies [116, 117]. Designing molecules with lipid groups leads to molecules with amphiphilic features which are extremely important for self-assembly [118-120]. To study the sole effects of the non-covalent forces, namely hydrogen bonding and solvophobic interactions, acting on the self-assembly of peptide amphiphiles, molecular simulations were used [121]. It was found out that pure solvophobic interaction favored micelle production rather than one-dimensional nanofibers. However, there are a few studies where solvophobic interactions led to the self-assembly of the molecules into one-dimensional structures [122, 123].

Protein aggregation based diseases, including type II diabetes which are related to the presence of amylin fibrils in the pancreatic islets [124], are becoming more common as the lifespan increases; however, effective treatment have not been found yet. One of the approach scientist concentrate on is to restrict or inhibit the hydrogen bonding in between these molecules through primary sequence modification [125], as amyloid and amylin fibrils assemble from antiparallel oriented peptides, in which the amide bonds contribute to the hydrogen-bonding network. Elgersma *et al.* studied the self-assembly of amylin amide bond derivatives into nanostructures with the ultimate aim to design β-sheet-breaker peptides to inhibit the aggregation of amylins [123]. The peptide backbone was modified at alternate amide bonds to generate depsipeptides, *N*-alkylated peptides and peptoid-peptide hybrids as aggregation inhibitors. Although, these peptides were expected to self-assemble into fibrils, instead helical ribbons and nanotubes were obtained which indicates the lack of β-sheet formation. Replacing the backbone amide with an ester moiety or *N*-alkyl group resulted in a weaker hydrogen-bond acceptor, which inhibited the aggregation

of peptides into fibrils. For both peptides, which assembled into helical ribbons and nanotubes (Figure 2.10), increased hydrophobicity is the proposed mechanism for the self-assembly.

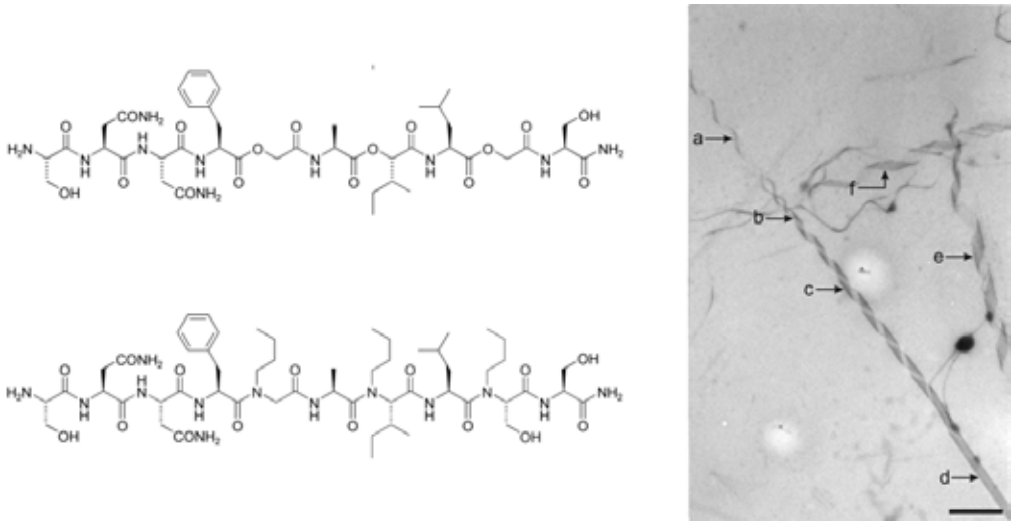

Figure 2.10. The chemical structures of amylin derivatives. Both structures assembled into helical fibrils and nanotubes. (Scale bar: 2 μm) [123].

2.6. Van der Waals interactions

Van der Waals interactions arise from fluctuations of the electron distribution of two closely spaced molecules. Shift of the electron cloud around the nucleus results in formation of an instantaneous dipole within the molecule, which in turn partially charges the other molecule such that the partial positive charge of one molecule will be attracted to the partial negative charge of the other molecule. Although van der Waals interactions do not usually play the main role in self-assembly, there are a few studies showing its leading role in the assembly process. Zhang *et al.* developed a simple synthesis method for gold nanobelts, which are proposed to self-assemble through van der Waals interactions [126]. Auroric acid ($HAuCl_4$) in polyvinylpyrrolidone (PVP) formed various structures;

triangular plates, hexagonal plates, spheres, as well as nanobelts were observed. The nanobelts were uniform in diameter (130 nm) and thickness (30 nm). Polyvinylpyrrolidone adsorption onto gold planes directs the growth of the belts. PVP adsorbs onto the {111} facets of the gold seeds, and the subsequent growth of the seeds on {110} facets in the absence of PVP results in the formation of triangular plates through van der Waals forces. The triangular plates then recrystallize to form the nanobelts, which have the same thickness and angle end structure.

Nanowires self-assembled from molybdenum sulfur iodine were experimentally characterized by electron microscopy and computer-simulated to fully understand the structure and the forces acting on that structure [127]. The electron microscopy images showed derivations from the previously predicted bundle structures, so the authors proposed a new structure. The electronic properties of the wire was determined by density functional theory (DFT), which presented weak bonding between neighboring strands. This weak bonding, attributed to van der Waals forces, proved that the wires indeed assembled into the newly proposed structure. It is suggested that the inter wire interaction is stabilized by Mo *d*-S *p* hybridization and minimization of van der Waals forces.

Chapter 3

Synthesis and Characterization of Peptide Nanofibers as Template for Synthesis of Inorganic One-Dimensional Nanostructures

This work is partially described in the following publication:

Acar, H., R. Garifullin, and M.O. Guler, "Self-Assembled Template-Directed Synthesis of One-Dimensional Silica and Titania Nanostructures", *Langmuir*, 27(3),p.,1079-1084, 2011.

3. Synthesis and Characterization of Peptide Nanofibers as Template for Synthesis of Inorganic One-Dimensional Nanostructures

3.1. Introduction

Self-assembled amyloid-like peptides [128] have emerged as a unique class of materials with potential applications as templates for nanotube [83] and nanowire [8, 82] growth, one-dimensional nanostructure organization [129], micromechanical system components [130] and interconnects for nanoelectronics [131]. Amyloid-like peptides provide suitable conditions for template-directed mineralization process with their inherent ability to self-assemble into fibrillar nanostructures [132, 133]. These organic-inorganic hybrid materials are important for bottom-up synthesis of one-dimensional inorganic nanostructures.

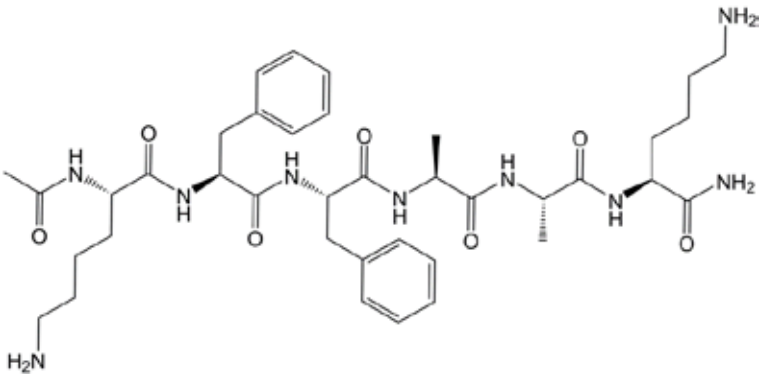

Figure 3.1. Ac-KFFAAK-Am Peptide

Here we synthesized an Amyloid Like Peptide (ALP) molecule, which is able to self-assemble into one-dimensional nanofiber in convenient conditions. The ALP

structure was inspired by amyloid proteins composed of extended sheet-like peptide secondary structures. Amyloid fibrils are the responsible from diverse group of diseases, including Alzheimer's disease, type II diabetes, and prion diseases [134]. For finding a compatible cure for these kind of diseases, it is crucial to investigate and understand the structure of the ALP nanofibers. Despite the fact that they formed from structurally unrelated group of proteins, all amyloid fibrils share similar biophysical and structural properties. The formation is a result of stacking of aromatic residues. The π-π stacking interactions plays a key role in the process of molecular recognition and self- assembly that leads to the formation of amyloid fibrils [135].

In this study, the ALP molecule was designed to form an extended hydrogen bonded supramolecular nanostructure. Enhanced stability of the resulting supramolecular nanostructure was achieved by the incorporation of amino acid residues which provide a directional and relatively strong intermolecular interaction, namely hydrogen bonding [136]. A diphenylalanine motif was employed to promote the β-sheet formation [137] through π-π stacking [138]. The amine groups on the side chain of lysine residues were used at both ends to functionalize the periphery of the nanostructures. Amines were exploited for seeding metal ions around the nanofibers.

3.2. Experimental

Peptide Synthesis: 9-Fluorenylmethoxycarbonyl (Fmoc) and ter. Butoxycarbonyl (Boc) protected amino acids, MBHA Rink Amide resin, and 2-(1H-Benzotriazol-1-yl)-1,1,3,3-tetramethyluronium hexafluorophosphate (HBTU) were purchased from NovaBiochem and ABCR. The other chemicals were purchased from Fisher, Merck,

Alfa Aesar or Aldrich and used as received, without any purification. Peptides were constructed on MBHA Rink Amide resin. Amino acid coupling reactions were performed with 2 equivalents of Fmoc protected amino acid, 1.95 equivalents of HBTU and 3 equivalents of N,N-Diisopropylethylamine (DIEA) for 2 h. The Fmoc protecting group removal was performed with 20 % Piperidine/DMF solution for 20 min. Cleavage of the peptides from the resin was carried out with a mixture of TFA:TIS:H_2O in ratio of 95:2.5:2.5 for 3 h. Excess Trifluoroacetic acid (TFA) was removed by rotary evaporation. The remaining peptide was triturated with ice-cold diethyl ether and the resulting white precipitate was freeze-dried. The peptide was characterized by a quadrupole-time of flight mass spectrometry (Q-TOF MS) (Figure 3.2). The mass spectrum shows the corresponding mass of the peptide; the purity of the peptide was assessed by RP-HPLC and found to be more than 95 % (Figure 3.3).

Liquid Chromatography-Mass Spectrometry (LC/MS): The peptide molecule is very soluble in water. 1mg peptide added into 1 ml water and sonicated for 15 minutes. Then LC/MS measurements were taken with Agilent Technologies 6530 Accurate-Mass Q-TOF LC/MS. Agilent Zorbox Extend-C18 coulomn (Rapid resolution HT 2.1X50mm 1.8-Micron) was used with 1 % Formic acid-Water (A) and 1% Formic acid- Acetonitrile (B) as mobile phase. The flow of mobile phase graduated as at first 5 minutes 2% B-98% A, from 5 to 20 minutes the rate of B increased to 100% and stayed there for 1 minute, after 21st minute the rate of B turned back to 2% again with the flow rate 0.2 ml/min. LC chromatogram was obtained at 220 nm (Figure 3.3).

UV-Vis and Fluorescence Spectrophotometry: 0.03 wt % peptide solution in ethanol was prepared and added into 1 cm quartz cuvvette. UV absorbance

measurements were taken with Varian Cary 100 UV-VIS spectrometer between 200-400 nm. Fluorescence measurements were done with Varian Cary Eclipse Fluorescence Spectrophotometer between 265-600 nm.

Fourier Transform- Infrared Spectrofotometry (FT-IR)*:* $1.33x10^{-2}$ M peptide mixed with four different solvents; ethanol, methanol, H_2O at pH 5 and 10. The reason of using those different solvents is the structural differences of the self-assembly of peptide in each solvent. For preparing the FTIR pellets, the samples in ethanol and methanol were evaporated with a vacuum oven, at 38°C and 400 mbar for 12 h, then 20 mbar for 12 h. The samples prepared in H_2O were lyophilized for 2 days. 1 mg of remaining powder was mixed with 100 mg of KBr for preparing pellets. Bruker Tenson 27 FT-IR spectrometer was used for FT-IR analysis in the range of 400-4000 cm^{-1}.

Differential Scanning Calorimetry (DSC): The measurements were done with TA DSC Q2000. Heating flow rate was 50^0C per minute. 5 mg of 1 wt % peptide gel in ethanol was measured.

Circular Dichroism (CD)**:** A 3.99 x 10-4 M ALP solution was prepared in different solvents and at different pH values. A Jasco J-815 CD spectrophotometer was used for CD analysis.

Scanning Electron Microscopy/Energy Dispersive X-Ray Analysis (SEM/EDX): An FEI Nova 600i Nanolab Scanning electron microscope with energy dispersing X-ray spectrometer (EDAX) was used. Samples calcined on silicon wafers were used for analysis.

Environmental Scanning Electron Microscopy (E-SEM): E-SEM experiments were performed with FEI Quanta 200 FEG. Small amounts of samples (ca. 5 µl) were cast on clean silicon wafer. The samples were dried with a critical point dryer prior to analysis.

Transmission Electron Microscopy (TEM): TEM was performed with FEI Tecnai G2 F30. Diluted samples were placed on a Lacey mesh ultrathin carbon coated copper grid. 2 % (wt/v) uranyl acetate solution was used for staining organic nanostructures. 10 µl of diluted sample solution was dropped on a grid for 1 min. Excess amount was removed by pipetting. Then, 2 % uranyl acetate solution was put on a parafilm sheet. The grid was put on the drop upside down for 5 min. After staining, the grids were dried in the fume hood at room temperature overnight. Inorganic samples were formed on steel meshes by calcination. After calcination, those meshes were put in 1 ml ethanol and vigorously sonicated for 5 min, to disperse inorganic samples in ethanol. Then, 2 µl of dispersion in ethanol were taken onto TEM grid.

Thermal Gravimetric Analysis (TGA): TA Instruments TGA Q500 was used with a heating rate of 20 ºC per min. 5 mg of peptide powder was used for TGA analysis.

Polarized Light Microscopy: An Axio Imager A1m optical microscope was used with two light polarizers. A drop of 1.33 x 10^{-2} M peptide sample was sealed between two sliders and characterized with a polarized light microscope.

Oscillatory Rheology: Rheology measurements were performed with an Anton Paar Physica RM301 Rheometer operating with a 25 mm parallel plate configuration at 25 °C. Each sample of 100 µl total volume with a final peptide concentration of

1.33 x 10^{-2} M was carefully loaded on the center of the lower plate and left untouched for 15 min before measuring. After equilibration, the upper plate was lowered to a gap distance of 0.5 mm. Storage moduli (G′) and loss moduli (G″) values were scanned in a time-dependent manner for 75 min with a constant shear strain of 0.5 % and 10 rad/s angular frequency.

Critical Point Dryer. Samples were dried at a critical point (1072 Psi, 31 ºC) with the Tousimis Autosamdri-815 B, Series C critical point dryer.

3.3. Results and Discussions

The peptide Ac-KFFAAK-Am (Figure 3.1) was designed and synthesized by Solid Phase Peptide Synthesis (SPPS) method to mimic the amyloid structure and form self-assembled peptide nanofibers by intermolecular forces. Phenylalanine residues used for π- π stacking formation and alanine for H-bonding. These forces are incorporate during the self-assembly of the peptide molecules into one-dimensional peptide nanofibers in convenient conditions. The amine groups of lysine at two ends were used for further mineralization. According to Hard-Soft Acid-Base (HSAB) Theory, we know that, as a hard base, amine group has affinity to hard acidic minerals [39].

After the synthesis of the ALP, the molecular weight of the product was determined by using Q-TOF Mass Spectrometer, and found 752 g/mol as expected (Figure 3.2). The purity of the product was investigated with Liquid Chromatography (LC) by the absorbance at 220 nm (Figure 3.3). The spectrum of the LC showed that the peptide product was pure more than 95%, which was sufficient to use without further purification.

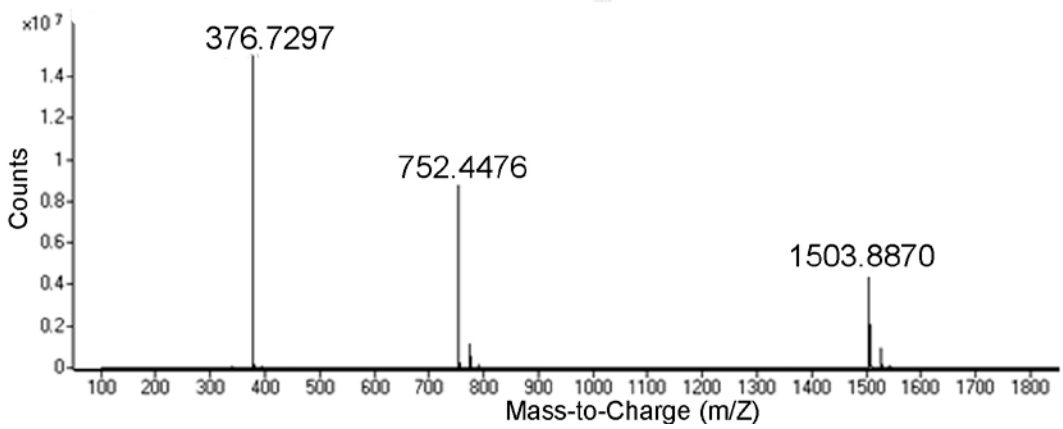

Figure 3.2. Mass spectrum of ALP molecule. MS: (m/z) calculated 751.92, [M+H] found 752.4476, [M+2H] found 376.7297. [2M+H] found 1503.8870.

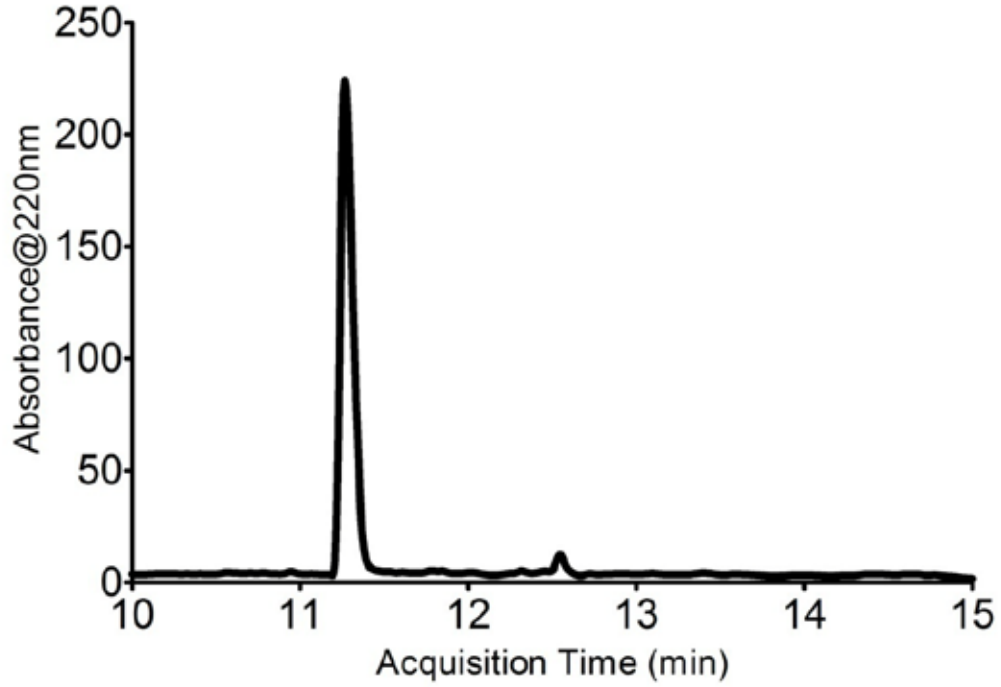

Figure 3.3. Liquid Chromatogram, absorbance at 220 nm.

The self-assembly conditions of the peptide were investigated by solubility tests in various solvents (Table 3.1). A solubility test was performed by adding 1 mg of peptide into 100 µl of solvent turned out to be minimum gelation concentration (1.33 x 10^{-2} M) for water (at pH 10) and ethanol, because peptide could completely form

gel at this concentration and the medium did not have any residual solvent residing at the top of gel. The ALP molecule readily dissolved in methanol and in water. The initial pH of the aqueous solution was 5 and 10 µl of 1 M NaOH solution was added into the aqueous solution to raise the pH for neutralization of charges on amine groups of lysines to promote self-assembly. A self-supporting gel formation was observed at pH 10. In addition, the ALP molecule in ethanol also formed a gel after sonication at room temperature (Figure 3.4). The solubility of the ALP molecule was also tested in hexane, dichloromethane, acetone, toluene, benzene, tetrahydrofuran and acetonitrile. The peptide remained as a white precipitate in these solvents even after sonication for 30 min and heating up to 50 ºC.

Table 3.1 Solubility Tests

Solvents	**Solubility**
Water	*Gel > pH 10* *Soluble < pH 5*
Ethanol	*Gel*
Methanol	*Soluble*
n-Hexane	*NOT Soluble*
Dichloromethane	*NOT Soluble*
Acetone	*NOT Soluble*
Toluene	*NOT Soluble*
Benzene	*NOT Soluble*
Tetrahydofuran	*NOT Soluble*
Acetonitrile	*NOT Soluble*

The ALP gels in ethanol were composed of a 3-D network of nanostructures as observed by SEM (Figure 3.4b and Figure 3.5). According to TEM images, the diameters of the ALP nanofibers were about 20 nm, and the lengths were in the micrometer range (Figure 3.4e). Furthermore, as clearly observed in Figure 3.4e, the peptide nanofibers had affinity to form bundles by twisting around themselves. These bundles stayed as three-dimensional scaffolds in ethanol (Figure 3.5)

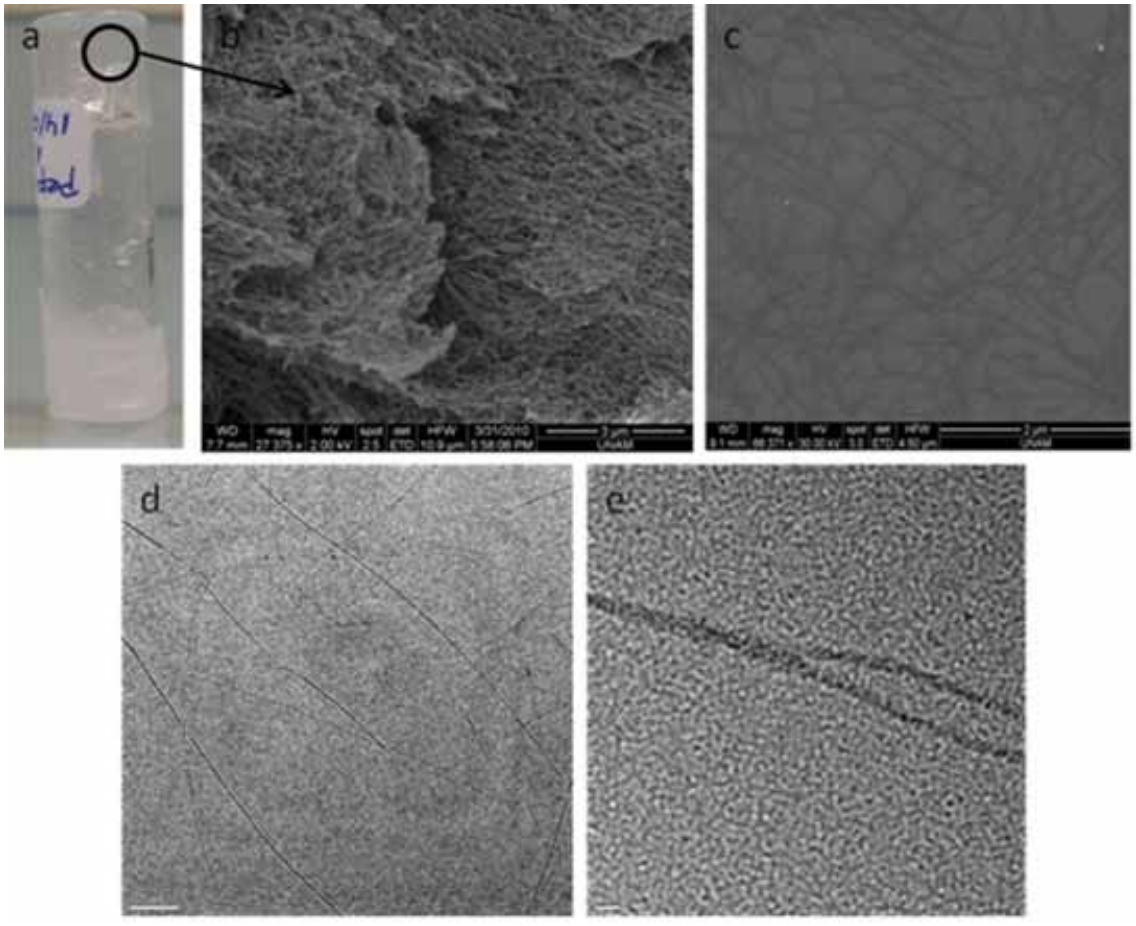

Figure 3.4. (a) Peptide gel (1 wt % peptide in ethanol); (b) SEM image of peptide fibers, 3 nm Au/Pd coated, scale bar: 3 µm(c) 2 µm (d) TEM image of peptide fibers in, scale bar: 500 nm.; (e) 20 nm.

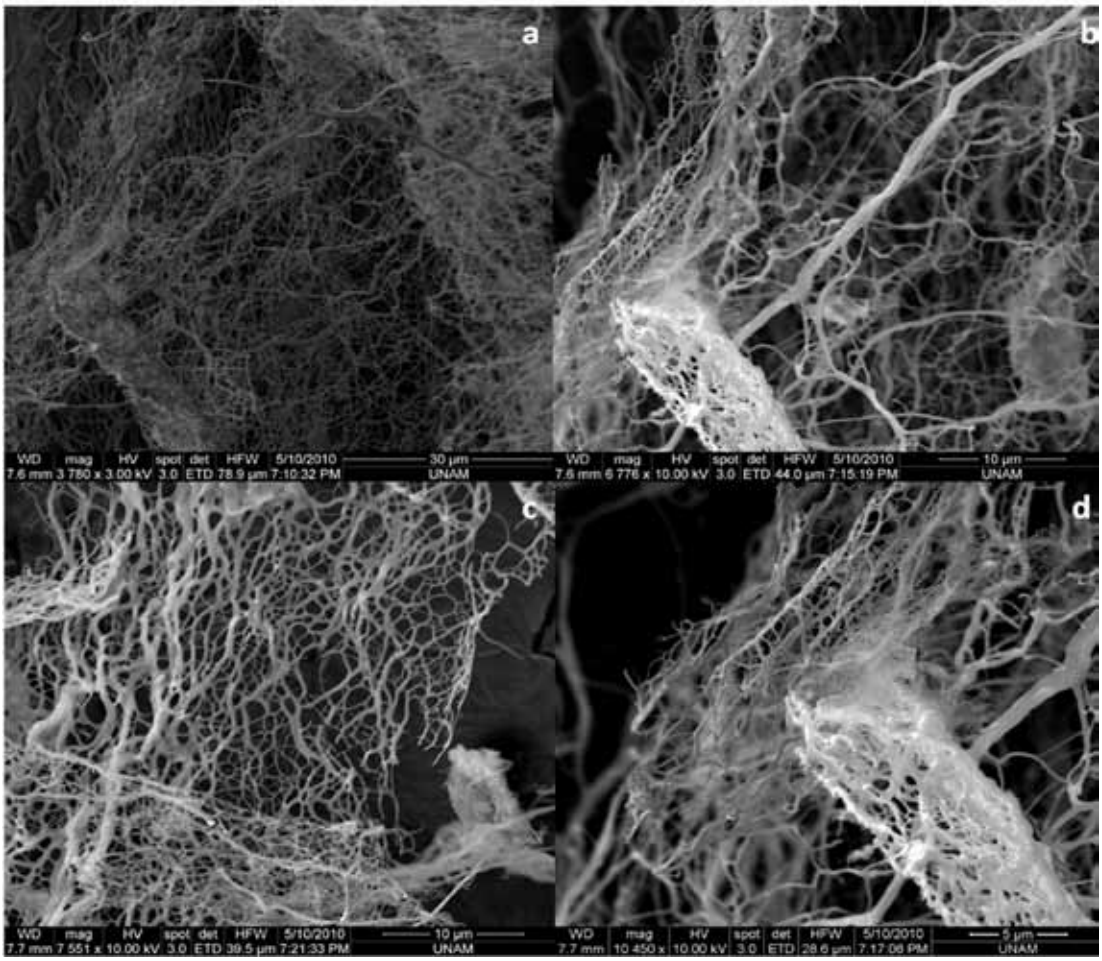

Figure 3.5. SEM images of the peptide fiber bundles in ethanol, dried with critical point dryer.

The gel formation was investigated by oscillatory rheology measurements. In this method, viscoelastic behaviour of the sample at constant frequency of oscillation is characterized by the storage modulus (G') and the loss modulus (G''). The storage modulus (G') and the loss modulus (G'') were recorded as a function of time. The values of storage modulus remained significantly higher than the loss modulus during the measurement, thus supporting visual evaluation of the mixture as a gel. A self-supporting gel formation was observed for both gels in ethanol (Figure 3.6a) and in H_2O at pH 10 (Figure 3.6b). According to the results, it was observed that the gel

strength increased with time. Two possible reasons for changes in G' and G'' with time could be gel aging and solvent evaporation. With time, gel aging can result in stiffer gels. Additionally, the concentration of peptide might increase upon solvent evaporation resulting in stiffer gels.

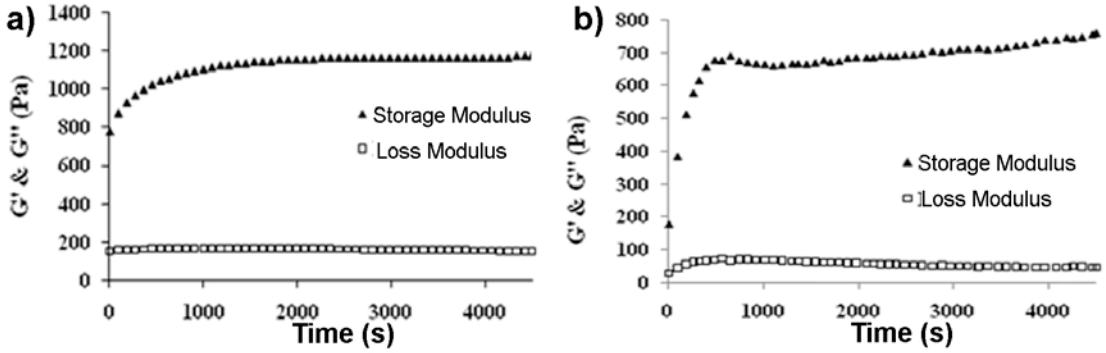

Figure 3.6. Time dependent oscillatory rheology measurements of gels (a) in ethanol and (b) in H_2O at pH 10.

Circular dichroism (CD) measurements were performed to study the effect of peptide secondary structures on nanostructure formation in varying concentrations and solvents (Figure 3.7 and Figure 3.8). This method shows the absorption bands of optically active chiral molecules. The experiments were done with peptide concentration of $3.99x10^{-4}$ M (0.03 wt %) prepared in different solvents such as methanol, ethanol and water. The ALP molecules formed gel in ethanol and in H_2O at pH 10 and were soluble in H_2O at pH 5 and methanol. The CD spectrum of the ALP sample in ethanol revealed a higher intensity than in methanol because of the higher degree of aggregation of the twisted β-sheet structure (Figure 3.7). The CD signals around 235 nm and 220 nm indicate β-sheet structure in H_2O both at pH 10 and at pH 5 (Figure 3.8). The typical β-sheet structure reveals signals at 195 nm and

216 nm [139, 140]. The red-shifted signals indicate that the predominant secondary structure forming the nanostructures is a twisted β-sheet [141]. The CD spectrum of all peptides in water, looked like PolyProline II (PP-II) structure [142-145] (Figure 3.8). This formation could be due to the alanine residues of peptide [146].

Although the peptide solution in methanol did not form any gel, the CD spectrum of this solution showed a structure between extended and β-sheet (Figure 3.7). The solution of gel in ethanol showed a hybrid structure, too. The dominant structure of gel is like PP-II, but also β-sheet formation was observed.

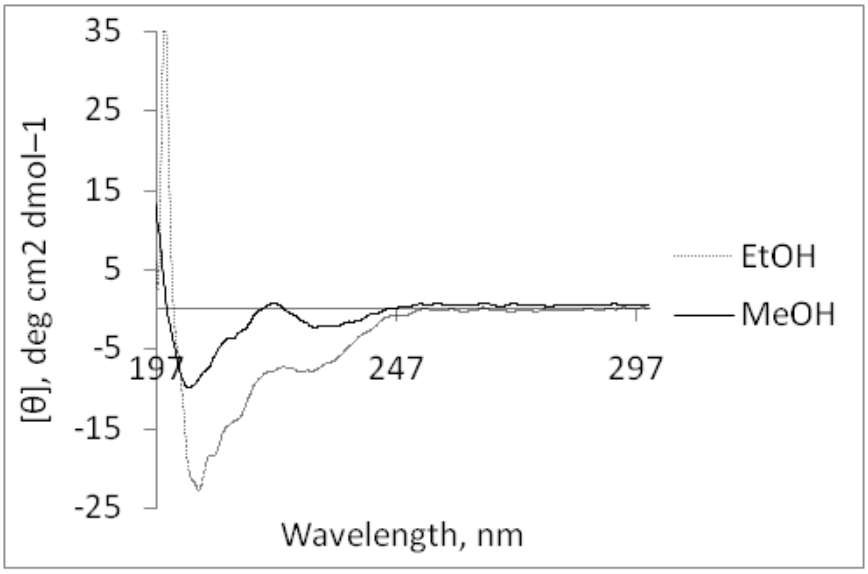

Figure 3.7. CD spectra of 0.03 wt % peptide solution in ethanol and methanol

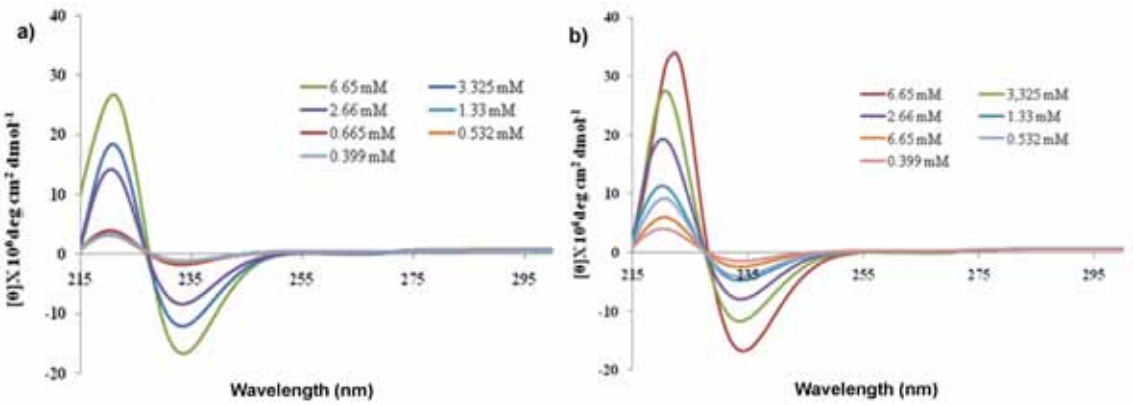

Figure 3.8. CD spectra of ALP in H_2O with different concentrations a) at pH 10 and; b) at pH 5.

When the peptide molecules individually dispersed at certain concentrations in ethanol, they self-assembled into the peptide nanofiber structure by highly specific interactions such as hydrogen bonding (through alanine residue) and π-π stacking (through phenylalanine residue). The peptide nanofibers as product have hierarchical architectures such as liquid crystalline orderings [147]. The liquid crystalline ordered structures shows birefringence between two cross polarized lenses under light microscopy. Birefringence indicates the presence of ordered micro domains in solution [148].

To characterize the orientation of peptide nanofibers in ethanol solution, 1.33×10^{-2} M peptide gel placed between two cross polarized lenses under light microscope. Figure 3.9 shows optical micrographs of the gels. A characteristic Schlieren texture [149] of lyotropic liquid crystal phase was observed in the ALP gels [147, 150]. This texture indicates the hierarchical ordering of the peptides in the medium.

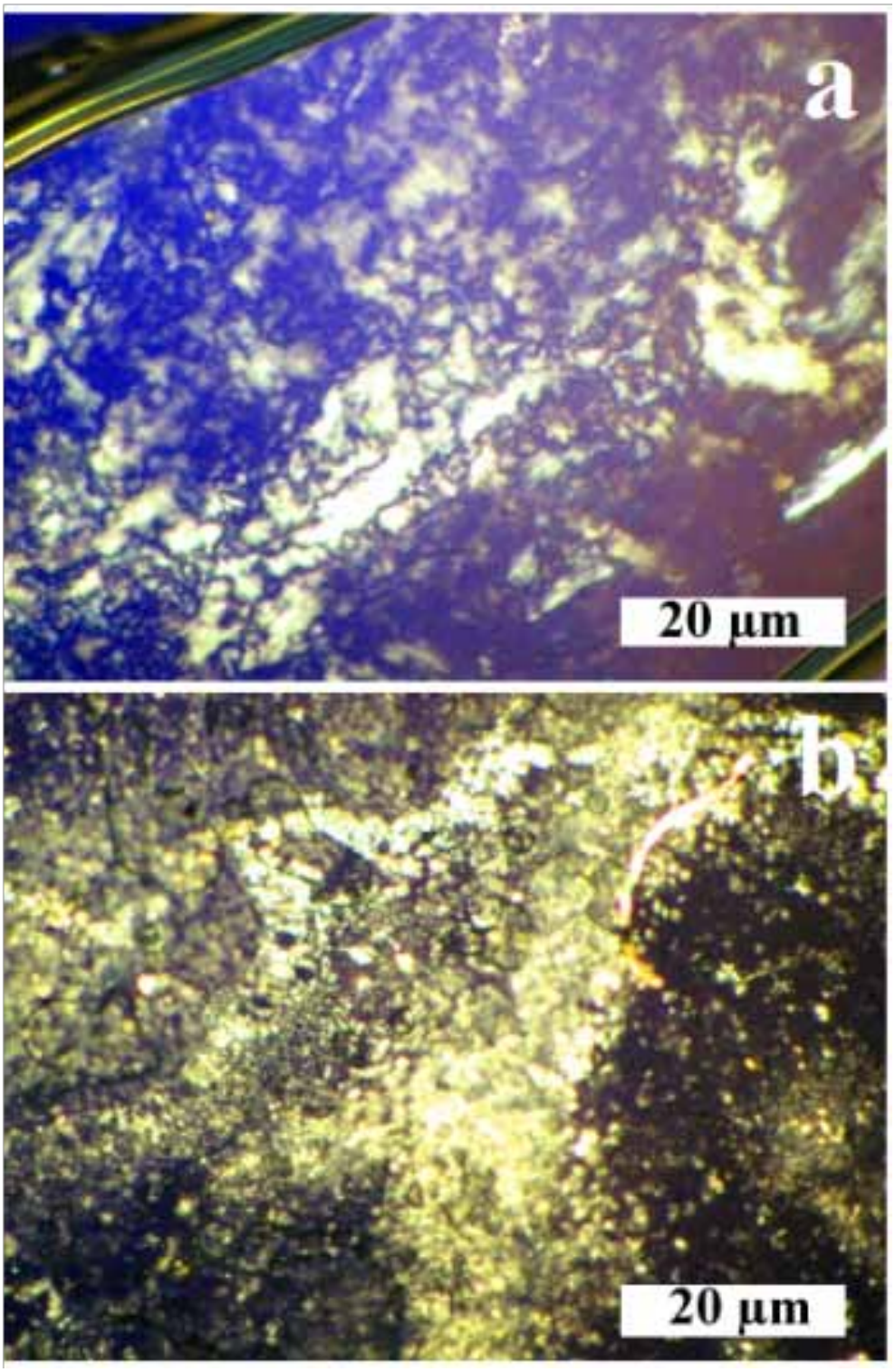

Figure 3.9. Birefringence effect of self-assembled ALP nanostructures (a) in ethanol, (b) in H_2O at pH 10, magnification 500X.

FT-IR measurements were performed with dried samples of the ALP solutions in ethanol, methanol and water at pH 5 and 10 (Figure 3.10).

The Amide-A bond, due to the N-H streching vibrations are observable around 3225-3280 cm^{-1}. This vibration does not depend on backbone comfomation, but it is very sensitivr to the strength of H-bondings [151]. Amide I (1600-1700 cm^{-1}) region is very important to determine the backbone conformation and H-bonding pattern. Independent from the amino acid sequence of the protein, the exact position of the band shows the conformation. In this region, the peaks; first around 1615-1637 cm-1 and second around 1685-1696 cm^{-1} show β-strand [152]. The peak near 1680 cm^{-1} clearly was assigned to β-turns in the structure [151]. Amide II bond (1510- 1580 cm^{-1}) derives mainly from in plane N-H bending.

In prepared samples; the Amide-A (associated with the -NH stretching frequency) band was observable around 3296 cm^{-1} in methanol and in H_2O at pH 5, where the peptide was completely dissolved, attributed to the -NH group of the peptides involved in hydrogen bonding [153, 154]. The Amide-A band was at around 3325 cm^{-1} in ethanol and in H_2O at pH 10, where the peptide molecules formed a gel due to self-assembly. Also, Amide-I (indicating the existence of C=O stretching vibrations) generated two peaks around 1687 and 1633 cm^{-1} [155, 156]. The splitting of the peak can be due to the interactions between repeating peptide units [153]. The Amide-I peak of the peptide in ethanol and in H_2O at pH 10 was found around 1645-1706 cm^{-1}.

The FTIR data showed us the Amide-I region which occurs in the region 1600-1700 cm^{-1}(Figure 3.10). Hydrogen bonding and the coupling between transition

dipoles are among the most important factors to form amide bands. Amide I bands in the spectral range 1620–1640 cm^{-1} and 1648-1660 cm^{-1} with peptide can be attributed to β-sheet and α-helix structures, respectively. The peak around 3200-3300 cm^{-1} occurs due to the N-H stretching. Also, around 1200-1300 cm^{-1}, the amide III region can be seen.

In ethanol solution, although the peaks around 1695 cm^{-1} were ascribed to an antiparallel β-sheet structure [151], the higher frequencies could also be due to turns (Figure 3.10). The CD (Figure 3.7) and FT-IR spectra of the ALP samples were indicative of β-twist and β-turn structures of the self-assembling ALP molecules.

Table 3.2. FT-IR peaks of some basic peptide secondary structures and regions

Structure	Wavenumber (cm-1)
Antiparallel β-sheet	1690
β- turns	1675-1685
β-sheet	1615-1637
α-helix	1655
Random coil	1645
Amide-A	3225-3280
Amide-B	3088
Amide-I	1600-1700
Amide-II	1510-1580

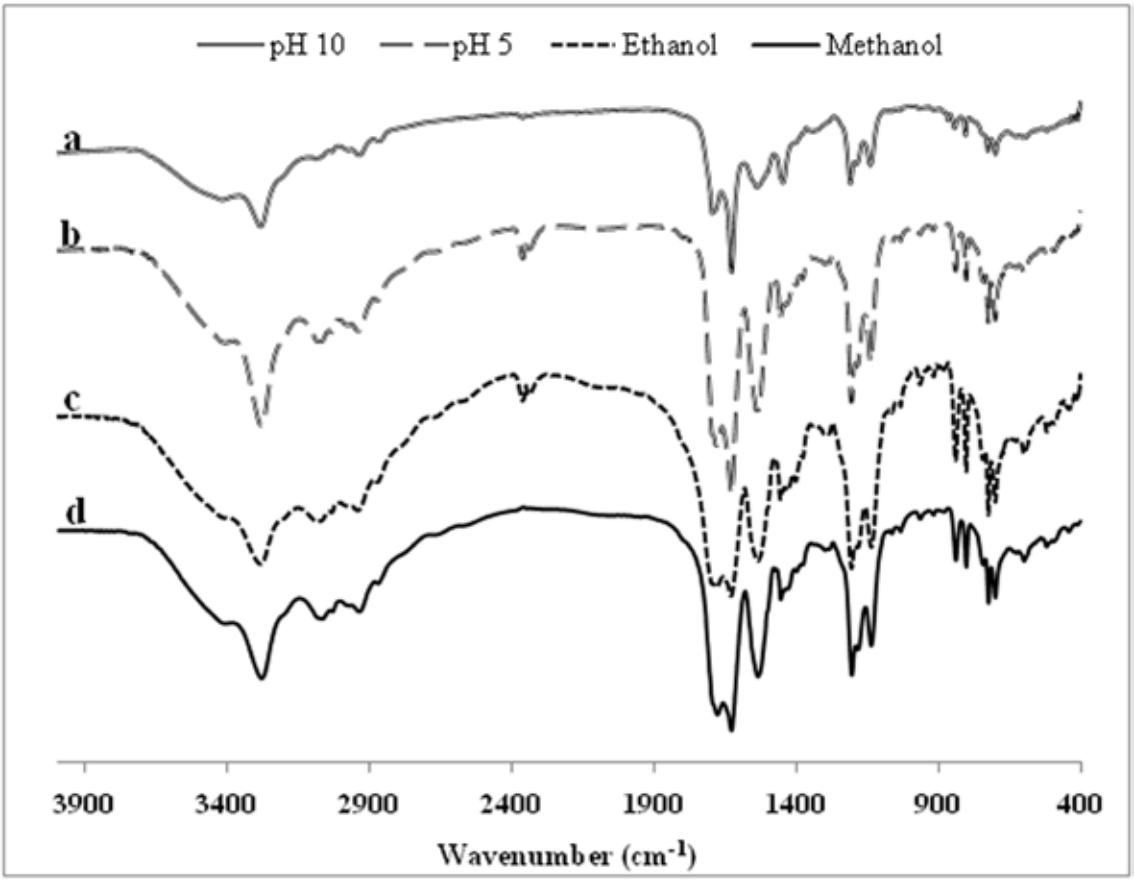

Figure 3.10. FT-IR spectra of the ALP samples; (a) in H_2O at pH 10, (b) in H_2O at pH 5, (c) in ethanol, and (d) in methanol.

We investigated UV absorption properties of the peptide molecule in ethanol, methanol and in H_2O at pH 5 and 10. We observed absorption around 260 nm in all solvents, which is the characteristic absorption band of phenylalanine residues in the peptide (Figure 3.11) [157-159]. The fluorescence emission properties of the peptide molecules were also investigated. Fluorescence emission peaks around 283 and 304 nm were observed upon excitation of adjacent phenylalanine residues at 260 nm, indicating excimer formation due to π-stacking (Figure 3.12) [158-160]. Excitation of phenylalanine rings around this absorption wavelength causes a fluorescence around 300-350 nm which is due to the π-π* transition [159]. The UV-Vis absorption

and fluorescence spectra of the peptide solutions in different solvents were quite similar, indicating somewhat similar degrees of self-assembly in all of the solvents (Figure 3.11 and Figure 3.12).

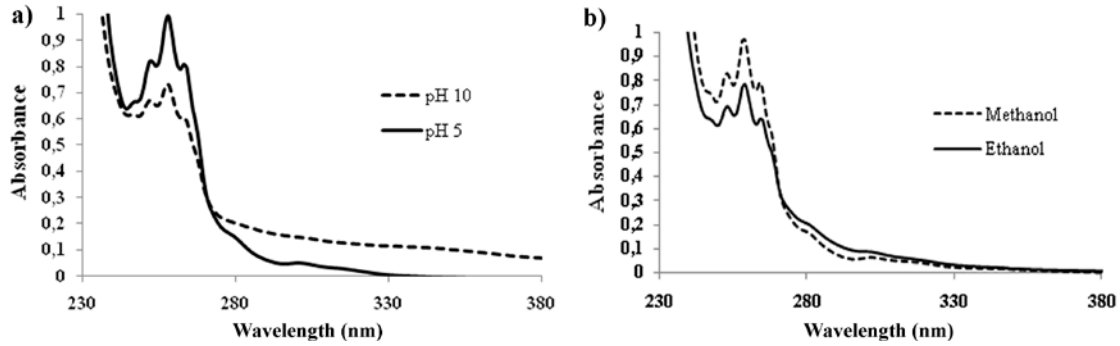

Figure 3.11. UV-Vis absorption spectra of the ALP; (a) in H2O at pH 5 and pH 10, (b) in ethanol and in methanol.

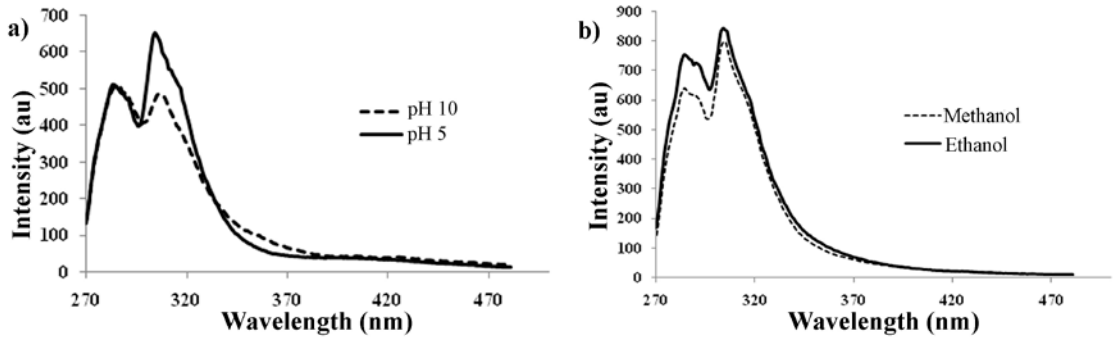

Figure 3.12. Fluorescence emission spectra of the ALP; (a) in H_2O at pH 5 and 10, (b) in ethanol and methanol.

The Thermal Gravimetric Analysis (TGA) was performed to determine the evaporation temperature of the peptide molecule. As seen at Figure 3.13, the powder of peptide molecule was heated up to 750ºC. The sample started to evaporate after 200ºC and approximately 60% of the weight was lost at 350ºC. At around 550ºC, the peptide powder burnt out completely.

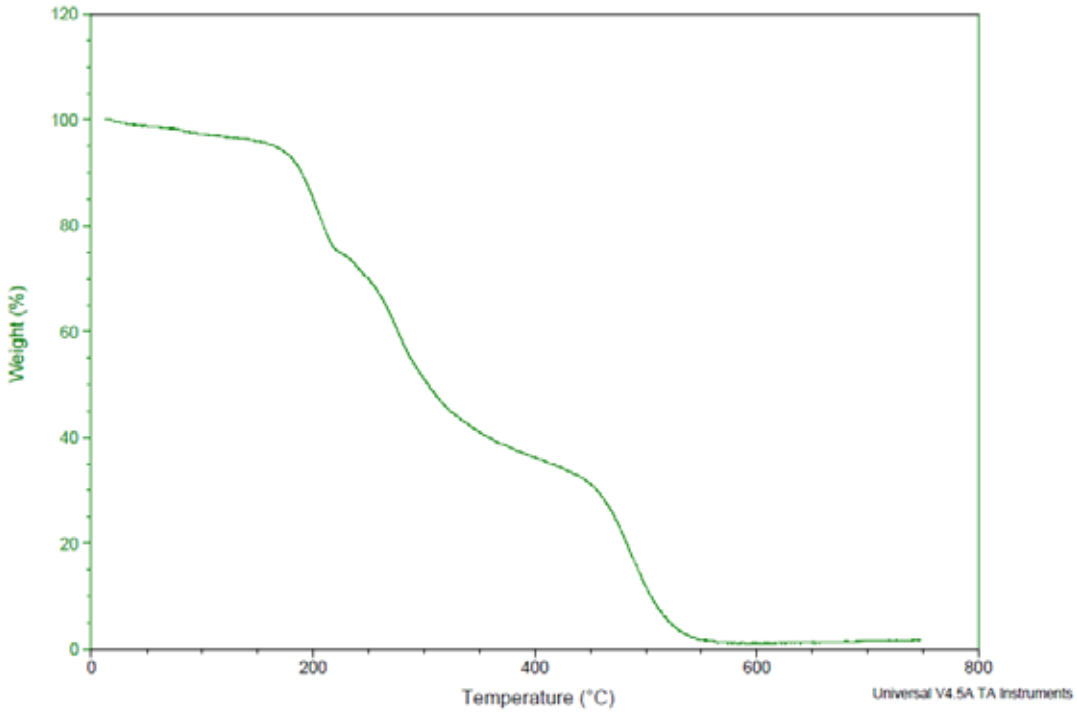

Figure 3.13. Thermal Gravimetric Analysis of peptide powder.

This chapter demonstrates the synthesis of a peptide molecule having ability to self-assemble into one-dimensional fibrillar form with special functional groups and having affinity to bind particular inorganic ions was designed and synthesized. The physical and chemical properties of the designed peptide and self-assembled one-dimensional nanofibers were characterized.

Chapter 4

Template-Directed Synthesis and Characterization of Silica Nanotubes and Their Application as Explosive Detection

This work is partially described in the following publications:

Acar, H., R. Garifullin, and M.O. Guler, "Self-Assembled Template-Directed Synthesis of One-Dimensional Silica and Titania Nanostructures", *Langmuir*, 27(3),p.,1079-1084, 2011.

Yildirim, A., et al., "Template-directed synthesis of silica nanotubes for explosive detection", *ACS applied materials & interfaces*, 3(10),p.,4159-64, 2011.

4. Template-Directed Synthesis and Characterization of Silica Nanotubes and Their Application as Explosive Detection

4.1. Introduction

Inorganic nanotubes are attracting a great deal of interest due to their potential applications in sensing, catalysis and biotechnology [161, 162]. Silica is one of the most studied materials to produce nanotubes because of its inert nature, hydrophilicity, and ease of surface functionalization [163]. Silica nanotubes are typically prepared within the pores of anodic alumina membranes by chemical vapor deposition or sol-gel methods [164-166]. Wall thickness and pore size of the tubes can be controlled by changing the reaction conditions. However, the size of the tubes is restricted with the pore sizes of the membranes and it is not possible to produce tubes thinner than 50 nm. Alternatively, silica nanotubes were prepared around the organic or inorganic templates such as carbon nanotubes [167, 168], ZnO [169], and PbSe [170] nanowires, gold nanorods [171], surfactants [172, 173], peptides [174] and gel systems [175, 176]. Depending on the template used, variety of nanotubes with different sizes, pore diameters and wall thicknesses were synthesized. However, large scale production of thin (< 50 nm) and long (< 1 μm) silica nanotubes is still rare [177]. These high aspect ratio silica nanotubes would be indispensible in especially, catalysis and sensing applications because of their high surface area and ability to form highly porous networks.

With this insight, we prepared very thin and long silica nanotubes by using amyloid-like peptide [178] nanofibers as template [179]. The nanofibers not only act as a template but also they catalyze the silica formation because of the amine groups

on their surfaces. The self-assembly of peptides was achieved by a specially designed short peptide sequence, Ac-KFFAAK-Am, that forms sheet-like hydrogen bonded structures. Functional groups (-NH_2) on side chains of lysine residues served as the nucleation centers for successive deposition of inorganic precursor materials. Transformation of deposited material to target inorganic material and removal of organic template were achieved by the calcination process at an appropriate temperature. The simple preparation process of target inorganic materials makes the ALP-templated process very lucrative not only for laboratory scale preparation, but also for industrial large scale applications.

A wide variety of detection methods and materials are studied in very chalenging and important area of detection explosives. Fluorescent quenching based sensing methods are very promising for rapid and sensitive detection of explosive vapors [180]. The mechanism of fluorescence quenching sensing is based on photo-induced electron transfer from excited fluorescent molecules to explosives [181]. Previously, conjugated polymers [180-184], fluorescent organic nanofibrils [185, 186], dye doped porous silica films [187-190] and surface decorated nanoparticles [191] were used for fluorescence quenching based sensing of explosives. The performance of fluorescent porphyrin dyes strongly depends on the formed mesostructured substrate material and its pore size [187] In this work, we utilized the Meso-tetrakis-p-carboxy-phenylporphyrin ($TCPPH_2$) doped silica nanotubes, synthesized through peptide nanostructure templating, for explosive sensing. The fluorescent silica nanotubes (FSNT) can be dispersed in ethanol solution or in water and can be directly casted on the surfaces to form a porous network. The porous fluorescent silica nanotube surface provides sensitive detection of nitro-aromatic explosives;

2,4,6-trinitrotoluene (TNT) and 2,4-dinitrotoluene (DNT) [187-189]. When the sensor surface exposed to TNT or DNT vapor its' fluorescence quenched significantly within seconds because of the high surface area of the FSNT surface. In order to demonstrate the effect of surface area on sensor performance, we prepared $TCPPH_2$ dye doped nonporous silica thin film (film thickness is 170 nm) and silica nanoparticle (particle sizes are around 60 nm) surfaces. Both thin film and silica nanoparticle sensors demonstrated slower fluorescence quenching than fluorescent silica nanotube sensor against TNT because of their less porous (lower surface area) structure. Furthermore, the selectivity of the prepared fluorescent silica nanotube sensor is tested with vapors of similar aromatic molecules which are; nitrobenzene (NB), toluene, xylene, benzoic acid (BA) and dihydroxybenzoic acid (DBA). The results indicated that FSNT sensor highly selective and sensitive to TNT and DNT.

4.2. Experimental

Peptide Synthesis and characterizations were done as described at Chapter 3.

Calcination process: The ALP nanostructures were mineralized by tetraethyl orthosilicate (TEOS). Silica samples were incubated for 1 week at room temperature. 100 µl of each sample was casted on a steel mesh and dried with a critical point drier. The mineralized samples were placed in an oven. The oven started to heat up starting at room temperature to 350 °C for 10 min with a heating rate of 7 °C/min.

Critical Point Dryer: Samples were dried at a critical point (1072 Psi, 31 ºC) with the Tousimis Autosamdri-815 B, Series C critical point dryer.

Scanning Electron Microscopy (SEM)/Energy Dispersive X-Ray Analysis (SEM/EDX): FEI Nova 600i Nanolab scanning electron microscope with EDAX

energy dispersing spectrometer was used. Samples calcinated or acidic methanol washed on silicon wafers were used for analysis.

Transmission Electron Microscopy and Scanning Transmission Electron Microscopy: TEM and STEM were performed with FEI Tecnai G2 F30. Diluted samples were placed on a Lacey mesh ultrathin carbon coated copper grid. Inorganic samples were formed on steel meshes by calcination. After calcination, those meshes were put in 1 ml ethanol and vigorously sonicated for 5 min, to disperse inorganic samples in the ethanol. Then 2 µl of dispersion in ethanol were taken onto TEM grid.

Atomic Force Microscopy. AFM images of the FSNT sensor surface were recorded using model MFP-30 from Asylum Research operated in tapping mode at a frequency of 246 kHz. AFM images were taken at 512×512 pixels resolution. Image was taken with spring constant 40 N/m and the set point and scanning speed were 0.7–1.0 V and 1.0–1.5 Hz, respectively.

UV-Vis Absorption and Fluorescence Spectroscopies. UV-Vis absorption spectra were recorded by Varian Carry100 spectrophotometer. Fluorescence spectra were recorded by Varian Eclipse spectrophotometer.

Self-Assembled Template Formation, Silica Mineralization and Silica Nanotube Preparation: Silica mineralization was achieved by using tetraethyl orthosilicate (TEOS) as a precursor. TEOS (20 µL) was added on to the gel (1 mL) and the sample was aged for 1 week. Then, samples were washed with excess amount of acidic methanol (10 µL of 1 M HCl per 1 mL methanol). 5 mL acidic methanol was added into the silica coated peptide fiber gels and vortexed for 3 min. Later, the solutions were centrifuged at 10,000 rpm for 5 min. Supernatant was taken off and

fresh acidic methanol was added. This procedure was repeated for 5 times. At the last repeat after vortex, the solution was not centrifuged and sample for TEM imaging was taken from this solution.

Fluorescent Silica Nanotube (FSNT) Sensor Surface Preparation: After template removal, SNTs were dispersed in 1 mL of ethanol and 20 µg $TCPPH_2$ was added in 100 µL of ethanol. The solution was incubated 1 day at room temperature. Then, the solution was diluted with ethanol (1:50). Finally, 100 µL portions of the diluted solution was coated on glass substrates by drop casting and dried in oven at 60 °C. The glass substrates were sonicated in ethanol before coating.

Nonporous Silica Thin Film Preparation: For control experiment, a nonporous silica thin film was prepared according to a previous report [187]. In a standard procedure, 2.25 mL of TEOS, 2.05 mL of ethanol, 0.1 mg $TCPPH_2$ in 0.2 mL of ethanol, 0.2 mL of water, and 5 µL HCl (0.1 M) were mixed and stirred at 60 °C for 90 min, then 0.4 mL HCl (0.1 M) and 0.35 mL water were added and the solution was further stirred for 15 min at room temperature. Finally, the sol was aged at 50 °C for 15 min. 3 mL of aged sol diluted with 3 mL ethanol and coated on glass substrates with spin-coating at 2000 rpm.

Silica Nanoparticle Sensor Surface Preparation: Silica nanoparticles with diameters around 60 nm were prepared according to Stöber method [192]. Briefly, 0.25 ml of water, 10 ml of ethanol and 2.56 ml ammonia solution (26%) were mixed with 1.5 ml TEOS in 40 ml ethanol. The resulting solution was stirred at 25 °C for 24 h. The particles were collected by centrifugation (9000 rpm, 30 min), washed several times with water and ethanol and dried in a vacuum oven. 20 mg of particles

dispersed in10 ml ethanol and 0.2 mg $TCPPH_2$ was added in 0.2 ml ethanol and stirred overnight. The particles were collected by centrifugation (9000 rpm, 30 min) and dispersed in 10 mL of ethanol. 0.1 ml of the dye doped silica nanoparticle dispersion was diluted with 0.9 ml of ethanol and 75 µL portions of the dispersion was drop casted on clean glass substrates. The substrates dried in oven at 40 °C.

Fluorescence Quenching Experiments: The fluorescence quenching experiments were performed similar to the previous reports [180, 182, 183]. Approximately 0.1 g of analytes were placed into a 15 mL vial and covered with cotton to prevent direct contact of the analyte molecules with the films and to maintain constant analyte pressure. For nitrobenzene, toluene and xylene which are liquid at RT, a small droplet placed into a vial and covered with cotton. The FSNT surfaces were exposed to the analyte vapors for a specified period of time and then fluorescence measurements were carried out immediately. Measurements were performed at room temperature and it is assumed that the vial atmosphere was saturated with analyte vapor [175].

4.3. Results and Discussions

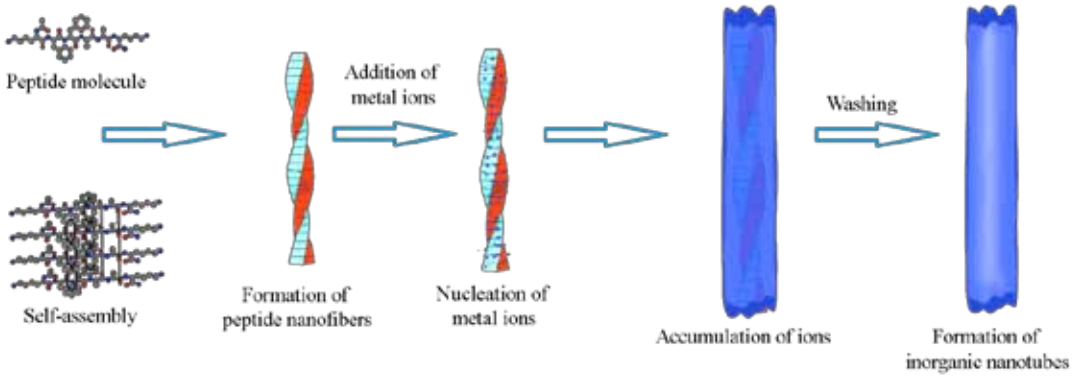

Scheme 4.1. The formation of peptide nanofibers, nucleation and accumulation of inorganic materials around it and obtaining of inorganic nanotube by calcination of the organic peptide.

The designed, synthesized and characterized peptide molecules self-assembled in ethanol, through supramolecular interactions such as hydrogen-bonding and π-π stacking as explained in Chapter 3. As shown in Scheme 4.1, the obtained peptides nanofibers with functional amine groups at periphery of them. The amine groups were used as nucleation sides of inorganic ions of tetraethyl orthosilicate (TEOS). After the accumulation of silica around the peptide, the organic peptide part of the one-dimensional nanostructures were removed by washing (since peptides are soluble in water and methanol as described at Chapter 3) or calcination at appropriate temperatures.

Silica mineralization were performed by using tetraethyl orthosilicate (TEOS) as a precursor. In general, silica nucleation from TEOS occurs in the presence of catalysts [193, 194]. The amine groups of the ALP molecule acted as a base and started nucleation of the silica on the nanostructures. Therefore, no other catalyst was needed for silica formation. After formation of peptide nanofibers in ethanol, 2 eq.M.

of TEOS was mixed along with the peptide nanostructures. The TEOS containing peptide nanofiber gel was aged for one week. Later, the samples were dried at room temperature and placed in an oven for calcination. The sample was calcined at 350 ^{o}C for 10 min. The obtained samples were contains bulk silica structures due to sintering.

During formation of the inorganic nanostructures, the nucleation process is an important mechanism in shape and size control. We observed that inorganic materials grow on the organic template with the help of the chemically active groups. When the concentration of the template was high enough, the individual organic nanostructures were found to interact and bundle due to the Ostwald ripening mechanism. Otwald ripening occurs spontaneously because larger particles are more energetically favored than smaller ones [195-197]. During the calcination process, inorganic nanostructures were found to fuse because of the high temperature of the medium. Uncontrolled growth and fusion of nanostructures could decrease the surface area of the material during calcination [198, 199]. To overcome the fusing of the nanostructures, 3-D networks were protected by critical point drying. The nanostructures were isolated from each other before calcination. By this process, the space among nanofibers was preserved. A higher yield of individual nanostructures was obtained by decreasing the time of calcination and preserving the space among nanofibers.

The silica nanostructures after critical point dryer and calcination were observed by TEM (Figure 4.1) and SEM (Figure 4.2). The EDX spectra of the calcined silica nanostructures did not reveal carbon and nitrogen signals.

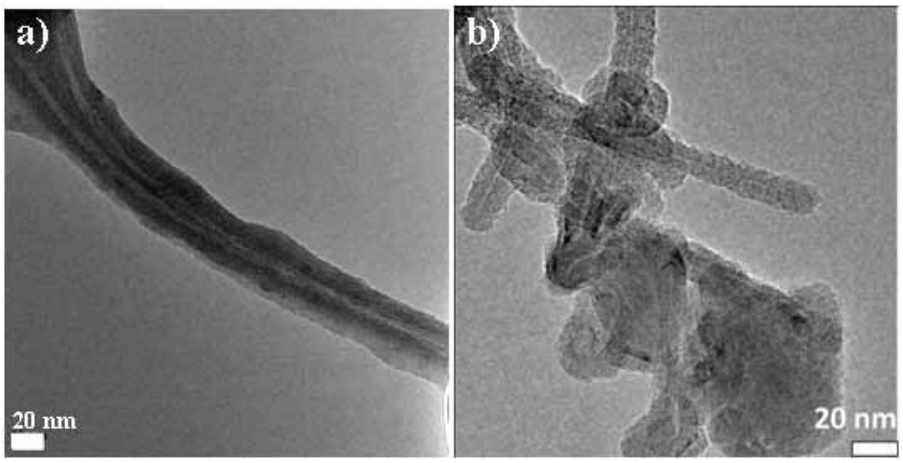

Figure 4.1. TEM images of the silica nanotubes after calcination. Both scale bars: 20 nm.

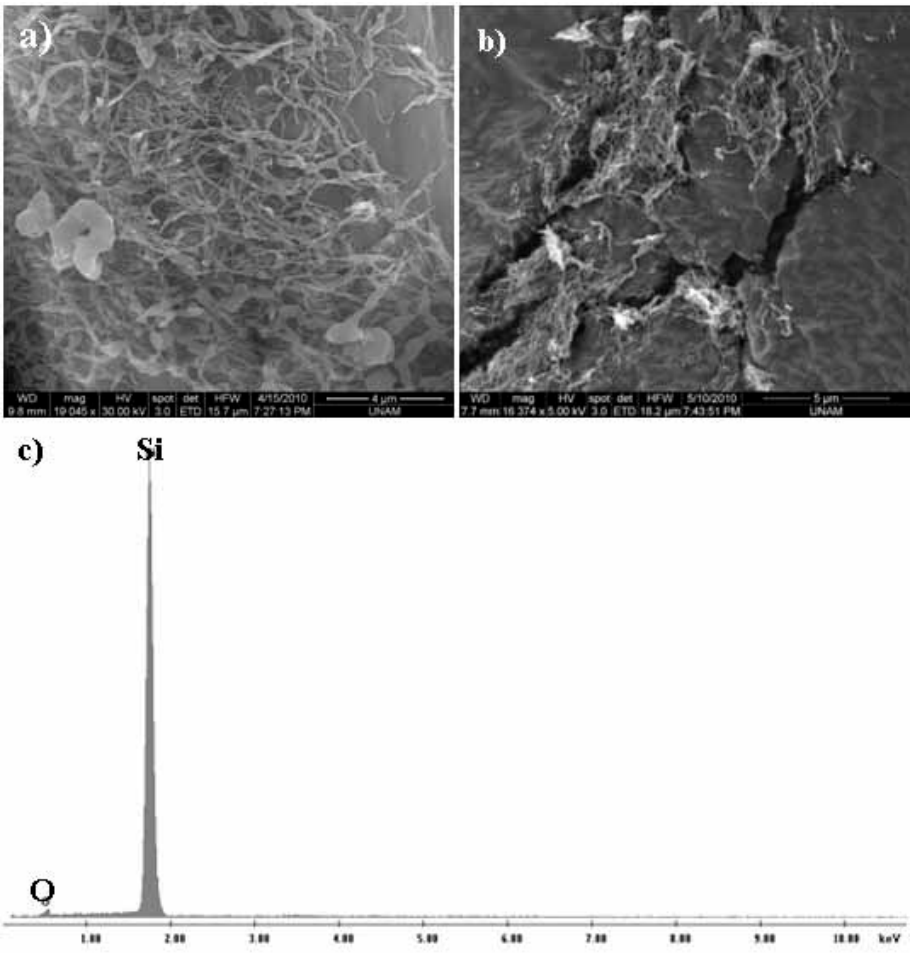

Figure 4.2. SEM images of critical point dried silica nanostructures after calcination at 350 ºC scale bars; a) 4 µm, b) 5 µm and c) EDX spectrum of the samples.

The exactly same amount of TEOS precursor was also processed without the peptide nanofibers as templates to observe the effect of template-directed synthesis. According to the SEM images, no defined structures were observed from these template-free silica particles (Figure 4.3).

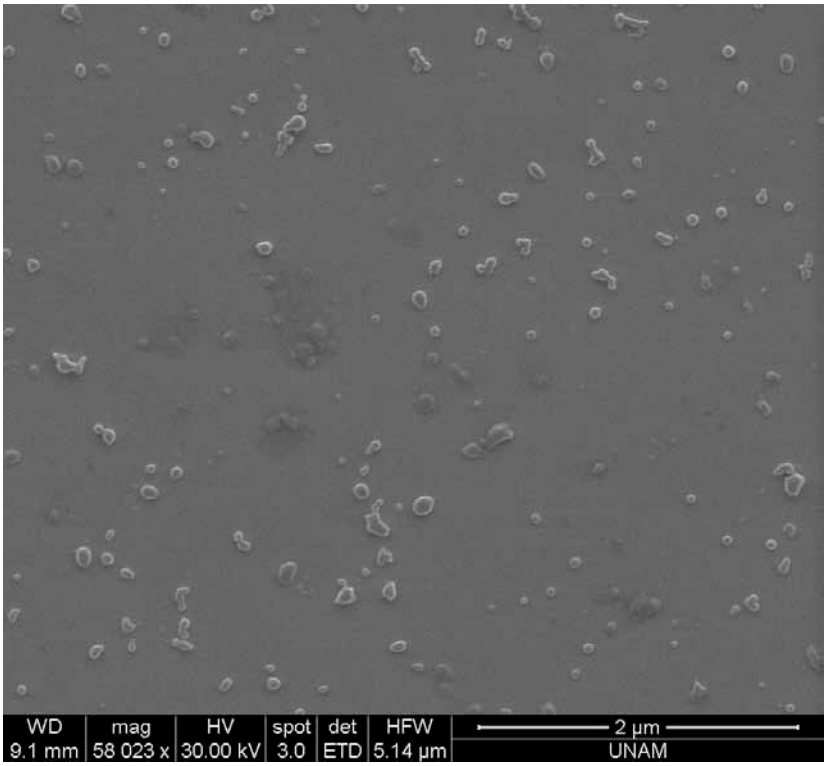

Figure 4.3. Silica structures synthesized without peptide nanofibers as templates.

The organic peptide nanofibers are soluble in acidic water and methanol as described at Chapter 3. Since the adsorption of flurescent dye occurs physically at liquid phase, calcination procedure was not necessary to performe. The silica coated peptide nanofibers were washed with acidic methanol for 5 times. The samples were vortexed and centrifuged at 10,000 rpm for 5 min, after addition of methanol. The

remained sample was dispersed in acidic methanol. The Meso-tetrakis-p-carboxy-phenylporphyrin ($TCPPH_2$) dye was added and the dispersion was aged for 1 day for physisorption of the dye to the silica network. The STEM images of samples were also taken and formation of one-dimensional individual silica nanotubes were observed. Nitrogen signal was not observed in the EDX spectrum of the region seen on TEM image (Figure 4.4), which is an evidence of the removal of the peptide molecules. The carbon and copper signals were caused by TEM grid.

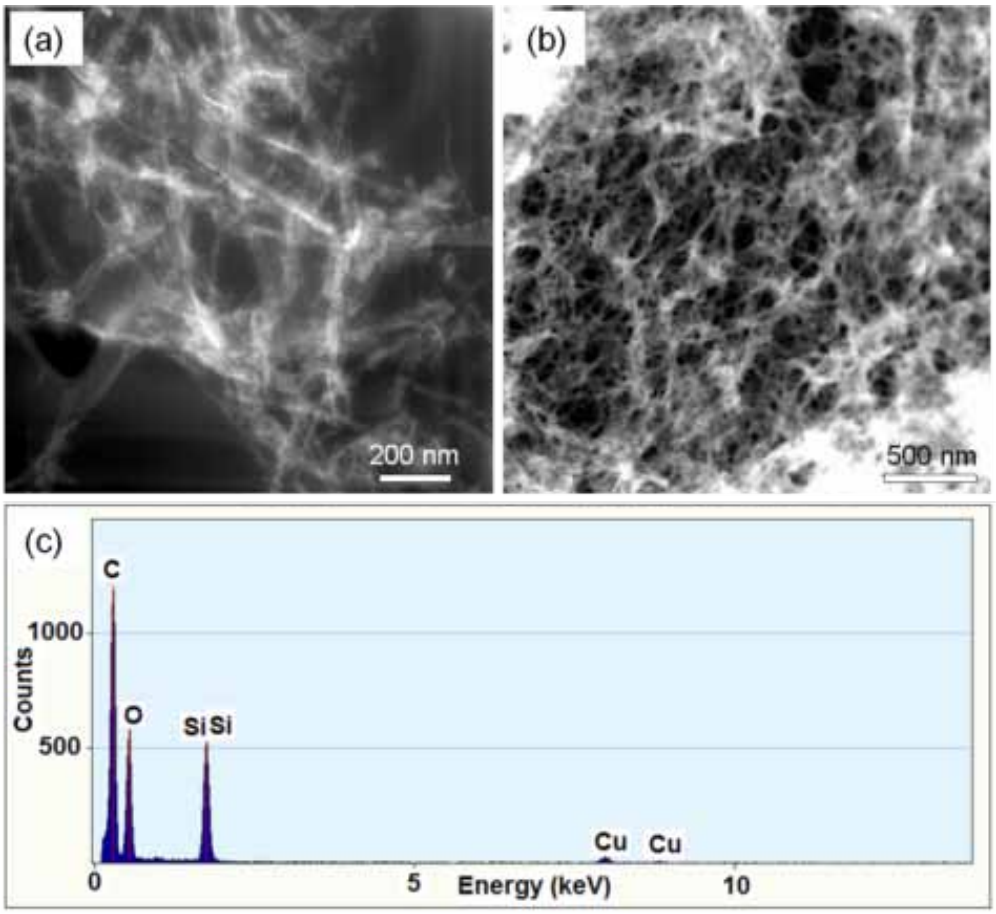

Figure 4.4. a)-b) STEM images and c) EDX spectrum of the silica nanotubes after template removal by washing.

After the observation of formation of silica nanotubes with peptide nanofiber templates, Meso-tetrakis-p-carboxy-phenylporphyrin ($TCPPH_2$) dye was used for doping silica nanotubes for explosive sensing. The fluorescent silica nanotubes were be dispersed in ethanol solution or in water and directly casted on the surfaces to form a porous network. Sensor surfaces were prepared by drop casting of fluorescent silica nanotubes dispersions on glass substrates (Scheme 4.2).

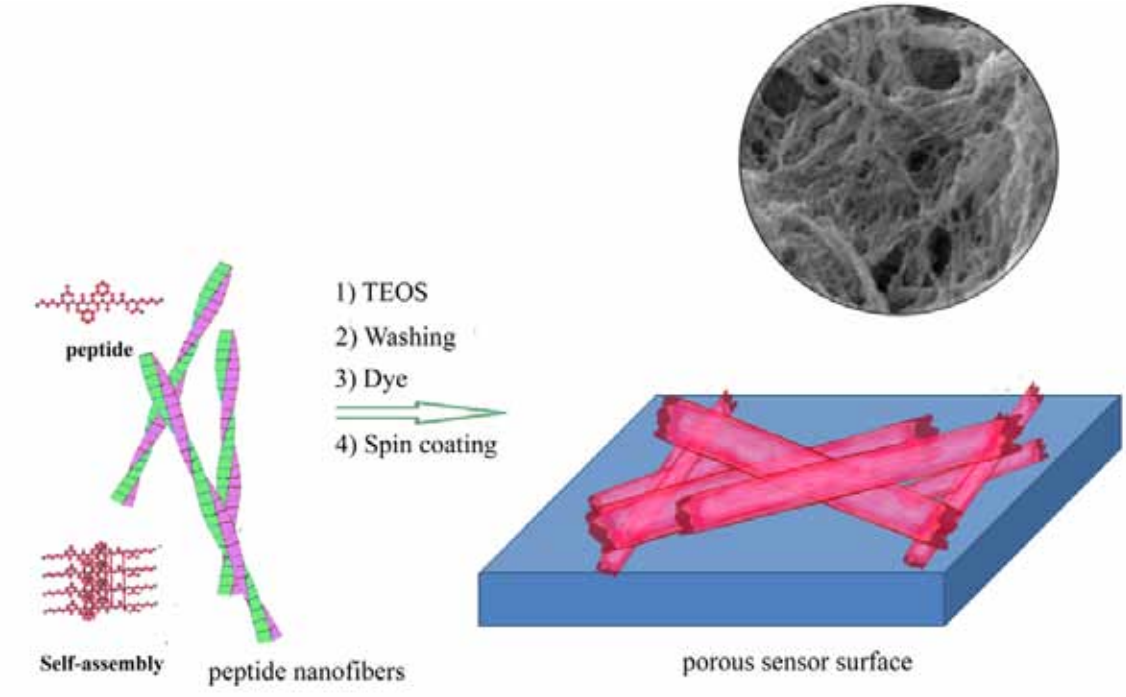

Scheme 4.2. The peptide nanofibers formed, the nucleation and accumulation of inorganic materials around the peptide nanofibers completed, the inorganic nanotubes were obtained by washing-off the organic part. After addition of the fluorescent sensitizer dye, the silica nanotubes spin coated on a surface for sensor development.

The fluorescent silica nanotube (FSNT) sensor surface was characterized with atomic force microscopy (AFM). The AFM image indicates very thin nanostructures

(individual nanotubes) and as well as thicker structures which were formed by aggregation of nanotubes (bundles) (Figure 4.5).

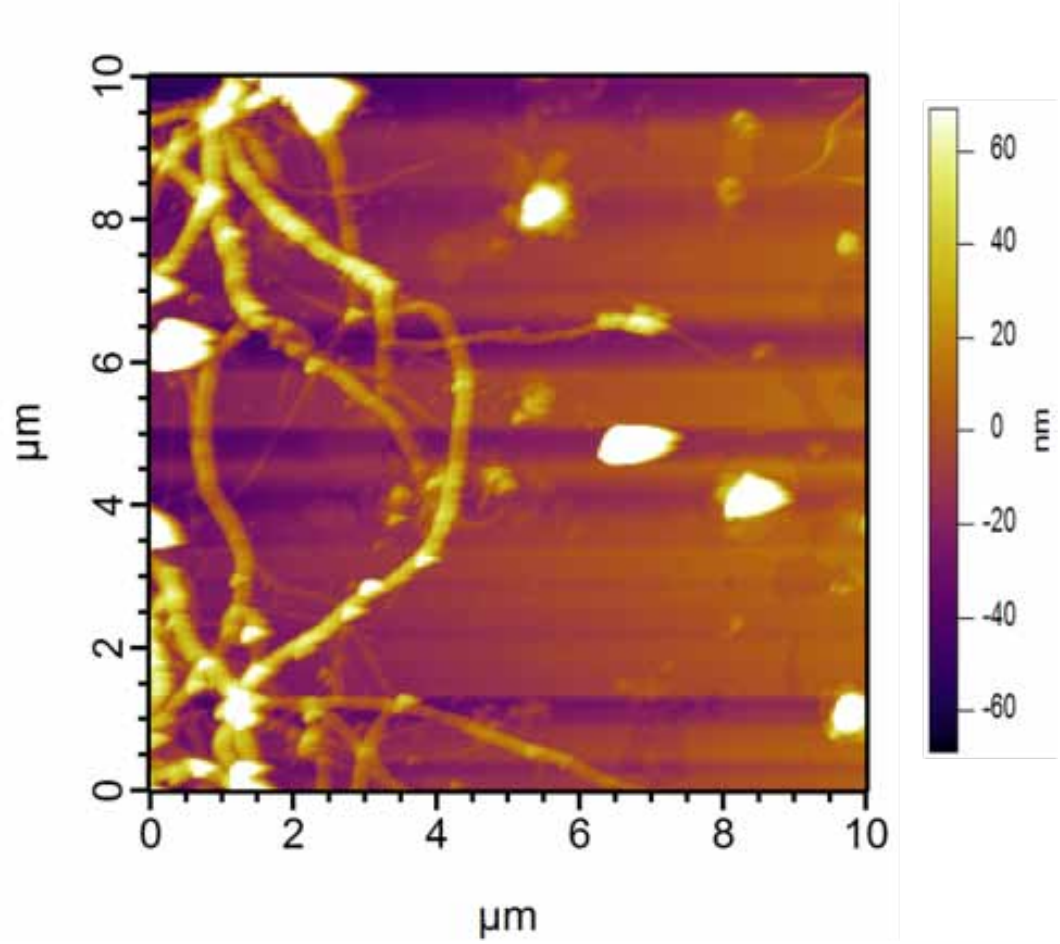

Figure 4.5. AFM image of the fluorescent silica nanotube sensor surface.

Randomly oriented fluorescent silica nanotubes formed a highly porous network. The absorption and emission spectra of fluorescent silica nanotubes on a glass surface were showed in Figure 4.6. The identical emission spectra of $TCPPH_2$ in ethanol and in SNTs confirmed incorporation of dye molecules in the silica network.

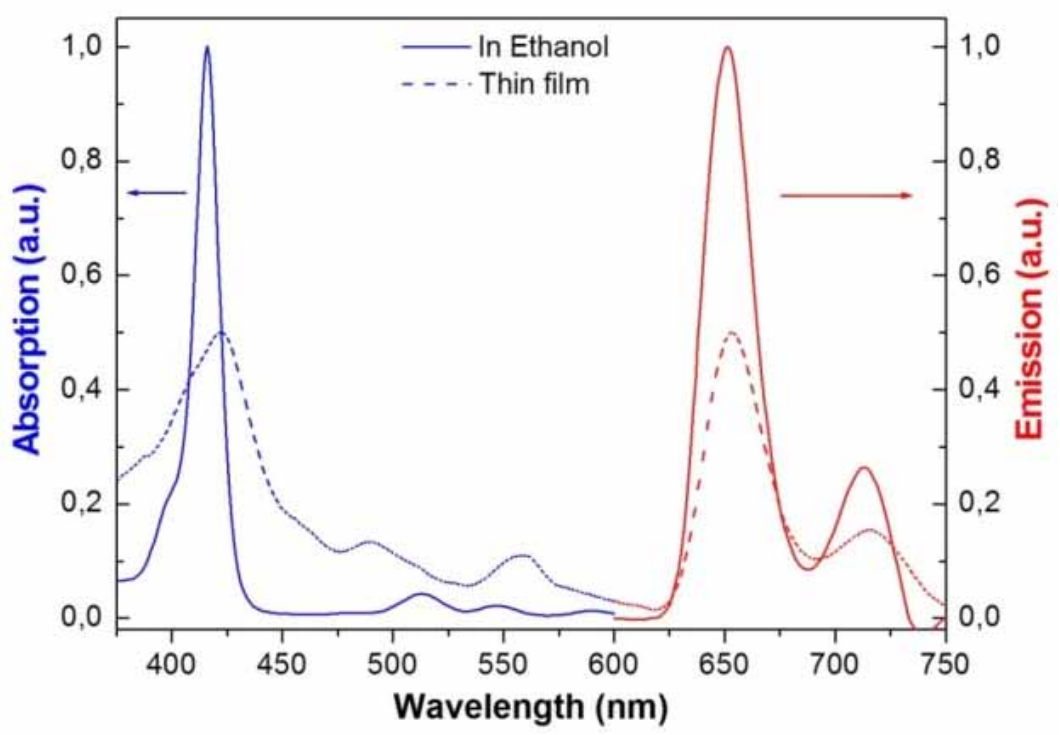

Figure 4.6. Absorption (blue) and emission (red) spectra of $TCPPH_2$ in ethanol (dashed line) and in silica nanotubes (solid line).

Figure 4.7 shows the fluorescence quenching of the FSNT sensor against TNT exposure on its vapor pressure (10 ppb) at RT. Fluorescence of the sensor was quenched 8.7% in 15 s and 29.3% in 10 min after exposure to the TNT vapor. The reason of the fluorescence quenching is the photo-induced electron transfer between excited $TCPPH_2$ molecules and TNT. When TNT molecule binds to $TCPPH_2$ dye the excited electron of dye molecule transferred to the LUMO of the TNT molecule rather than relaxation by emitting of light [187]. The FSNT sensor also exhibited a significantly high fluorescence quenching efficiency after DNT vapor exposure (Figure 4.7b). The quenching efficiency for DNT was found to be 16.5% after 15 s and 33.3% after 10 min, which is higher than the quenching values obtained for TNT. It is known that the vapor phase fluorescence quenching efficiency of an

analyte is mainly determined by its vapor pressure, the exergonicity (-ΔG°) of electron transfer between dye and analyte and the binding strength of analyte. The binding constant of TNT to electron-rich porphyrin ring is higher than that of DNT because of its extra electron-withdrawing nitro group.[200] On the other hand, vapor pressure of DNT (180 ppb) is 18 fold higher than the vapor pressure of TNT at room temperature. As a result of these two competing factors sensor exhibited a better quenching efficiency against DNT exposure. In Figure 4.7b, fluorescence quenching of the sensor with nitrobenzene (NB) is also presented. NB resulted a relatively low quenching (7.5%) after 10 min compared to TNT and DNT. Binding constant of nitrobenzene to porphyrin ring is expected to be lower than TNT and DNT because it contains only one electron withdrawing nitro group so it resulted in a low quenching of fluorescence although, it has a comparatively high vapor pressure (~300 ppm) at room temperature.

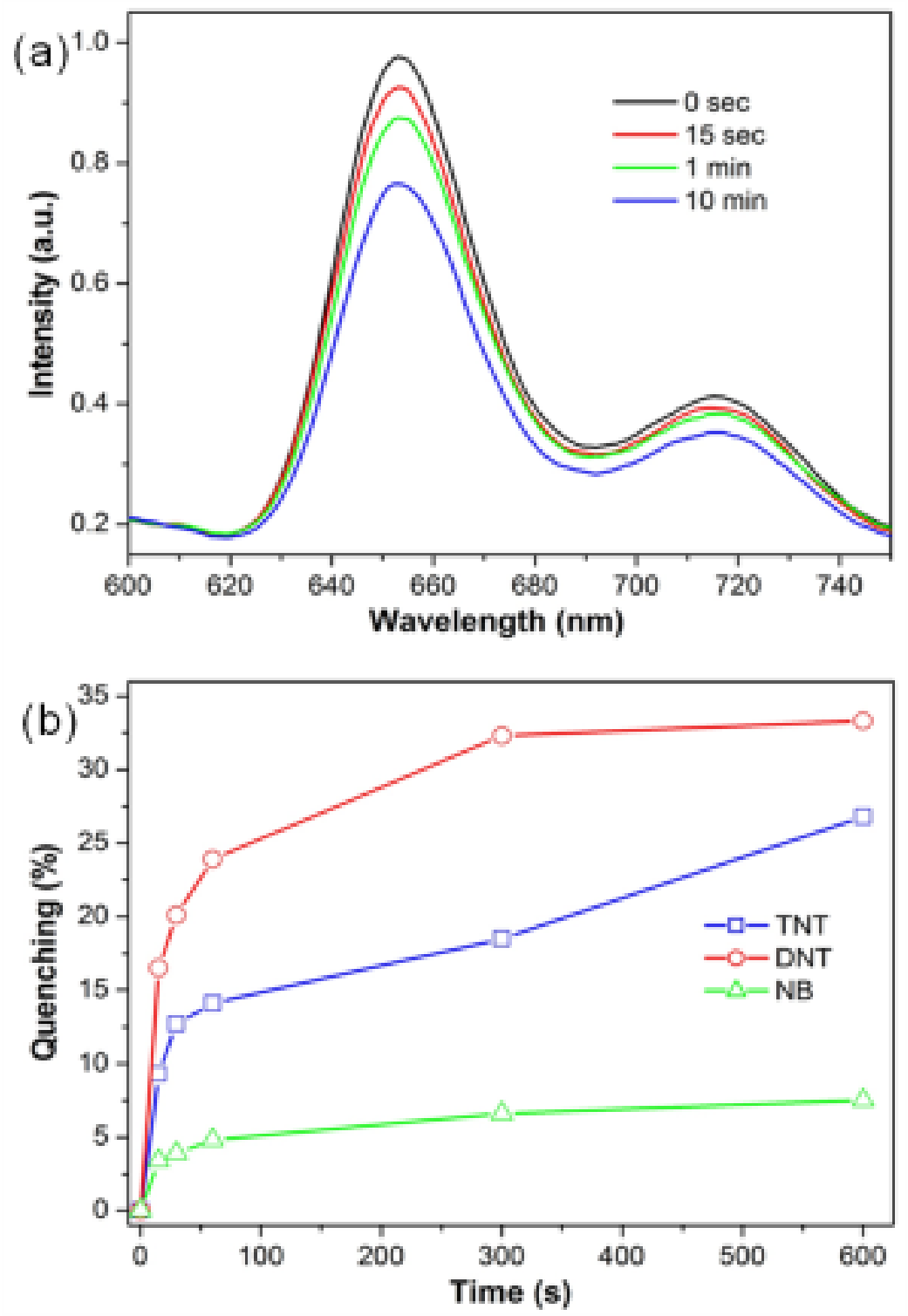

Figure 4.7. (a) Fluorescence quenching of FSNT surface with TNT. (b) Quenching efficiencies of the sensor upon exposure to TNT, DNT, and NB with respect to time.

The fast response and high quenching efficiency of the sensor can be attributed to the high surface area of porous fluorescent silica nanotube network and also high affinity of the $TCPPH_2$ to the TNT and DNT. Porous structure provides fast diffusion of the analyte molecules, and high surface area enhances analyte dye interaction. In order to demonstrate the effect of high porosity on fluorescence quenching, we prepared two $TCPPH_2$ doped control surfaces with lower porosities; a dense silica thin film and a surface composed of silica nanoparticles. The thickness of the silica thin film was determined as 170 nm with an ellipsometer. The silica nanoparticle sensor surface was investigated by SEM (Figure 4.8). The diameters of the particles were found to be around 60 nm. The particles spread to glass surface without aggregation and there were some uncoated parts. The fluorescence quenching performances of the control surfaces were tested with TNT (Figure 4.9). Both thin film and nanoparticle surfaces exhibited significantly lower fluorescence quenching (after 10 min 5.4% and 11.2%, respectively) compared to FSNT surface. The reason of the lower sensitivity of these two sensors is probably their lower surface areas. Also, it must be noted that nonporous thin film sensor exhibited lower quenching efficiency than slightly porous nanoparticle film.

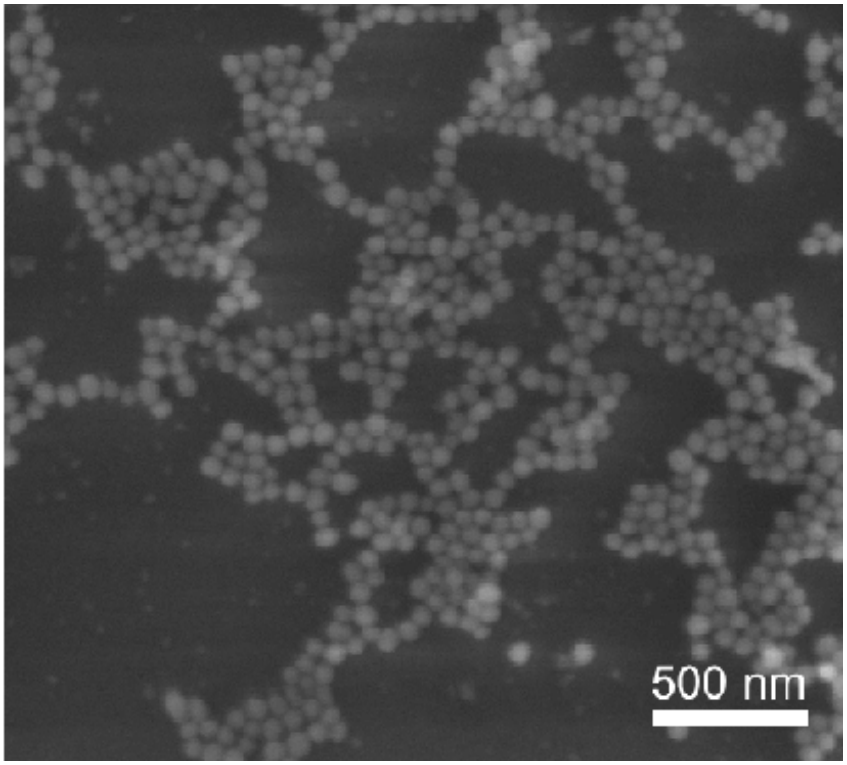

Figure 4.8. SEM image of silica nanoparticles on the sensor surface.

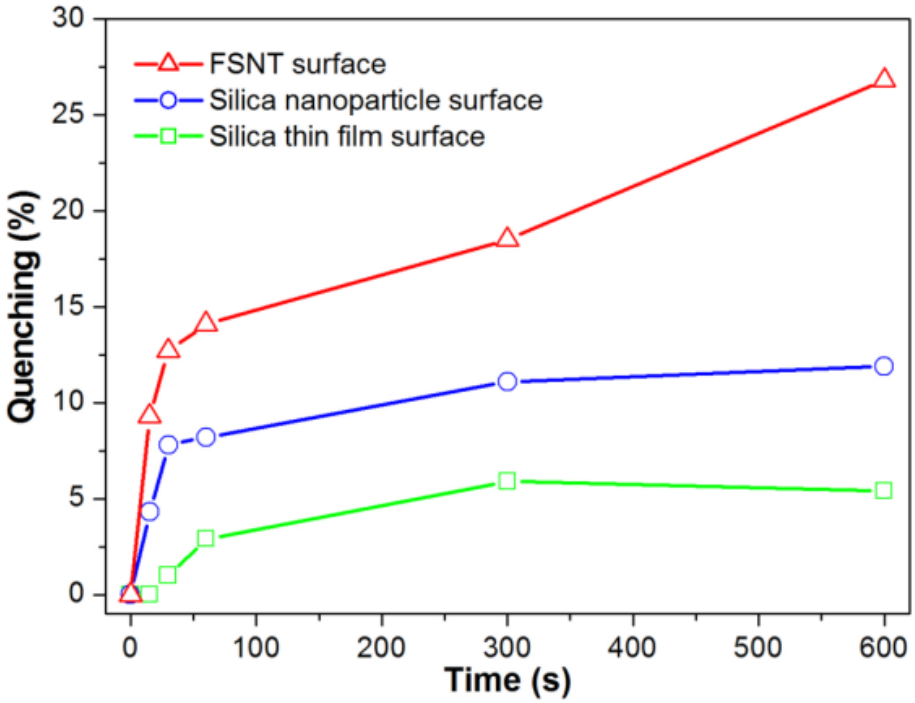

Figure 4.9. Quenching efficiencies of FNST, Silica nanoparticle and silica thin film sensors upon exposure to TNT with respect to time.

The selectivity of the sensor was tested with four other aromatic compounds (Nitrobenzene, Toluene, Xylene, Benzoic acid and Dihydroxy benzoic acid) in addition to TNT and DNT, and results are presented in Figure 4.10. None of the chemicals quenched the fluorescence of the sensor, significantly even after 10 min of exposure showing the high selectivity of the sensor against nitro-explosives (TNT and DNT).

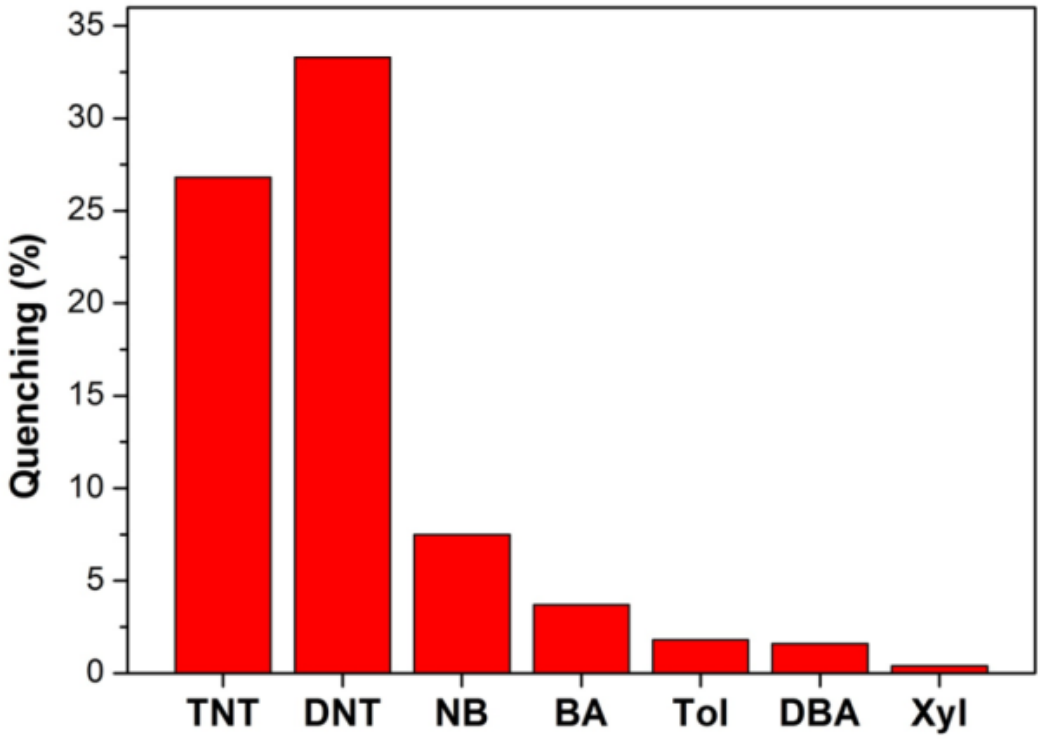

Figure 4.10. Quenching efficiencies of 7 analytes tested after 10 minutes exposure. The FSNT sensor is found to be very selective to the TNT and DNT. NB (nitrobenzene), BA (benzoic acid), Tol (toluene), DBA (dihydroxybenzoic acid), Xyl (xylene).

In summary, we studied fluorescence quenching based explosive sensing performance of dye doped peptide nanofiber (ALP) templated high aspect ratio silica nanotubes. We fabricated silica nanotubes by using a template directed bottom-up

synthesis method. The ALP template also catalyzed silica mineralization by the amine groups. These high-aspect-ratio inorganic nanostructures have a vast potential with their high surface area. Silica nanotubes with high surface area are especially interesting for use in catalysis [201, 202].

To provide explosive sensing property to the silica nanotubes, they were doped with a fluorescent dye. The fluorescent nanotube coated surfaces revealed fast fluorescence quenching against DNT and TNT due to its porous structure. The high selectivity of the FSNT sensor for nitro-explosives was demonstrated by testing the sensor with other control aromatic compounds. The ALP templated high aspect ratio silica nanotubes present a promising platform with their high surface area for sensing and catalysis applications.

Chapter 5

Template Directed Synthesis and Characterization of Titania Nanotubes and Their Application as Dye-Sensitized Solar Cell

This work is partially described in the following publication:

Acar, H., R. Genc, M. Urel, T.S. Erkal, A. Dana, and M.O. Guler, "Self-Assembled Peptide Nanofiber Templated One-Dimensional Gold Nanostructures Exhibiting Resistive Switching", *Langmuir*, 2012.

5. Template Directed Synthesis and Characterization of Titania Nanotubes and Their Application as Dye-Sensitized Solar Cell

5.1. Introduction

Proteins and peptides can assist forward the synthesis of nanostructured inorganic materials in an eco-friendly strategy via bio-mineralization process. Nature inspired synthetic peptide fiber networks have wide applications including bioactive tissue scaffolds [31, 32], carrier agents [33, 34], and template-directed synthesis of inorganic materials [36, 203]. Recently, the high mechanical stability of peptide nanofiber networks was shown [37, 38]. Self-assembly property of amyloid-like peptides (ALPs) can be successfully exploited to obtain one-dimensional nanostructures, such as organic nanowires and nanotubes [204, 205] which may find applications in electronics [35] and sensors [206]. The synthesis of TiO_2 hybrid nanowires using amyloid protein fibrils as templates, and their application in hetero-junction hybrid solar cells was reported elsewhere [207].

The improvement of the quality of human life in near future highly depends on sustainable green energy sources. Solar energy is the most accessible and the easiest to collect sustainable energy source on earth. Dye Sensitized Solar Cells (DSSCs) are a promising and an inexpensive alternative to silicon based solar cells. Although there are many semiconductor materials available for DSSC construction, TiO_2 is one of the most commonly used alternative because of its advantages such as being abundant, bio-compatible, environmentally friendly and inexpensive. TiO_2 nanostructures have many application areas such as gas sensors, lithium ion batteries, photo-catalysts and solar cells [208].

DSSCs have different components for light harvesting, electron transport and hole transport, which make them easier to study with each material to optimize the overall performance [209]. Since electrons and holes are transported in different media, separate optimization in each interface can be done. To achieve better efficiency from DSSCs, studies on the morphology of the TiO_2 semiconductor is significantly important. There are several parameters that should be possessed by TiO_2 component of DSSCs, such as pure anatase phase, optimum surface area for better dye absorption and hole conduction, pore volume and pore diameter, and well-connected network of individual nanostructures [210]. Due to high-surface-area supporting the dye molecules and electron-transport properties of the titania nanoparticles, they serve as one of the most common semiconductor electrode for DSSCs [211].

Application of TiO_2 nanoparticles in DSSCs limits the power conversion efficiency by electron trapping in the nanoparticle film. The incident photon promotes electron injection from sensitizer dye to metal oxide, on which dye is chemisorbed as a monolayer, and then excited electron is transferred through metal oxide to supporting transparent conductive glass by trap-limited diffusion (random walk). The metal oxide is in contact with redox electrolyte (I_3^-/I^-), which is necessary for regeneration of the oxidized dye on the photoanode surface. The redox system is reduced at platinized cathode, thus completing regenerative cycle.

During the operation, photoexcited electrons from dye should be injected and transported through the TiO_2 semiconductor electrode. But, at the same time, these photoexcited electrons can be captured by the electrolyte through the direct contact between electrolyte and the areas of TiO_2 which is not covered by dye via the

recombination of redox ions. The time scale for injection and transport of the electron by TiO_2 is comparable with the time scale of the recombination by the electrolyte [212]. The competition between these time scales determines the photon-to-current conversion efficiency of the DSSC. One of the major problem of DSSCs is this loss of electron at the TiO_2/electrolyte interface [213].

On the other hand, the transport of charge carries through the titania tubes is more facile because of its inherent nature to produce lower diffusion resistance [214]. One-dimensional nanostructures such as nanowire [215], nanorods [216] are able to transport electrons before the recombination process take place, which is necessary for high cell efficiency [217]. Highly ordered architectures offer longer electron diffusion paths and shorter electron transport time constants than randomly oriented titania nanoparticle films [218]. In fact, wire-like architecture acts as a “box” that delimits medium through which electron travels. If this “box” is smaller than the mean free path of the electron we may expect enhancement in electron mobility [36].

The peptidic assemblies can be effectively used as soft templates in the synthesis of inorganic and organic-inorganic hybrid nanostructures [219]. Bottom up approach, realized through mineralization process of self-assembled templates, leads to high-surface area hybrid nanofiber network. Calcination of hybrid material network on the surface of FTO glass yields in functional electrode with nanostructured anatase titania layer. Staining of obtained layer with N719 photosensitizer dye enhance it with photoactivity. Photoactivity and overall performance of fully functional devices based on our engineered materials are assessed in dye sensitized solar cell experiments.

Here we demonstrated the peptide-templated synthesis of TiO_2 nanotubes. The synthesized nanotubes with their high surface area and abundant mesopores demonstrated high dye-loading and yield.

5.2. Experimental

Materials: The peptides are designed and synthesized as reported previously in Chapter 3. Fmoc and Boc protected amino acids, MBHA Rink Amide resin, and HBTU were purchased from NovaBiochem and ABCR. The other chemicals were purchased from Fisher, Merck, Alfa Aesar or Aldrich and used as received. 3-mm thick fluorine doped tin oxide (FTO) glass (sheet resisivity of 8 Ω/sq), photosensitizer dye Ruthenizer 535-Bis TBA (N719), Iodolyte AN 50 electrolyte and Meltonix 1170-60 thermoplastic were purchased from Solaronix.

Characterization Methods: Small amounts of samples (ca. 5 µL) were cast on clean silicon wafer. Some of the samples were dried with a critical point dryer prior to analysis to take the image of 3D network structure. Samples were dried at a critical point (1072 Psi, 31 ºC) with the Tousimis Autosamdri-815 B, Series C critical point dryer. Photovoltaic current-voltage (J-V) measurements of the cells were taken from the active area of 0.25 cm^2 (0.5cmx0.5cm). Cells were scanned between (-1, 1 V) and (-100 and 100 mA). A NEWPORT full spectrum solar simulator with Air Mass (AM) 1.5 filter from Oriel was used as a light source in J-V measurements. Simulator was operated at the following parameters: 1.5 AM, 100 W/cm^2 and 25°C. Transmittance of the cells measured by Cary 5000 UV-Vis-NIR spectrophotometer. Reflectance measurements were done by Diffuse Reflectance Sphere (DRA 2500) mounted on Cary 5000 spectrophotometer.

Preparation of nanostructured TiO_2 paste: 1 wt% peptide gels were prepared (5 mg peptide in 500μL ethanol) and aged overnight. Later gels were diluted by additional 500 μl of ethanol and 5 molar equivalents of titanium (IV) isopropoxide [Ti(*i*-Pro)$_4$] (Alfa-Aesar) was added as a titanium precursor to the self-assembled peptide nanofibers in ethanol. The samples were incubated for 24 hours at room temperature. Mineralized gels were washed with methanol centrifugated several times. Obtained titania nanostructures were dispersed in 500 μl ethanol and to this mixture 250 μl α-terpineol (Alfa Aesar) and 500 μl ethyl cellulose solution (Alfa Aesar, 10% in ethanol) was added. The final mixture was used as the nanostructured TiO_2 paste.

***Solar cell preparation and characterization*:** Since our paste is more diluted and less viscous, we applied our TiO_2 nanotubes on surfaces by drop casting. All TiO_2 - applied FTO glasses were heated to 450^0C for 2 hours for twining into the anatase form, semiconductor phase. After heating in the oven, the FTO glasses were sinked into 0.03 mM Ruthenizer 535-Bis TBA (N719) (Solaronix) dye for 24 hours. The counter-electrode was prepared by sputtering 25 nm Pt onto glass surface. Iodolyte AN 50 (Solaronix) was used as an electrolyte and was injected between electrodes of the solar cells.

BET analysis: Template-free synthesized TiO_2 particles and TiO_2 nanotubes were calcinated in alumina crucible in oven at 450^0C, separately. Autosorb iQ Station 1Autosorb iQ was used for BET analysis. Surface Area and Porosity of the samples were determined.

Inductively coupled plasma- mass spectrometry (ICP-MS) analysis: ThermoFisher PlasmaLab ICP-MS was used for the analysis. All DSSCs were disassembled after photovoltaic measurements. 50 µl of HF (48%, Sigma Aldrich) was dropped on the titania film on FTO surface of each sample and kept for 10 min in polyethylene dishes. The solution was diluted 4 orders of magnitude for ICP-MS analysis.

Dye adsorption: The amount of the dye adsorbed on the solar cells was measured by Cary 100 UV spectrometer. For desorption of dye from TiO_2 paste,1:1 ethanol:0.1M NaOH solution was prepared [220-222]. Each cell was immersed in 3 ml 1:1 ethanol:0.1M NaOH solution for 1 hour for desorption of dye. 6 standarts of N719 dye was prepared in this solution as; 0.01, 0.05, 0.1, 0.5, 1 and 5 µM in 3 ml, respectively. The spectrum of 5 µM N719 dye in this solution has a significant absorption peak at 515 nm. The calibration curve of the standarts was calculated by taking the intensity of absorption at 515 nm and $R^2 = 0,99$.

5.3. Results and Discusions

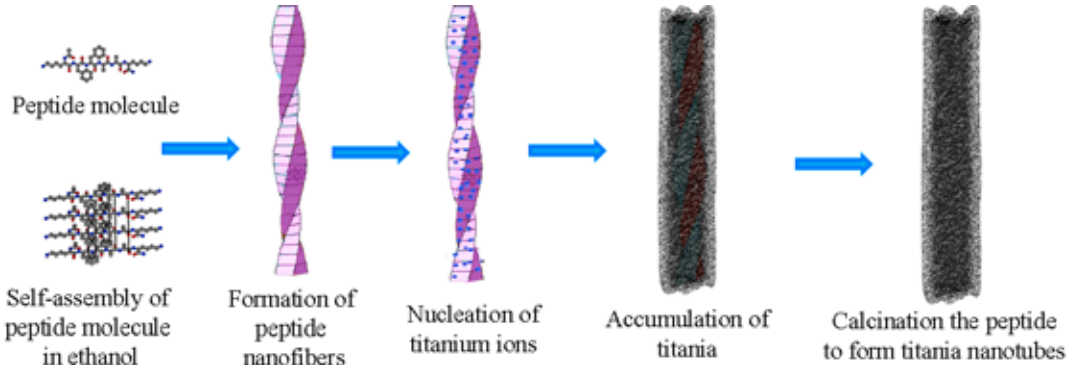

Scheme 5.1. Schematic illustration of self-assembly and mineralization of peptide nanofibers and formation of hollow nanotubes.

Amyloid-like peptides are a class of macromolecules that have inherent property of self-organization; this feature is realized through supramolecular assembly of individual peptide molecules into one-dimensional fibrillar structures. These engineered titania nanotubes were obtained through bottom up approach, where self-assembled peptide nanofibers (Scheme 5.1) were used as template for mineralization. Lysine residues in the sequence of the peptide took the role of nucleation and successive growth centers. Peptide self-assembly and mineralization both take place in solution, thus making this approach appealing from the technical point of view. To see the 3-D network of the mineralized peptide nanofibers, the sample was dried in Critical Point Dryer. After the drying procedure, the sample was directly taken to the oven for calcination at 450°C for transformation of titania into semiconductor anatase phase and elimination of organic peptide part. Thus, semiconductor titania nanotubes were obtained.

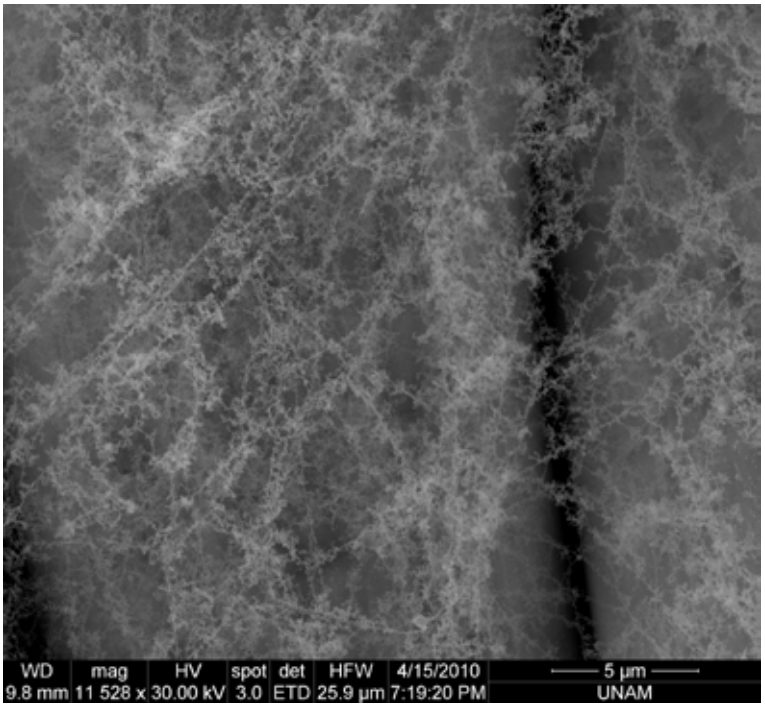

Figure 5.1. 3D network of titania nanotubes after Critical Point Dryer and calcination

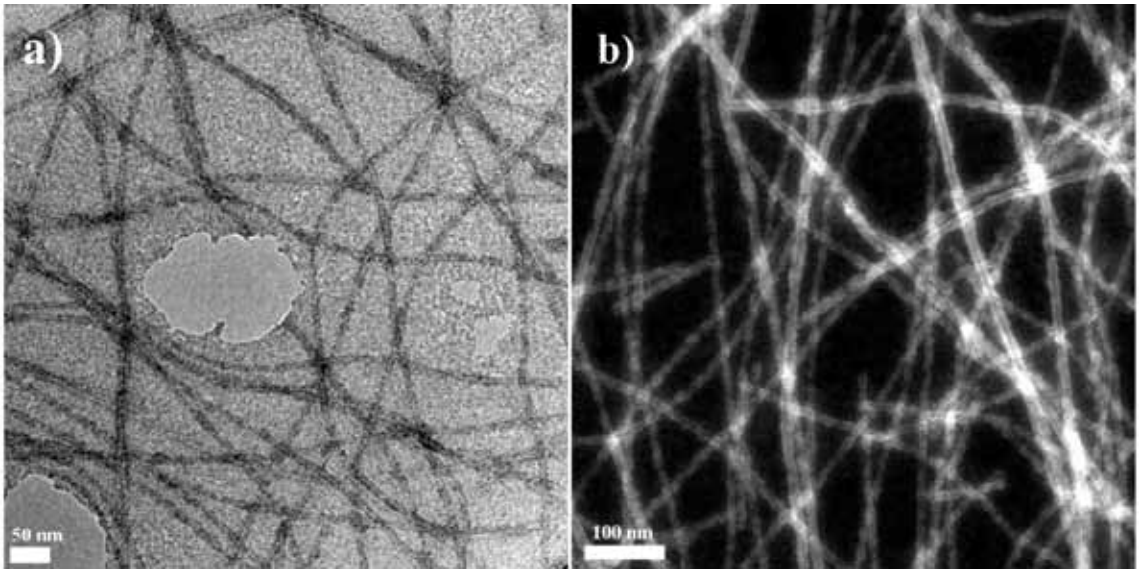

Figure 5.2. TEM images of critical point dried titania nanotubes after calcination at 450°C.

Exploiting soft fibrillar templates in nanofabrication processes makes synthesis of high-aspect ratio materials with high surface area possible [36]. In our case, we

obtained highly porous network of one-dimensional nanostructures (Figure 5.1). Due to geometry of the template-directed TiO_2, fast and directional charge transfer to the surface of the conducting oxide layer becomes possible (Scheme 5.2). This charge transfer enhancement should substantially decrease conduction losses in the electrode. Moreover, nanostructured titania with its high surface area provides increased interaction between TiO_2 and sensitizer. Three sets of the solar cells, which included template-free, and peptide templated anatase titania, were prepared.

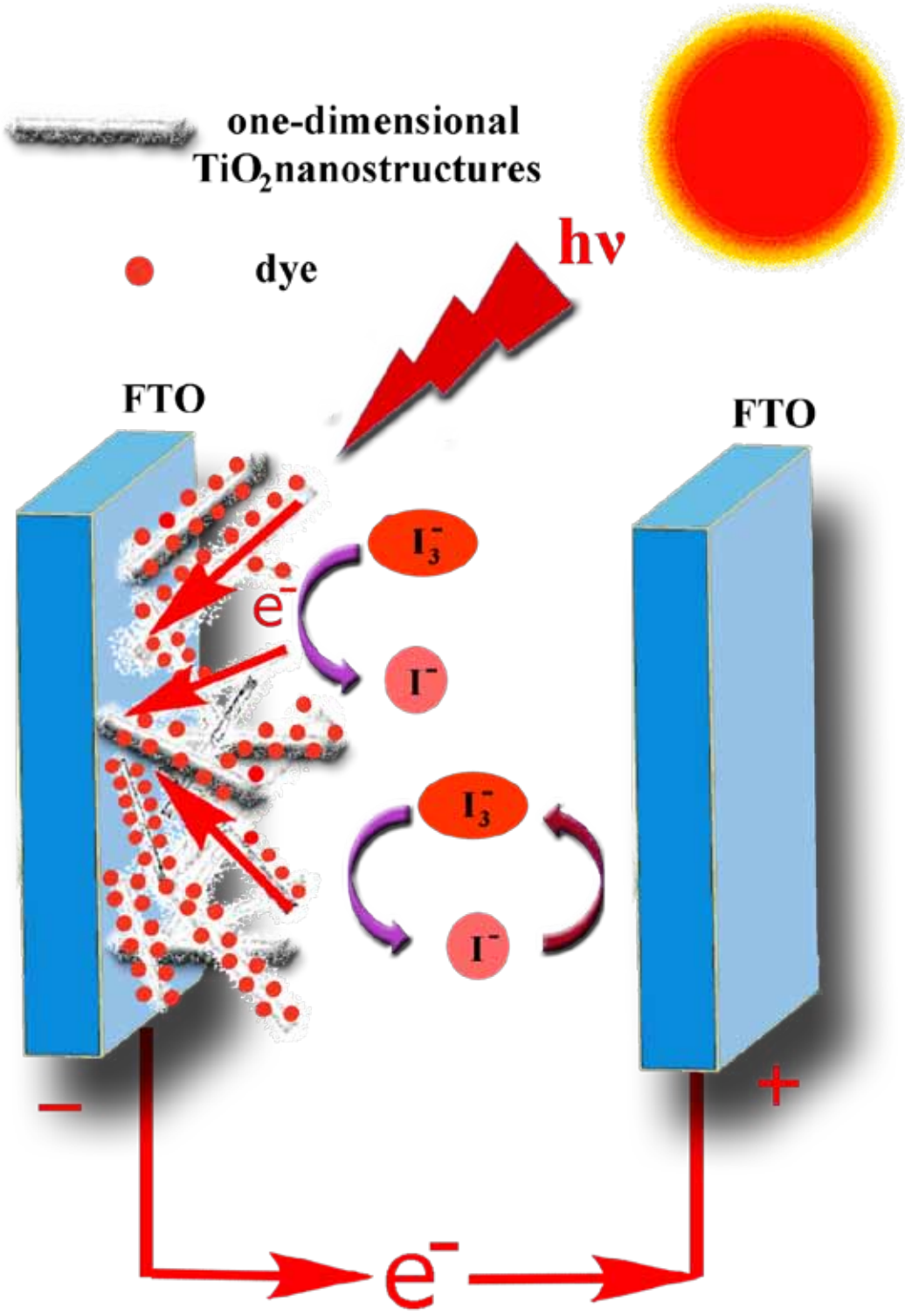

Scheme 5.2. The schematic illustration of DSSC constructed with one-dimensional titania nanostructures.

Template-free titania was used as a control for template effect achieved by means of peptide nanofibers. Template-free titania particles were synthesized exactly under the same conditions but with peptide template missing (Figure 5.3). The titania nanotubes and particles mixed with α-terpineol and ethyl cellulose solution separately to form paste. This paste was applied on the surface of FTO glass and calcinated on FTO. This calcination procedure led to a phase transformation and also discarded impurities and moisture on FTO surface which could affect the overall efficiency of the DSSC.

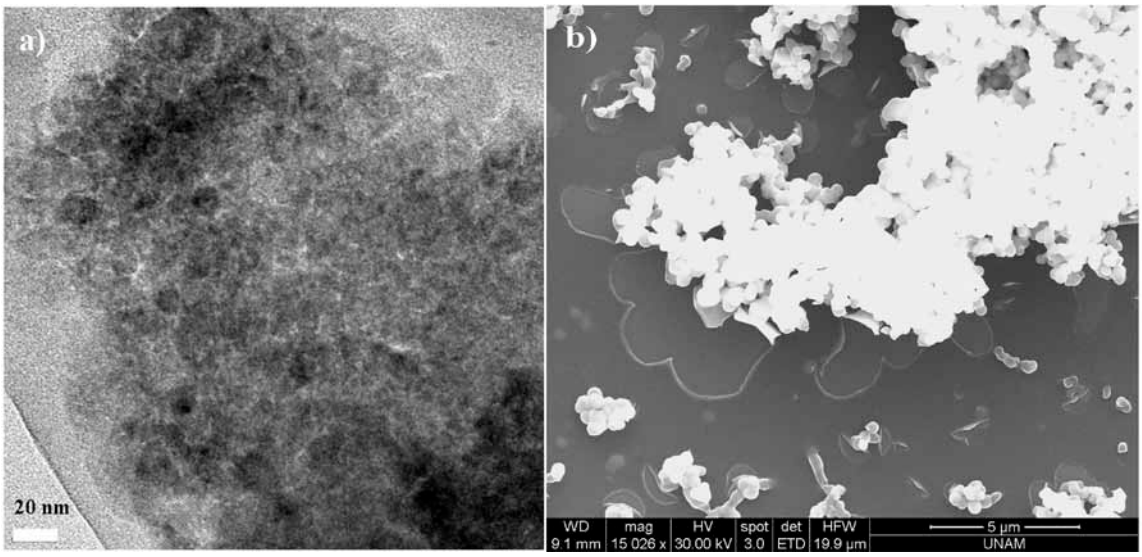

Figure 5.3. a) TEM and b) SEM images of calcined TiO_2 particles without the ALP template.

To obtain the one-dimensional TiO_2 at anatase phase, the semiconductor phase of titania necessary for DSSC construction, the nanostructures were annealed at 450 °C. This thermal material processing leads to anatase phase formation as shown in XRD spectra (Figure 5.4), and at the same time to organic template removal [223, 224]. In

XRD spectra, the shoulder at around 30 degree comes from rutile phase of TiO_2. It was previously demonstrated that the phase transformation of TiO_2 particles with the range of 15-40 nm (the diameter of the nanotubes we obtained are in this range) starts from the interfaces of the contacting anatase grains and the phase transformtion at the outer region is not as the same step as that in the inner region [225]. Another study of the same group showed that the rutile nucleates at interfaces of the contacting anatase grains (<60 nm) [226]. These studies explain the observation of small rutile peak at XRD spectra. Since the TiO_2 nanotubes are aroun 20-30 nm in diameter, the rutile phase transformaiton could be occur at teh contacting and outer regions of the nanotubes.

We have previously demonstrated complete thermal decomposition of peptide occurring at 350 °C in Chapter 3 [179]. Thus, 450 °C was sufficient for calcination of peptide organic template and phase transformation of titania. Calcination process takes place directly on FTO glass, which allows for minimization of solar cell assembly steps (Figure 5.5). Stained with sensitizer (N719) (Figure 5.10), peptide-templated materials were probed in Gratzel-type solar cell experiments. Fully functional solar cell devices had straightforward design: nanostructured titania was sandwiched between two electrodes with addition of liquid iodine/iodide electrolyte (Figure 5.6).

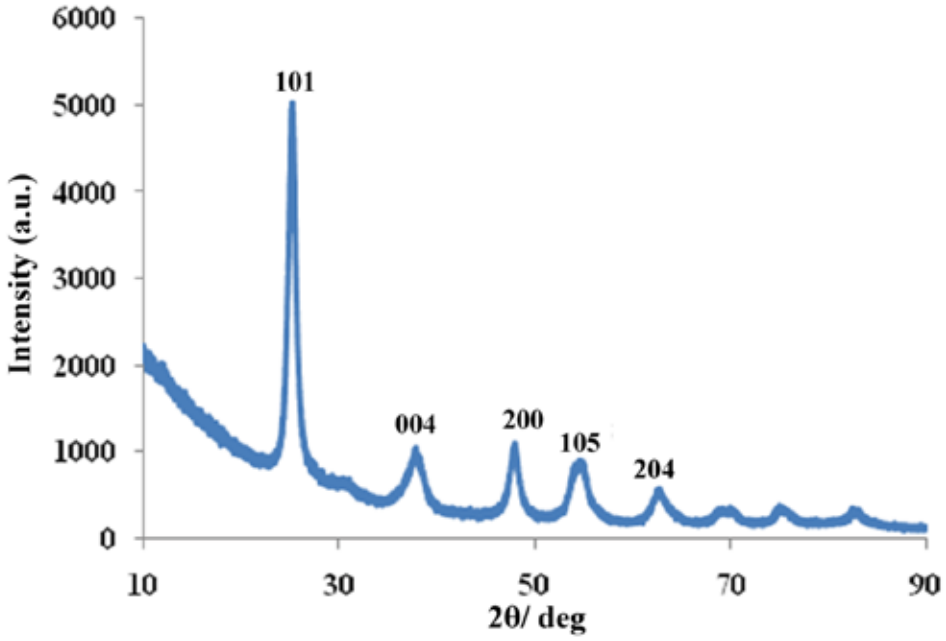

Figure 5.4. XRD spectrum of titania nanotubes after calcination

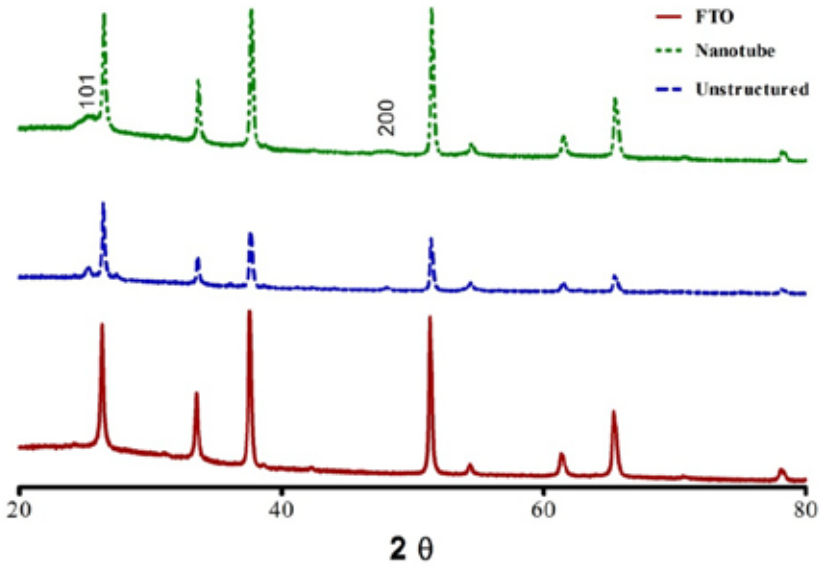

Figure 5.5. XRD spectra of template-free TiO_2 (blue), peptide templated TiO_2 nanotubes (green), on FTO and FTO only (red).

Figure 5.6. A prototype of the constructed DSSC.

The morphology of the titania nanotube film on FTO surface was analyzed with SEM imaging after calcination of titania. The one-dimensional titania nanostructures were observable. To ensure material composition of anodic titania, surfaces were analyzed by energy dispersive X-ray spectroscopy; Ti and O peaks were observed in EDX spectra (Figure 5.7)

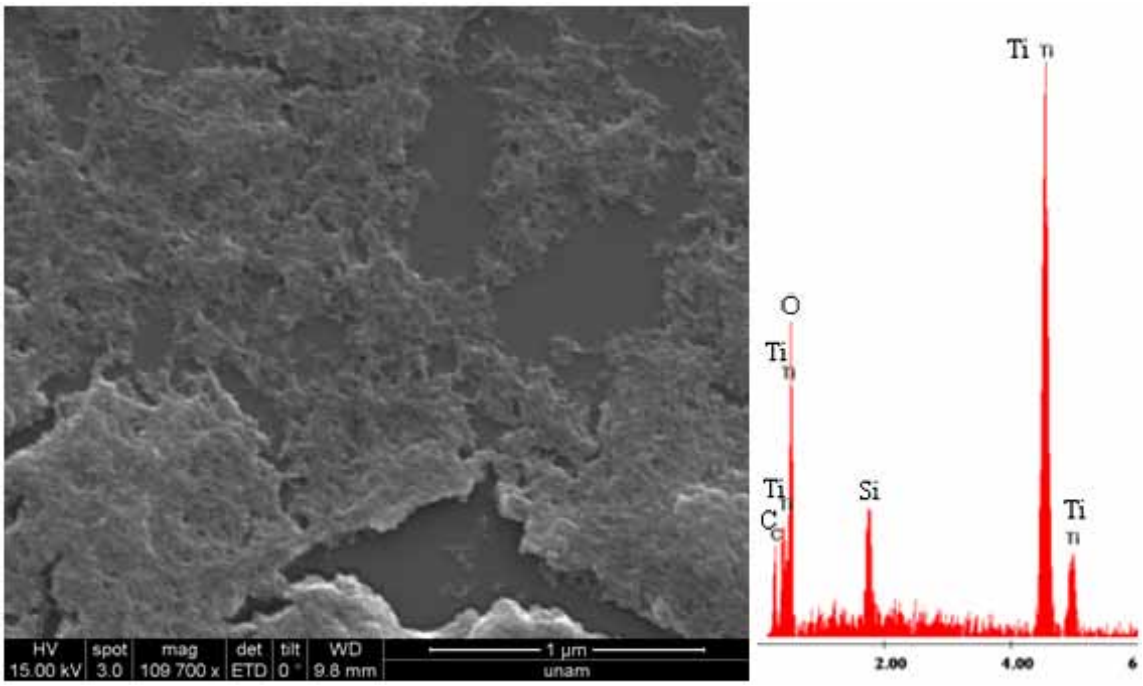

Figure 5.7. Titania nanotubes on surface after calcination and EDX spectrum of the surface.

The amount of titania on the FTO surface is an important parameter which affects the overall efficiency of the DSSC. The total TiO_2 amount on the surfaces differed slightly for solar cells within the sets and more significantly between the sets. Accurate measurements of the titania amounts were achieved by inductively coupled plasma – mass spectrometry (ICP-MS). After the cell efficiency measurements, the cells were disassembled and the titania on FTO was digested in hydrofluoric acid (HF). The amount of titania in HF solutions were analyzed by ICP-MS in all sets and compared. The amount of template-free titania particles was found about 2 times more than titania and nanotubes synthesized by peptide nanofiber templates. It could be due to the three-dimensional structure of bulk titania nanotubes (Figure 5.1) which inhibit the sintering and aggregation of titania during the calcination process. On the other hand, since template-free titania particles have no particular shape and size

(Figure 5.3), they re-assemble on the surface during the calcination to form denser aggregations. Thus, after the calcination, the amount of adhered titania is higher for template-free particles.

The specific surface area of the titania structures have been characterized using nitrogen gas sorption method, which relies on Brunauer-Emmett-Teller [125] theory. The specific surface area (SSA) is a property of solids which is the total surface area of a material per unit of mass. The measurements showed that the specific surface area of nanotube network was more than 5 times greater than that of template-free unstructured titania particles (Figure 5.8 and Figure 5.9). The SSA of template free titania particles found 27.010 m^2/g (Figure 5.8) and 150.628 m^2/g for titania nanotubes after calcination. The adsorption and desorption graphics of the samples are taken with multi points. For BET analysis, the points that taken to calculation should be as linear as possible. The 6 points taken to calculation of BET analysis (while it should be at least 3) for both of samples to find the accurate results.

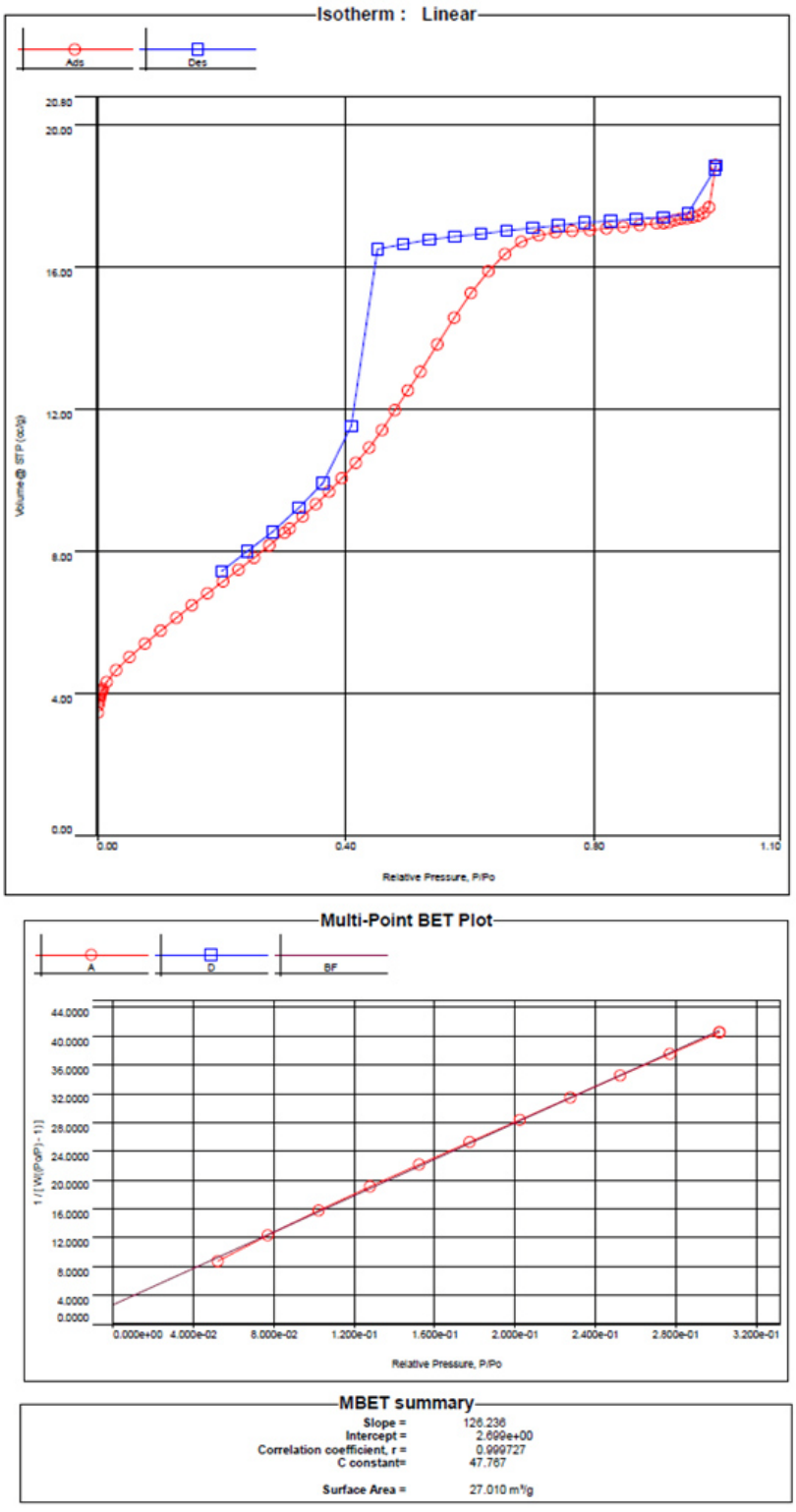

Figure 5.8. a) The isothermal histogram and, b) MultiPoint BET analysis based on the histogram of template-free TiO_2.

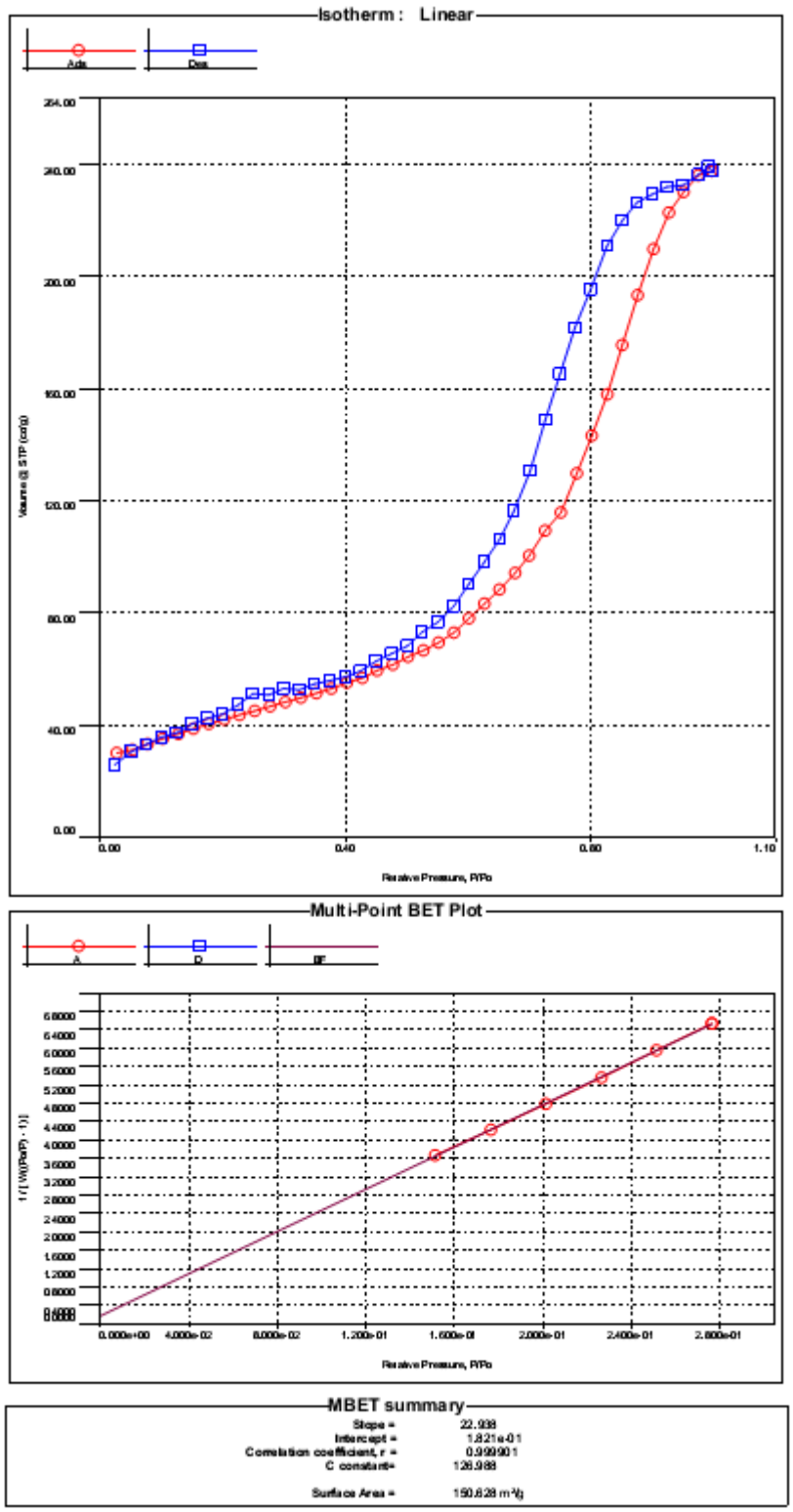

Figure 5.9. a) The isothermal histogram and, b) Multi-Point BET analysis based on the histogram of peptide nanofibers templated TiO_2 nanotube network.

The porosity and surface area of titania component should be optimized for DSSCs. The pore size should be large enough to allow the easy diffusion of electrolyte, while avoiding the recombination of redox in the electrolyte [227]. For this purpose, one-dimensional nanostructures offer the best morphology. Since N719 dye molecules are not likely to aggregate under ordinary conditions, the dye should have been adsorbed as monolayer (Figure 5.10) [228, 229]; therefore, increasing the surface area will cause increase in the efficiency of the solar cell. The amount of adsorbed dye is expected to be greater for nanotubes compared to template-free titania.

For the desoption of dye fro titania, 1:1 ethanol:0.1M NaOH solution [220-222] was prepared. The spectrum of 5 µM N719 dye in this solution has a significant absorption peak at 515 nm (Figure 5.11). For drawing the calibration curve, 6 standarts of N719 dye was prepared in this solution as; 0.01, 0.05, 0.1, 0.5, 1 and 5 µM in 3 mL, respectively (Figure 5.12). The calibration curve of the standarts was calculated by taking the intensity of absorption at 515 nm and $R^2 = 0,99$. To calculate the adsorbed dye on titania surfaces, the cells sinked into 3 ml of 1:1 ethanol:0.1M NaOH solution for 1 hour for desorption of dye.

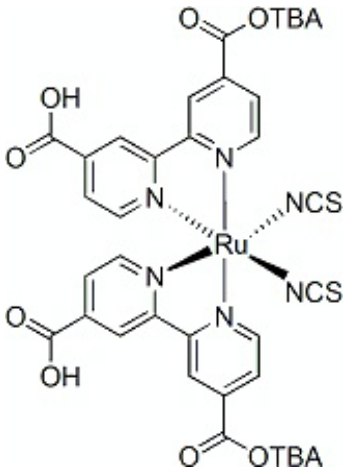

Figure 5.10. The chemical structure of N 719 dye.

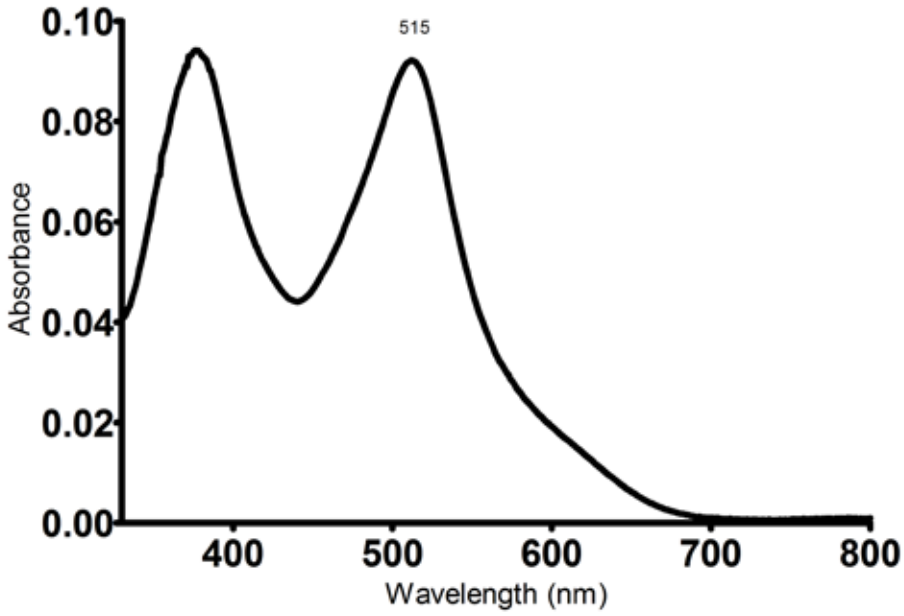

Figure 5.11. UV-Vis absorption spectrum of N719 sensitizer dye.

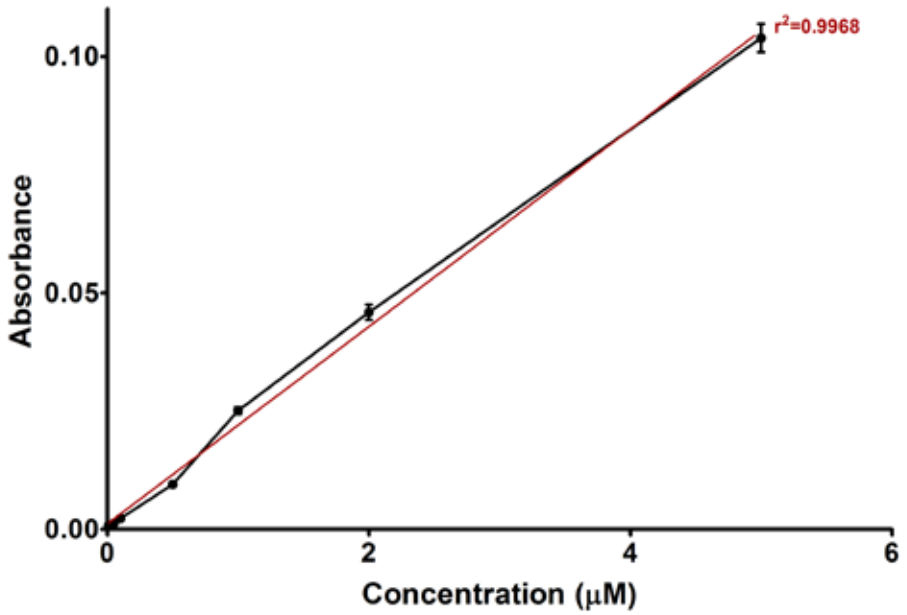

Figure 5.12. Linear concentration calibration curve of N719.

Indeed, according to the measurements, the average amounts of adsorbed dye were found as 3 times more for nanotubes compared to template-free particles, as expected and compatible with the surface area measurements (Table 5.1).

Dye amount adsorbed by material accounts for current density and also effects the device performance [230]. The porous morphology of the titania nanotubes synthesized by peptide molecule as template, provides more surface area for adsorption of dye. Furthermore, one-dimensional hollow structure is enhancing the direct and fast transportation of electron through semiconductor to the electrode before recombination. The efficiencies of the DSSCs were analyzed by solar simulator. Expectedly, devices with nanostructured materials exhibited significantly greater performance (Figure 5.13). Surprisingly, differed from each other, devices based on nanotubese had comparably greater efficiency. Observed difference in

performance was attributed to the radial distribution of TiO_2 in templated one-dimensional nanostructures. The J-V characteristics of the photovoltaic devices prepared using the active layers discussed above, are shown in Figure 5.13.

To evaluate the performance of a solar cell, “fill factor” is a key parameter. It is the ratio of the actual maximum obtainable power to the product of the open circuit voltage and short circuit current. Although fill factor values of titania particles and nanotubes were comparable, open circuit voltage values for templated materials were around 760 mV, while template-free material did not exceed 630 mV. This clearly demonstrates the crucial role of the peptide-templated materials in enhancing overall efficiency of the device performance.

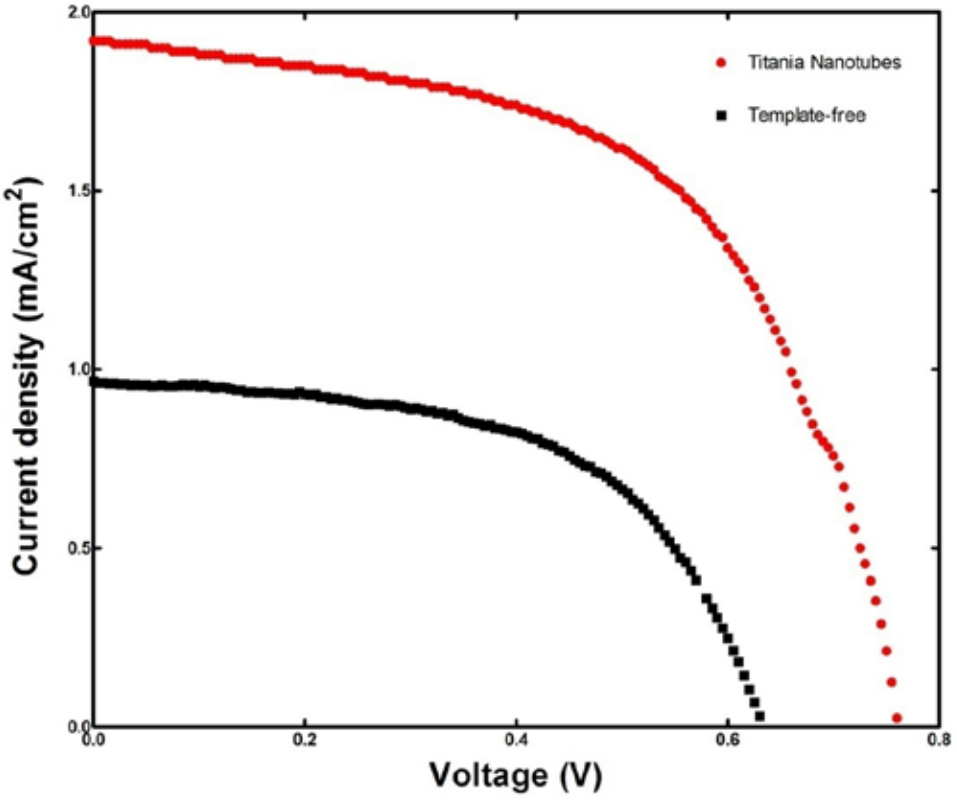

Figure 5.13. Representative J-V spectra of devices based on template-free, peptide templated nanotube materials.

As discussed above, the efficiency of the DSSC directly depends on the amount of electrodic titania and dye adsorbed on it. Thus, the measurements of all the parameters were crucial for more adequate comparison of efficiencies DSSC constructed from different titania structures. By taking all the parameters into account, the efficiency of titania nanotubes was significantly higher than all other structures (Figure 5.13 and Table 5.1). The difference in photonic efficiency of one-dimensional nanostructure was because of their better conductivity properties.

Material	**J_{sc} (mA/cm^2)**	**V_{oc} (mV)**	**Fill Factor**	**Efficiency (%)**	**Surface Area (m^2/g)**	**Average Adsorbed Dye (μM/g)**
Nanotubes	1.92	760	0.57	0.83	150.63	0.066
Template-free	0.61	630	0.56	0.34	27.01	0.022

Table 5.1. Efficiencies and other parameters of representative DSSCs from titania nanotubes and particles.

Dye-sensitized solar cells are an interesting field in which the titania nanostructures may enhance the efficiency of the energy conversion by increasing surface area [231]. Mimicking the natural biomineralization process by means of this kind of simple and controllable self-assembling molecules can be an interesting way to produce bulk amounts of inorganic nanostructures for various industrial and technological applications.

The explained inexpensive and “green” synthesis method of one-dimensional TiO_2 nanostructures for dye sensitized solar cells by using peptide nanofibers, can offer an

attractive and promising way for the rising field of sustainable energy. Also, the differences between nanotubes, nanowires and template-free particles were revised and clarified.

Chapter 6

Template Directed Synthesis and Characterization One-Dimensional Au Nanocomposites and Their Conductivity Properties

This work is partially described in the following publication:

Acar, H., R. Genc, M. Urel, T.S. Erkal, A. Dana, and M.O. Guler, "Self-Assembled Peptide Nanofiber Templated One-Dimensional Gold Nanostructures Exhibiting Resistive Switching", *Langmuir*, 2012.

6. Template Directed Synthesis and Characterization One-Dimensional Au Nanocomposites and Their Conductivity Properties

6.1. Introduction

Recent developments in controlled assembly of inorganic nanoparticles into functional macro-structures with tunable properties provided promising results in diverse applications [232]. One of the simple and cost effective methods for shape and size controlled assembly of nanoparticles is template directed synthesis [25]. In this approach, deposition of the inorganic material on the template can be obtained either by molecular cross-linking or use of complementary interactions, such as electrostatic interactions. Hence, control over the shape and the size of the nanostructures can be achieved by geometry and surface properties of the template material [233, 234]. Patterns can be made up of wide variety of materials including solid inorganic materials (e.g. gold and silver) or biological materials (e.g. DNA, viruses and polymers) [235]. Recently, there is an increased amount of reports on incisively designed template materials using biomimetic approaches. Amyloid like peptide (ALP) nanostructures also provide different opportunities for controlled aggregation of metal nanoparticles into one-dimensional nanostructures due to their exciting physical, mechanical, and chemical properties [25, 236]. ALP nanostructures can be specifically designed to have chemically active groups offering metal binding sides on their external surface. Schebeil *et al*. studied layer by layer electro deposition of gold and silver on ALP nanofibers and obtained conductive peptide-nanoparticle hybrids comparable with solid metal wire [8].

The design, synthesis and characterization of the peptide used here as a template was described in Chapter 3. The anionic gold complex affinity on free amine groups is a well-known strategy [237]. We used this strategy for formation of nucleation of inorganic ions on peptide nanofiber templates.

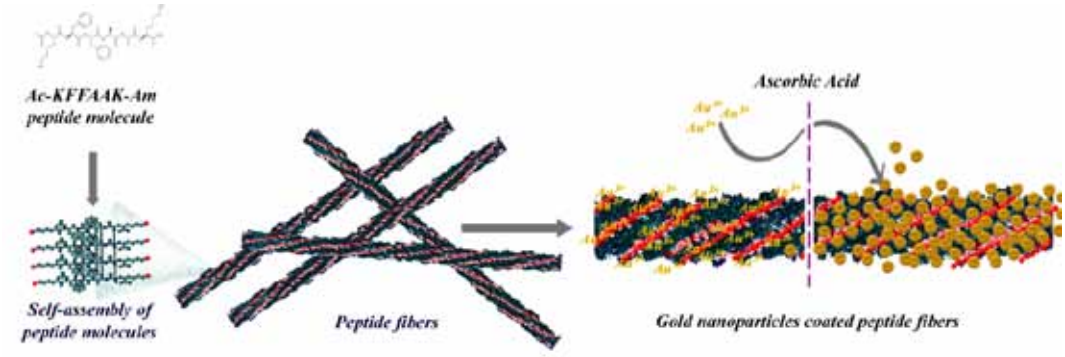

Scheme 6.1. Schematic presentation of gold nanostructure formation using peptide nanofibers as template.

In this work, nanofibers of amyloid like peptides were used as a template.A multi-step seeding mediated growth method was adapted for template directed nanostructure synthesis where the nanocomposites have a potential use in electronic device development as conductive materials [238]. Several parameters such as pre-seeding time periods,the crystallization after the addition of reducing agent, presence of a reducing agent and its concentration and peptide concentration, were studied to understand their effect on the structural properties of one-dimensional gold nanostructures and continuity of the template role of the peptide nanofibers. Particle assembly on the ALP nanofibers was obtained by reduction of ionic gold via ascorbic acid. Structural properties of the peptide nanofibers and assembled one-dimensional

gold nanoparticles were characterized. In addition, conductivity of gold-peptide nanofiber hybrid was tested for potential electronic applications.

6.2. Experimental Section

Peptide synthesis and characterization described in Chapter 3.

Preparation of gold nanocomposites in ethanol: $6.65x10^{-6}$ mol peptide was mixed in 500 µL of ethanol and sonicated for 5 min at 35 °C for formation of clear self-supporting gel. Gold ion solution in ethanol was added immediately after gel preparation. $6.65x10^{-6}$ mol $KAuCl_4$ (Alfa Aesar) was dissolved in 50 µL of ethanol and the gel mixed gently with a pipette tip. Samples left on the bench at room temperature. Then $6.65x10^{-6}$ mol L-(+)-ascorbic acid (Alfa Aesar) was dissolved in 10 µL of water. The solution at pH 2 was added directly into the gold seeded gel.

Preparation of one-dimensional gold nanocomposites via a multi-step seed mediated growth methodology: Multi-step seed mediated growth methodology [239] was adapted for amyloid like peptide nanofibers which were used as template. First, $6.65x10^{-6}$ mol peptide was dissolved in 500 µL ethanol (13.3 mM) and sonicated for 5 min at 35 °C for formation of self-supporting gel. Nuclei formation was carried out by adding $1.33x10^{-6}$ mol $KAuCl_4$ (Alfa Aesar) dissolved in 10 µL of ethanol (one fifth of the total amount of gold) into the gel immediately after preparation and mixed gently with a pipette tip. To change the pH of the ascorbic acid solution, 1 M NaOH was used to obtain reducing agent solution at neutral pH, and alkaline pH, 0.02 mM and 0.06 mM of NaOH was added, respectively. 10 µL of the ascorbic acid solution in water was added into 1 mL of pre-seeded gels. Solutions were aged at room temperature and samples were diluted to targeted peptide concentration by

using $1.33x10^{-6}$ mol $KAuCl_4$. Later, 10 µL of ascorbic acid solution was added into the sample following a gentle mix with pipette tip. The solution was incubated for 30 min. The seeding and reducing cycle was repeated until the desired peptide concentration. Dilution factor was kept at 10% until reaching the peptide concentration of 8.86 mM. Lower peptide concentrations were obtained with sequential dilutions of pre-seeded peptide gel by 50% with fresh solutions of $KAuCl_4$ until reaching the peptide concentration of 0.4 mM. Samples after each cycle was aged for overnight and used for further characterizations.

UV-Vis Absorbance: UV-Vis absorbance measurements were performed on a Varian Cary 5000 UV-Vis-NIR spectrophotometer. 1 mm quartz cuvettes were used for spectrophotometer analysis. Spectrophotometric analysis of gold nanoparticle formation on the pre-seeded peptide nanofibers with gold precursor ($KAuCl_4$, 13.3 mM) reduced by changing amount of ascorbic acid an incubation time is shown in Figure 2.

Scanning Electron Microscopy (E-SEM): SEM experiments were performed with FEI Quanta 200 FEG. 10 µL of the sample was dropped onto clean silicon wafer. Coating of the samples was not performed.

Transmission Electron Microscopy and Scanning Transmission Electron Microscopy: FEI Tecnai G2 F30 instrument was used for TEM analysis. Diluted samples were placed on a Lacey mesh ultrathin carbon coated copper grid. 2% (w/v) uranyl acetate solution was used for staining bare peptide nanofibers. 10 µL of diluted sample solution was dropped on a grid for 1 min. Excess amount was removed by pipetting. Then, 2% uranyl acetate solution was placed on a parafilm

sheet. The grid was put on the drop upside down for 5 min. After staining, the grids were dried in the fume hood at room temperature overnight. No staining was performed for gold nanoparticle coated peptides. Gold nanoparticles formed on the surface of peptide nanofibers prepared with 13.3 mM peptide and equivalent amount of KAuCl4 in ethanol, imaged after 1 week of incubation at room temperature (Figure 1).

Atomic Force Microscopy (AFM): Atomic force microscopy experiments were carried out using a commercial system, Asylum Molecular Force Probe 3D (MFP3D). Multifrequency Kelvin Probe Force Microscopy was used for measuring the surface potential and capacitance. A low frequency (fe= 27.5 KHz) sinusoidal bias was applied to the tip during tapping mode imaging, and both harmonics (at low frequency (fe= 27.5 KHz) corresponding to surface potential and 2fe corresponding to tip-sample capacitance) were recorded. Topography was also recorded simultaneously. A DC bias was also applied to the tip superimposed with the sinusoidal bias. The time harmonics of the electrostatic force were measured by Standford Research Systems SR830 and SR844 lock-in amplifiers. The samples were scanned at a rate between 0.15-0.5 Hz. Commercial Cr/Pt coated cantilevers were used, with resonance frequencies about 70 kHz and spring constants of 2-4 N/m. Tapping drive frequencies were selected to favor repulsive mode imaging. Biases to the contacts on the surface were applied by using Keithley 2400.

Preparation of contacts for AFM and probe station electrical measurements: A p-Si <100> 4-inches wafer was coated with 1 μm thick SiNx as an isolation dielectric layer. Contacts with different gap lengths between 2 – 50 μm were formed

by photolithography and subsequent metallization (sputtering of 35 nm of Au/Pd). The peptide and gold nanocomposites were drop-casted on to the substrates after dilution.

6.3. Results and Discussion

Affinity of the anionic gold to form complex with free amine groups is a well-known strategy [237]. Herein, an amyloid like peptide was designed to form nanofibers of microns in length with amine groups on their exterior surface (Scheme 6.1). The amine groups located on the periphery of the peptide nanofibers can bind to $AuCl_4^-$/$AuCl_2^-$ ions by electrostatic interactions [240, 241]. The electrostatic interactions between $AuCl_4^-$/$AuCl_2^-$ ions and protonated amine groups (since the reactions occur in pH 2) cause gold adsorption on the outer surface of the peptide nanofibers [242]. Moreover, the ALP nanofibers formed self-supporting gels in ethanol (Figure 6.1), which is a well-known slow reducing agent for gold [243, 244].

The structural properties and corresponding surface plasmon resonance [212] characteristics of the nanostructures were examined by TEM imaging and UV spectrophotometer to determine appropriate ratio of the peptide and $KAuCl_4$. After one week of incubation at room temperature, particle formation around the peptide nanofibers were observed. However, using higher molar ratios of $KAuCl_4$ and peptide (2 and 3 molar ratios) led to a dramatic increase in the number of free randomly distributed gold nanoparticles (Figure 6.1b, Figure 6.2). Nanoparticles formed at the external surface of the peptide nanofibers did not show characteristic plasmon peak at 550 nm (Figure 6.3); however, strong peak at 320 nm was observed due to ionic $AuCl_4^-$ in solution [245]. Absence of size dependent localized plasmon

resonance effect might be because of the small particle size below the critical value or hindrance of SPR feature as a result of the closer gap between the particles located through the peptide nanofibers [246].

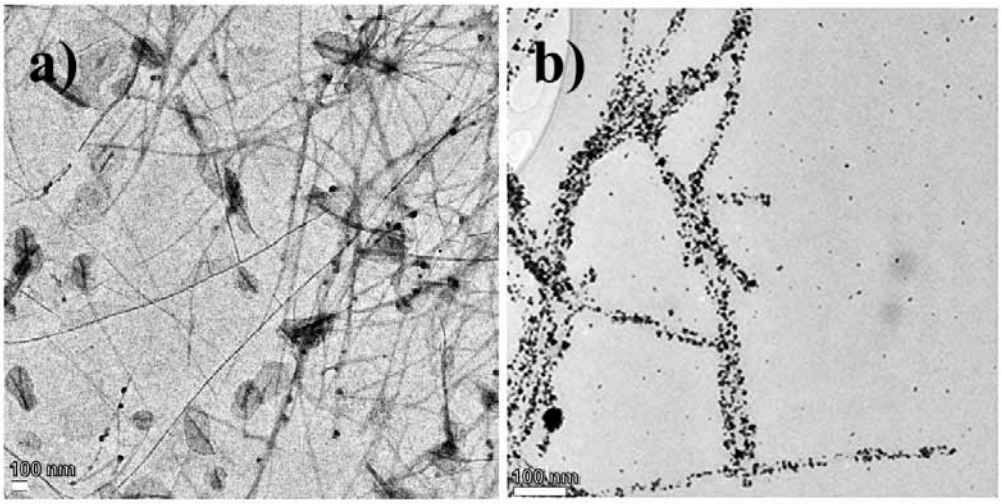

Figure 6.1. Representative TEM images of a) peptide nanofibers stained with uranyl acetate and b) gold nanoparticles formed on the surface of peptide nanofibers.

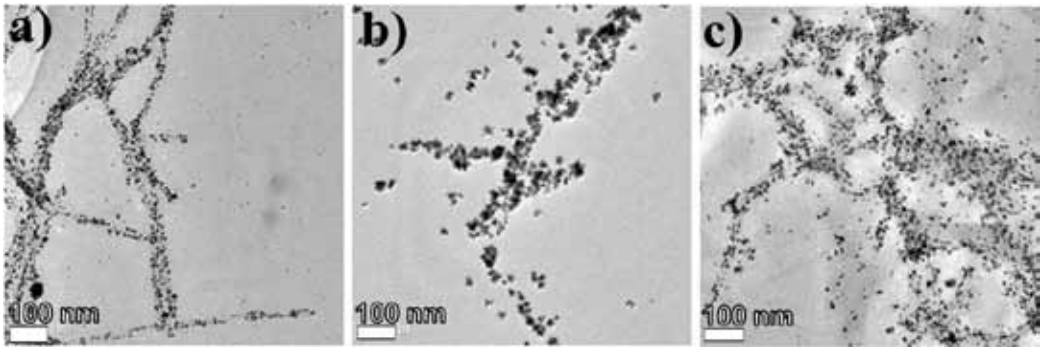

Figure 6.2. TEM images of gold nanoparticle formation on the peptide nanofibers (13.3 mM) in ethanol at different $KAuCl_4$ to peptide molar ratios; a) 1, b) 2 and c) 3.

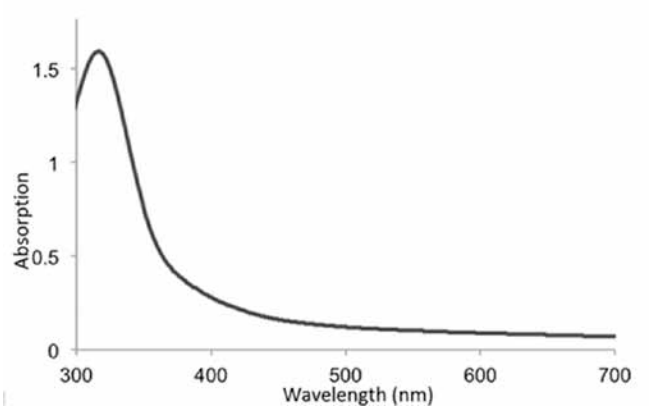

Figure 6.3. Absorbance of the gold nanoparticles coated peptide nanofibers ($KAuCl_4$/peptide ratio is 1 molar ratio).

Although, nanoparticle alignment around the peptide fibers were observed in the samples prepared using ethanol, full arrangement of nanoparticles in one-dimension was not seen because of low reduction capacity of ethanol. Thus, ascorbic acid, which is a well-known reducing agent in preparation of one-dimensional gold nanostructures by facilitating the coordination of metal precursor at post-seeding stages was used as a reducing agent [247-249]. Ascorbic acid reduction potential was tested using different approaches: i) direct addition of ascorbic acid into gold precursor and ii) addition of ascorbic acid into peptide nanofibers system, which were pre-seeded overnight with gold salt. In the first approach, neither a color change nor nanoparticle formation was observed whereas micron-sized randomly distributed aggregates were seenin the SEM images (Figure 6.4).

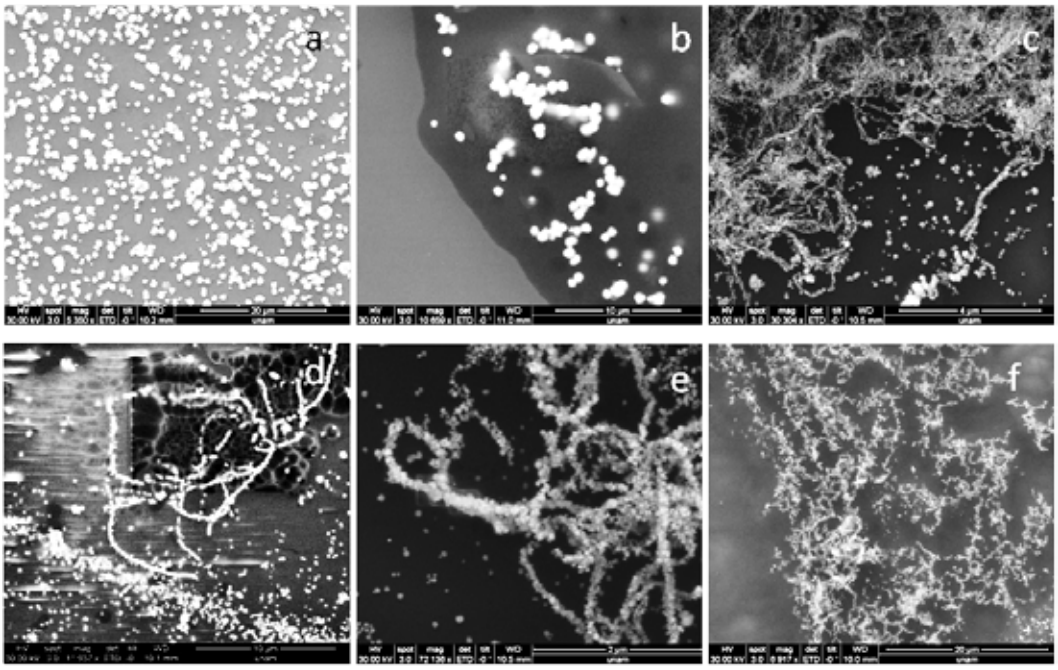

Figure 6.4. SEM images of a) micron sized gold aggregates formed in the absence of peptide after 2 days, and nanowire formation in the presence of peptide (13.3 mM) captured over time, b) 10 min, c) 30 min; d) 1 h, e) 1 day, f) 2 days after the addition of equal molar of ascorbic acid to pre-seeded peptide solution with gold ions in 1:1 molar ratio.

On the other hand, a change in a couple of minutes from yellowish to transparent color and later to dark brown was observed when ascorbic acid was added to pre-seeded peptide nanofiber solution. Reaction kinetics of ascorbic acid as a reducing agent was analyzed by UV-Vis absorbance spectrophotometry and electron microscopy techniques Consumption of gold ions can be tracked by change in characteristic peak at 320 nm and it was monitored by changing ascorbic acid concentrations over a time period. At increased ascorbic acid and constant $KAuCl_4$ concentrations, the peak at 320 nm showed fast decrease until one to one molar ratio of ascorbic acid to gold (Figure 6.5). The same samples were analyzed by SEM and we observed that the number of free particles was increased with ascorbic acid

concentration increase. The UV spectrum of the same sample showed a broad peak with a maximum around 550 nm (Figure 6.5a). As shown in the inset of Figure 6.5a, peak maxima at 320 nm and 550 nm have inverse relation. To obtain maximum conversion of Au^{3+} to Au^{0} and minimize the formation of unbound nanoparticles, ascorbic acid concentration was determined by the data point where two lines intercept, revealing one to one molar ratio of ascorbic acid to gold. This ratio was taken as optimum ratio for this study.

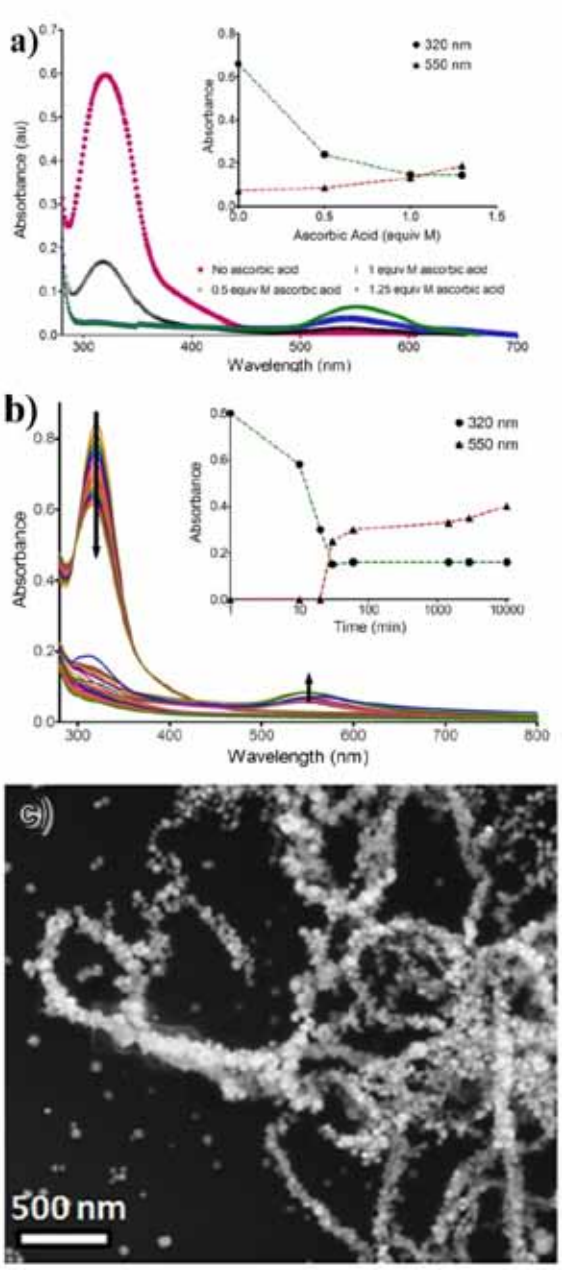

Figure 6.5. (a) Spectrophotometric analysis of gold nanoparticle formation on the peptide nanofibers at changing concentration of ascorbic acid at 60 min of incubation (Inset shows change in absorbance at 320 and 550 nm depending on the ascorbic acid concentration). (b) As time passes the absorption at 320 nm decreases while 550 nm increases at 13.3 mM ascorbic acid concentration (Inset shows relationship between peak maxima at 320 and 550 nm). (c) SEM image of gold nanoparticles formed on the peptide nanofiber template at optimized incubation time and reducing agent concentration.

Once the optimum ascorbic acid concentration was determined, time dependence of the particle assembly on peptide fibers were analyzed by adding ascorbic acid solution (13.3 mM) into pre-seeded peptide nanofibers with $KAuCl_4$ (13.3 mM), and the sample was monitored for over a week. After 30 min of incubation, the peak at 320 nm decreased 5 fold and no further change was observed (Figure 6.5b). On the other hand, the peak at 550 nm started to dominate after 30 min pointing formation of gold nanoparticles (Figure 6.5b, inset) in the surrounding medium which was also observed in SEM imaging (Figure 6.4). To figure out the optimum incubation time, the lowest value possible for both peak maxima at 320 nm and 550 nm was taken. The high-aspect-ratio gold nanostructures (Figure 6.5c) were obtained at this lowest point with less amount of unbound nanoparticles compared to the ones synthesized by incubation for longer time period (Figure 6.4). Therefore, we concluded that the optimum time for ascorbic acid to reduce the gold residues on the template surface with the formation of less amount of free nanoparticles is 30 min.

After optimization of the initial conditions, a multi-step seed mediated growth method, inspired from Jana *et al.*[250], was modified in order to obtain nanowires with higher organization by tuning the number of available amine groups and gel porosity which is correlated with the peptide concentration [251]. Mass transfer of the reactants was affected by the porosity of the peptide nanofiber gel: At higher peptide concentrations, there were more peptide nanofibers in the medium, and dense network of peptide nanofibers resulted in less porosity. Therefore, slower diffusion of the molecules was expected in the denser network preventing uniform distribution of reagents (Scheme 6.2) [252, 253]. Decreasing the peptide concentration to some extent can lead to decrease in the amount of peptide nanofibers in the medium. The

increased porosity eventually facilitated the macromolecular mobility resulting in a more uniform distribution of reaction species in the medium and minimization of random gold reduction. In order to see the consequences of this fact on the final nanostructure, gold nanowire formation through 5 consequent steps, corresponds to decreasing peptide concentration from 11.9 to 0.4 mM, was monitored by transmission electron microscopy (Figure 6.6 and Figure 6.7).

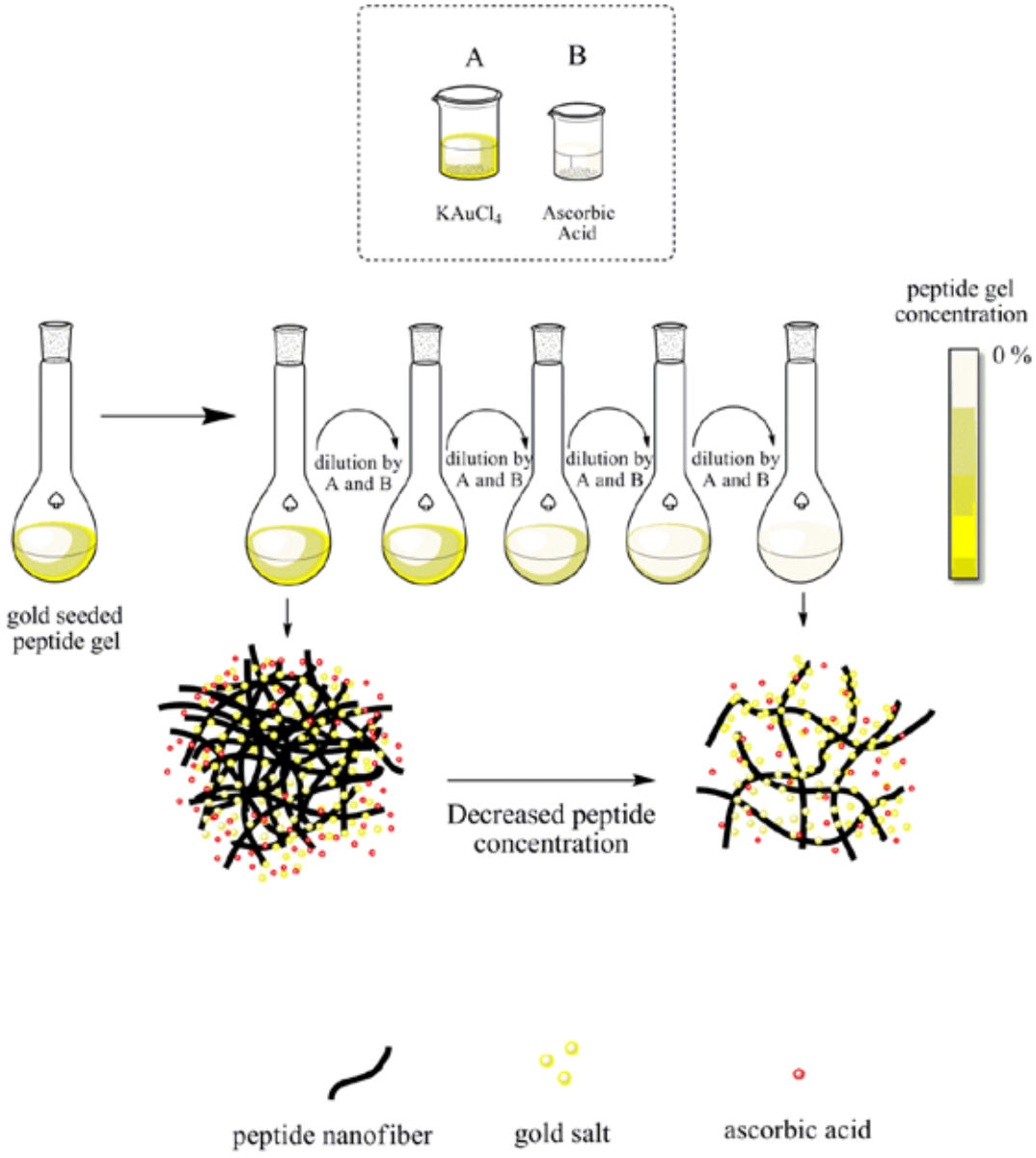

Scheme 6.2. Schematic illustration of multi-step seed mediated growth methodology.

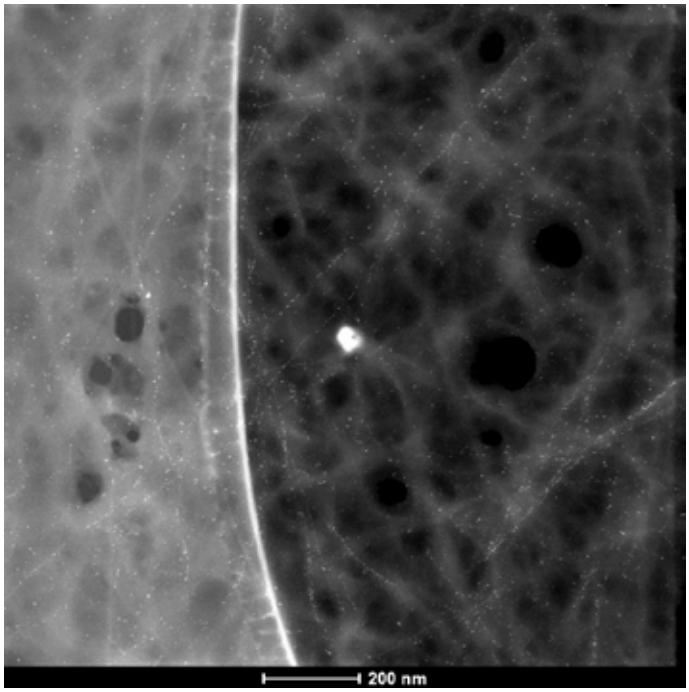

Figure 6.6. TEM image of 1-2 nm nanoparticles after the addition of first portion of the gold precursor. The $AuCl_4^-$/$AuCl_2^-$ ions bind to protonated amine groups and with the help of first ascorbic acid addition, gold nanoparticles were observed.

Ascorbic acid
increasing NaOH concentration
decreasing peptide concentration
11.9 mM
10.2 mM
8.9 mM
6.6 mM
1.6 mM
0.4 mM

Figure 6.7. Morphological characterization of the gold nanostructures formed on the changing concentrations of the peptide nanofiber template by STEM, and comparison of the effect of the reducing agent behavior at increased NaOH concentrations (0-0.06 mM). All scale bars are 200 nm.

After the addition of first portion of the gold precursor, the $AuCl_4^-$/$AuCl_2^-$ ions started to bind on protonated amine groups with the help of first ascorbic acid addition, hence gold seeds (about 1-2 nm nanoparticles) were observed (Figure 6.6). Afterwards, peptide concentration decrease from 11.9 to 8.9 mM (Figure 6.7), resulted a transition from nodule like nanowires to nanowires of compact arrangement of nanoparticles due to particle merging on the seeds formed in the previous stage.

In Figure 6.8a, gold nanowires were clearly observed in samples prepared by 6.6 mM peptide concentration where the packing of nanoparticles at around 3.50±0.71 nm is prominent. XRD pattern of these nanowires revealed a strong signal at 38°, which corresponds to (111) plane of Au crystal (Figure 6.8b**)** and indicated that the (111) plane was dominated and parallel to the support surface [254]. This result was consistent with STEM images (Figure 6.8a and Figure 6.7). Calculated intensity of (200)/(111) value of 0.165 was lower than that of the characteristic value of nanowires (0.249), which was defined at the standard file JCPDS [254]. No apparent surface plasmon peak was observed. However, a broad UV-Vis absorbance peak (Figure 6.8c) was seen between 500-700 nm. Similar broad signal for nanowires composed of nanoparticles arranged on a template was reported previously [255]. The nanofibers were coated with small diameter of gold nanoparticles and the electromagnetic properties of such closely separated nanoparticle arrays significantly

differed from those of monolithic gold nanorods due to presence of gaps between the nanoparticles. The Au nanoparticles were observed to have diameters below 15 nm and it is well established both theoretically and experimentally that Au nanoparticles and rods begin to exhibit SPR peaks when the characteristic size exceeds c.a. 30 nm. Therefore, it is reasonable not to expect transverse resonances due to few nm of Au nanoparticles configured around a typical fiber diameter of less than 10 nm. The longitudinal resonances were also absent due to the lack of continuous gold layer as well as the infinite nanofiber length, which would be necessary to observe well defined resonances even in the presence of a continous gold film. The results were consistent with the TEM images showing densely packed gold nanoparticle alignment on the ALP nanofiber surface [256, 257]. On the other hand, at peptide concentration below 6.6 mM, template effect was disturbed and nanoparticle agglomeration was observed (Figure 6.7). XRD patterns became too weak to calculate in this sample. As predicted, the modified multi-step seed mediated methodology favored controlled formation of high-aspect-ratio one-dimensional gold nanostructures composed of smaller gold nanoparticles with higher degree of packing (Figure 6.8a) compared to the bulk methodology where ascorbic acid was added directly to peptide gel (Figure 6.5c).

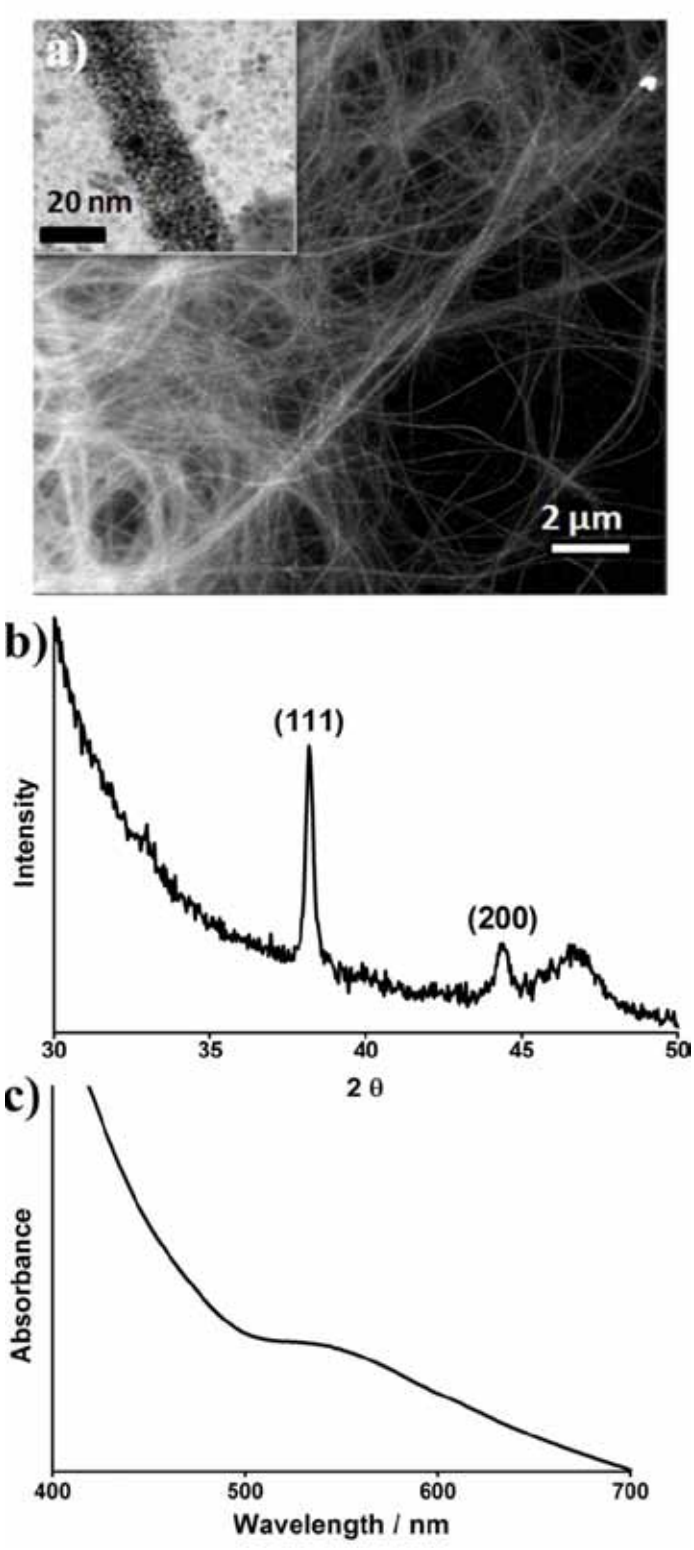

Figure 6.8 STEM image of gold nanowires synthesized using multi-step seed directed methodology a) 8.9 mM peptide concentration, b) XRD pattern, and c) the absorbance spectrum of the nanostructures

The reductive capacity of ascorbic acid is dependent on the pH of the environment [258-260]. At alkaline pH, ascorbic acid turns to ascorbate, which is a stronger reducing agent than its acid form and ascorbate concentration is associated with alkalinity of the environment (Scheme 6.3) [261, 262]. Therefore, influence of the reduction rate on gold nanowire formation at changing peptide concentration was evaluated by varying the NaOH amount in the initial ascorbic acid solution (The effect of NaOH concentration in the initial ascorbic acid solution on particle aggregation kinetics was studied). Increase NaOH amount in the ascorbic acid solution led to formation of uniform nanoparticles with diameter of about 20 nm. However, they were mostly located randomly on the clusters of peptide nanofibers with no apparent one-dimensional template effect. Instant color change from pale yellow to blackish purple was also indication of the aggregate formation. The fast reduction due to increased ascorbate concentration resulted in uncontrolled growth over the template (Figure 6.7).

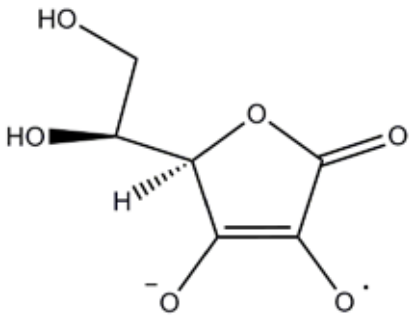

Scheme 6.3. Ascorbyl radical formed from Ascorbic Acid

As discussed above, the optimum time for ascorbic acid to reduce the ionic gold to form one-dimensional nanocomposites by using peptide nanofibers as template was

30 min. However, longer time periods for reduction between the dilutions could initiate formation of highly crystalline one-dimensional structures formed by gold nanoparticles. As shown in Figure 6.9a, peptide concentration of 6.6 mM revealed nanowires of fully merged gold nanoparticles with a fairly narrow and dominated (2Θ) at 38° corresponding to (111) crystal plane.

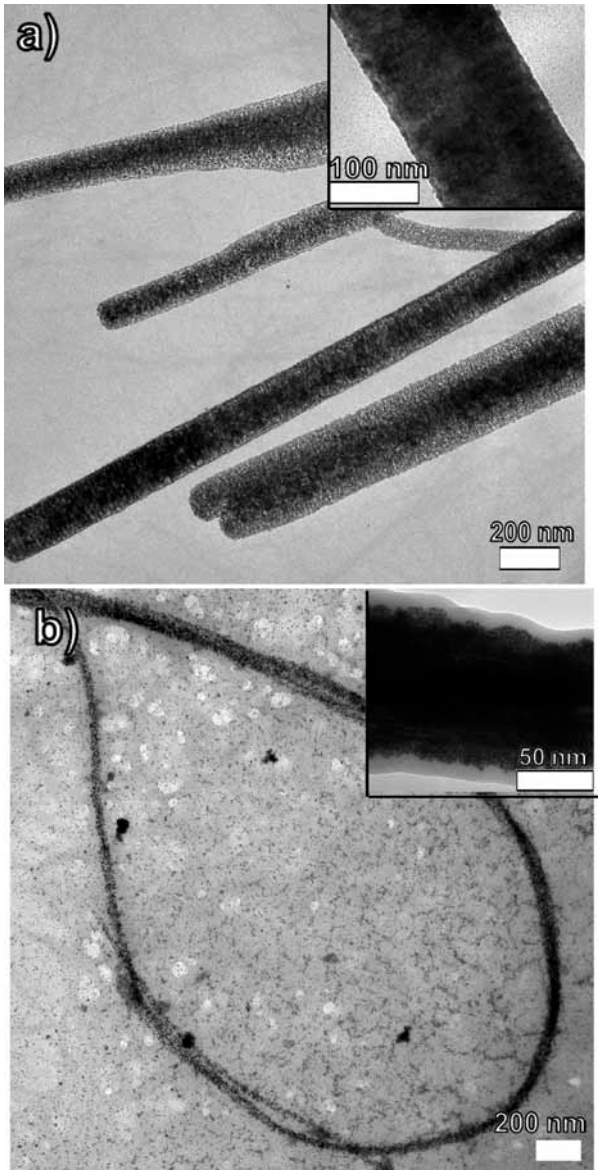

Figure 6.9. TEM images of gold nanostructures formed after 1 day of aging. a) Gold nanowires obtained in the presence of 6.6 mM peptide and b) peptide surrounded nanowires assembled in the presence of 11.9 mM peptide.

However, when the peptide concentration was increased to 11.0 mM, ~5 nm nanoparticles covered by a thick peptide layer on the gold nanostructures were observed (Figure 6.9b). As illustrated in Scheme 6.4, the formation of the string bag-like appearance was due to high peptide concentration. Incubating longer for post-seeding period did not initiate higher packing at this concentration but it promoted binding of free peptide molecules to gold nanoparticles similar to a capping agent and resulted in a new layer for the nuclei formation at the following seeding steps. This stepwise accumulation was completed with the formation of cable like packaging of the final structure with the peptide layer. These results demonstrated that by simply aging the samples for longer times between the dilutions, structural properties of one-dimensional gold nanocomposites can easily be tailored.

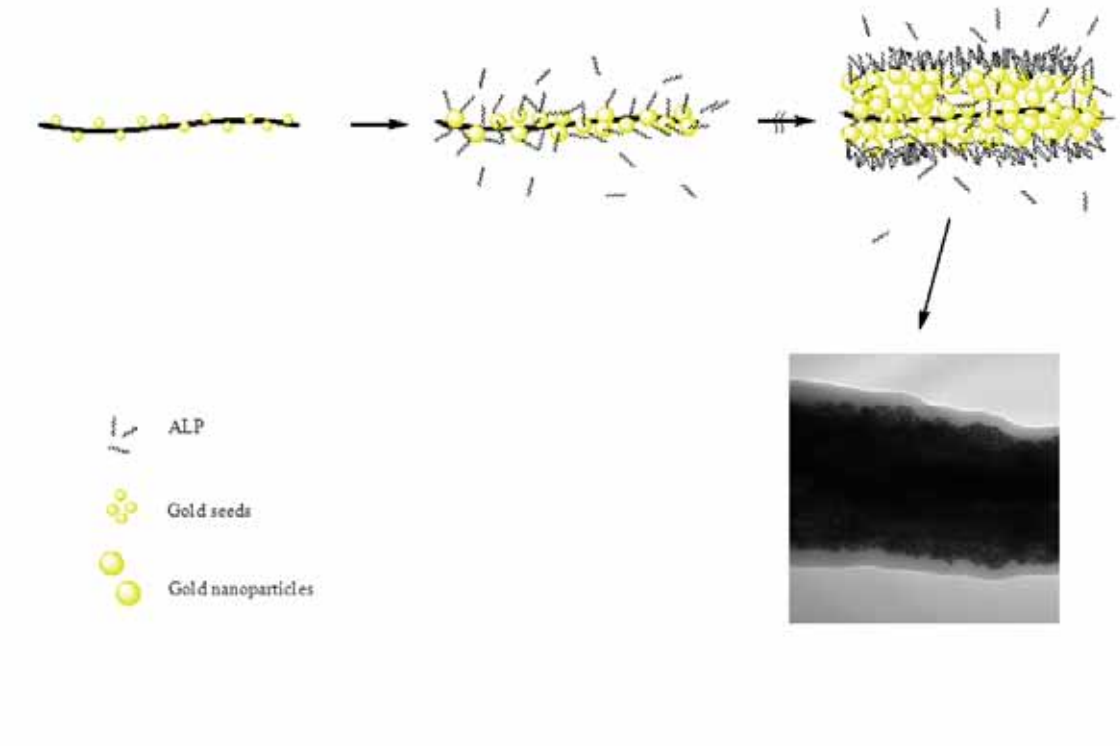

Scheme 6.4. The deposition of free peptide molecules around gold nanoparticles.

Presence of closely packed gold nanoparticles on the peptide nanofibers, separated by peptides or thin vacuum gaps, suggests that conductivity through dry film networks of such nanofibers can be considered essentially to be through electron tunneling in a series of molecular-break-junctions [263]. Conductance through random nanowire networks has attracted significant attention due to potential applications as semi-transparent contacts, or flexible/stretchable conductors and has been studied both theoretically and experimentally [264-267]. Considering their structural similarity, the conductivity mechanism of gold decorated peptide nanofiber networks are expected to be similar to nanowire networks if the gold encapsulation

can be considered as a continuous coating. If the gold nanoparticle coating is discontinuous (gold nanoparticles are separated by peptides or vacuum), tunneling is expected to dominate the conduction through individual nanofibers, and overall conductivity of the network is expected to be described by a more complex model involving tunneling dominated transport within and in-between nanofibers. Nanoscale electrical properties of individual fibers were investigated using atomic force microscopy. Gold-peptide nanofibers composite was drop-cast onto insulating substrates with AuPd contacts separated by a distance of 10 μm. No tunneling current can be observed between the nanofibers and contacts using moderate bias voltages below 5 V, current levels were below the 10 pA rms noise-level of the measurement system. Although the DC current is low, quasi-static charging can allow induction of significant changes in the surface potentials of nanostructures. In order to observe changes in the surface potentials of individual fibers under bias, multi-frequency Kelvin Probe Microscopy was used to simultaneously measure topography and surface potential, as shown in Figure 6.10 [268]. Bias was applied between the contacts (contacts A and B in Figure 6.10a), and a secondary bias was applied to the cantilever (contact C in Figure 6.10a). We observed that locations with different potentials exist along a nanofiber or nanofibers that are in contact with each other (Figure 6.10b and c). This suggested that gold nanoparticle decorated peptide nanofibers were individually near the percolation threshold, with occasional gaps between gold nanoparticles.

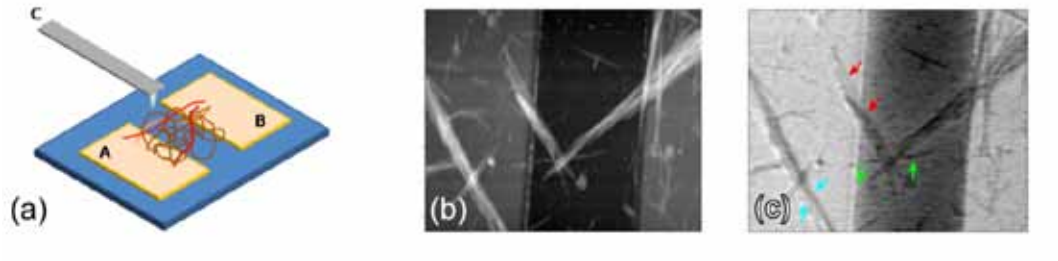

Figure 6.10. a) Dilute gold-peptide nanofiber network is dropcast on a silicon wafer with 1μm thick oxide barrier. A voltage can be applied to the cantilever (denoted by C), or to any of the AuPd contacts (denoted by A and B). b) Simultaneous measurement of topography, and c) surface potential show the low and non-uniform conductivity of the nanofibers. Several arrows are used to denote changes in surface potential along individual nanofibers or nanofibers in contact, when a bias of V_{AB} = 0.5 V is applied. In contrast, AuPd contacts show uniform surface potential distribution.

Current-voltage (IV) characteristics of dilute gels of gold decorated peptide networks were measured through contacts A and B in Figure 6.10a. Typically, samples revealed high resistance as would be expected from the low conductivity of individual nanofibers observed by probe station. When the resistive switching behavior was observable repeatedly, occasionally a high condcutivity path emerges (Figure 6.11a). Transition Voltage Spectroscopy (TVS) has been used to study conductance properties of molecular-break junctions [269, 270]. In TVS, Fowler-Nordheim presentation of the IV data was used by plotting $\ln(I/V^2)$ against 1/V. In such a plot, typically an asymmetric dip was observed for a tunnel junction, which was confirmed to be the case for the Au decorated nanofiber samples (Figure 6.11b).

The transition voltage from direct to Fowler-Nordheim tunneling;

$$V_T \approx \frac{2\hbar}{e\sqrt{m}}\frac{\sqrt{2\varphi}}{d}$$

is a function of tunneling gap *d* and effective tunnel barrier height φ, where *e* and *m* are the electronic charge and mass. V_T was observed to be modulated during cyclic voltage sweeps, which may indicate a change in the tunnel gap *d* or a modulation of the barrier height φ. Although it was difficult to determine without ambiguity the dominant mechanism leading to resistive switching, we speculated that electrochemical changes could be important. Due to applied bias, ions in the residual water may intercalate within the peptide nanofibers, causing swelling and contraction. Small changes in the fiber structure may modulate the effective tunnel gap and resulted in the observed hysteresis of the IV curve.

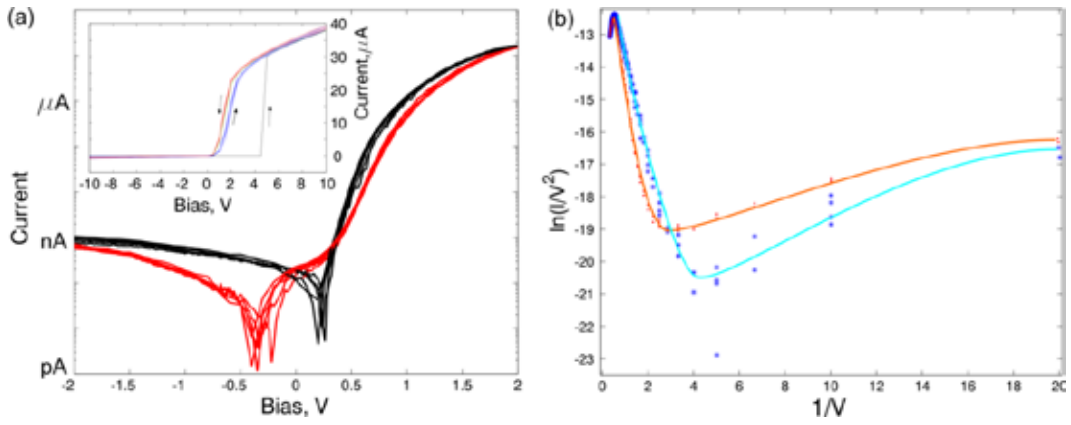

Figure 6.11. a) Cyclic current versus bias measurements revealed asymmetry in the conductance as well as hysteresis. The samples were typically high resistance initially, and switching to a high conductivity state occurs around 4.5 V bias (see inset). Several cycles were superimposed to show the extent of the repeatability of the measurements. b) The current was attributed primarily to tunneling as seen in the Fowler-Nordheim presentation, when $\ln(I/V^2)$ was plotted against 1/V for increasing (red) and decreasing (blue) bias sweeps. Solid lines were guides for the eye. The transition voltage from direct to Fowler-Nordheim tunneling is a function of

tunneling gap and effective tunnel barrier height, and was seen to be modulated during cyclic voltage sweeps.

Measurements performed on thin films of Au decorated and bare peptide nanofibers revealed a pronounced difference in the overall conductivity of the nanofiber network. Thicker films (as revealed by atomic force microscopy) of bare nanofibers exhibited current levels at picoampere level, while Au nanoparticle decorated nanofibers showed current levels at microampere level at similar biases. These observations suggested that the Au decorated nanofiber network possesses a much higher conductivity compared to bare nanofiber networks. Probe station based current measurements on even smaller number of bare nanofibers showed no detectable conductivity (with current levels below 1 pA for -10 to 10 V bias range, data not shown) on bundles of few nanofibers. In addition, an increase in ambient humidity was observed to increase the current levels in both bare and Au decorated nanofiber networks (Figure 6.12). These observations suggested that the measured conductivity (with current levels of up to 100 pA) in thin films networks of bare nanofibers may be solely due to the small ionic conductivity arising from presence of residual ions and condensed water on the films. Further elucidation of the role of ionic conductivity required a detailed study of the effect of humidity on conductivity of films and was left beyond the scope of this study. However, more than thousand-fold increase in the conductivity of Au decorated nanofibers along with reasonable agreement of the current-voltage dependence with the theoretical predictions point to a conduction mechanism dominated by tunneling between the Au nanoparticles on the nanofibers (Figure 6.12).

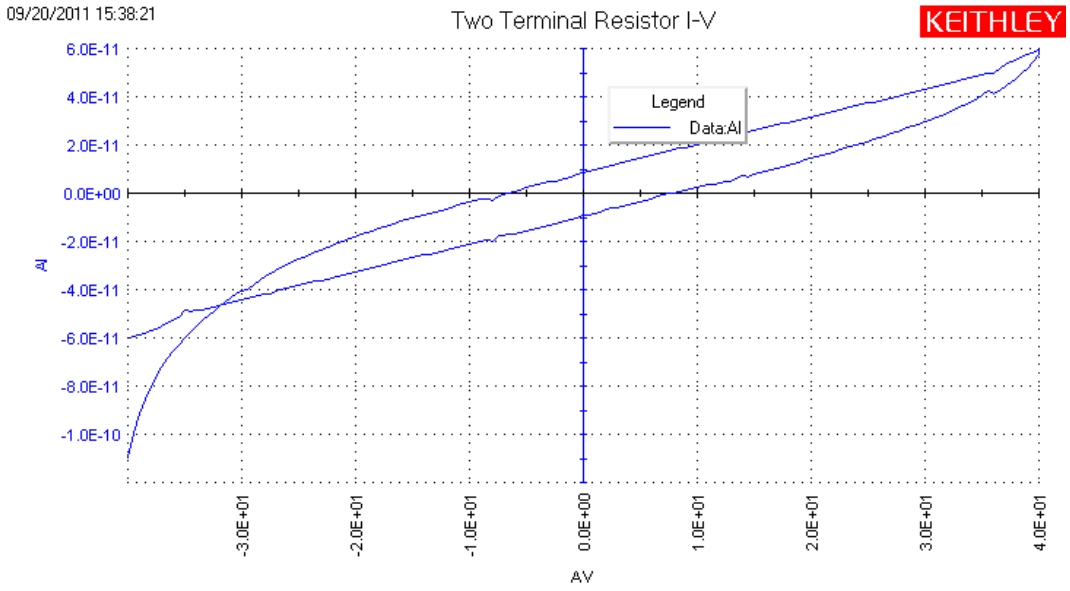

Figure 6.12. Conductivity measurements of bare peptide nanofiber was also measured. Current levels below 1 pA for -10 to 10 V bias range.

In conclusion, self-assembled amyloid like peptide nanofibers were used as template for one-dimensional growth of gold nanowires. Functional groups on the peptide nanofiber surface acting as binding moieties used for the initiation of seed mediated growth of gold nanoparticles. The effect of optimum ratios of peptide and gold precursor and peptide/ethanol, ascorbic acid concentration and reduction kinetics as well as the time interval of both seeding and post seeding after each dilution on morphology of the final structures were studied. A multi-step seeding mediated growth methodology for template directed synthesis of one-dimensional gold nanostructure was developed. Nanowires, noodle-like one-dimensional gold nanostructures and homogenous spherical gold nanoparticles were obtained in a controlled manner by the help of peptide nanofibers. The nanowires were highly conductive due to presence of large number of gaps between gold domains, and dry

films of peptide nanofibers showed tunneling dominated conductance as well as resistive switching. Transition voltage exhibited hysteresis, which was due to presence of electrochemical effects and related modulation of the effective tunneling gap and barrier height. This strategy can be extended to synthesis of wide range of metal and metal oxide nanoparticles depending on to the application. For example, ultrathin and long metal decorated nanofibers can in principle find use in applications where an optically transparent, low hazing and conductive coating is needed, such as in flexible displays, touch-interface devices and solar cells. The production strategy offers multiple parameters which would allow tuning of optical and electrical properties.

Chapter 7

Conclusion

7. Conclusion

Among the various materials in nanoscale, one-dimensional nanostructures such as nanofibers, nanowires and nanotubes have attracted tremendous attention. Nearly all materials, organic, inorganic or hybrid, have been used in the development of one-dimensional nanostructures. One-dimensional nanostructures provides excellent systems to investigate the transportation of electrical and thermal properties, and thier dependence on dimensionality. The dependence of inorganic nanostructures on ionic or metallic bonds to hold their structure together has enabled researchers to use various methods to synthesize uniform inorganic nanostructures. Self-assembly remains to be the leading mechanism for the design of one-dimensional organic nanostructures. In order to realize the enormous potential range of nanostructure applications, new nanofabrication capabilities, new methods for functionalization of molecules and more efficient bottom-up methods must be developed.

The difficulties about the production of one-dimensional nanomaterials at large-scale are mainly associated with the synthesis and fabrication with well-defined dimensions, morphology, phase purity and chemical composition. The “bottom-up” approach described here has many superior properties such as self-assembly of peptide molecules into fibrillar form and mineralization on them in the same medium. The separation of organic template and inorganic nanostructure also occurs in the same medium in ambient conditions.

Biomineralization occurs excellent in nature by numerous species, as a result of evolution in billions of years. In this thesis, the biomineralization procedure in Nature was mimicked. As exactly like the natural proteins, which are responsible

from the mineralization procedure in living organism, the peptide molecules designed and synthesized in this purpose. The peptide molecules designed to self-assemble into one-dimensional nanostructures in appropriate conditions. Furthermore, they designed with special functional groups which have affinity to bind with particular mineral ions in the medium. With those established special functional groups, peptide molecules self-assembled into one-dimensional nanostructures and used as templates for mineralization around them. The mineral ions accumulate around peptide nanofiber templates which results to formation of one-dimensional high aspect ratio inorganic nanostructures with high- surface area.

As described in this thesis, predetermined amount of peptide in appropriate conditions forms rigid peptide nanofibers. These peptide nanofibers are binding to particular mineral ions with electrochemical interactions. This “bottom-up” approach is suitable for mass production. The synthesized peptide nanofibers were used as templates for some inorganic mineralization. The physical and chemical properties of peptide nanofibers and synthesized inorganic materials have been characterized.

Silica mineralization was achieved in this study. After elimination of organic peptide nanofiber template from inside of silica, inorganic nanotubes were obtained. These inorganic silica nanotubes served as great nanostructures with their high surface area for explosive detection sensor development.

Using predetermined amount of peptide, self-assembly and mineralization under ambient conditions make the strategy convenient for bulk production. Self-assembled peptides nanofibers offer unique templating possibilities, which allow for synthesis of nanostructured materials with high surface area. The mineralization of titania

around these peptide nanofibers is also occurs by self-assembly of inorganic ions. Network of these one-dimensional titania structures possesses intriguing features, such as more effective electron transfer and reduced electron hole recombination, which in tandem result in enhanced photoactivity of the templated materials. Dye sensitized solar cell experiments have indisputably demonstrated superiority of nanostructured materials and one more time emphasized importance of bottom up approach realized via self-assembled soft templates. Titania mineralization and formation of titania nanotubes were also studied. The obtained titania nanotubes with porous and hollow structures and high surface area, used in Dye Sensitized Solar Cells. The high surface area supplied high amount of adsorption on the surface of titania semiconductor. Furthermore, one-dimensional structure enhance the transportation of electron through titania. The constructed Dye Sensitized Solar Cells showed better yield with compare to template free titania particles.

Gold mineralization resulted with gold nanoparticles around one-dimensional peptide nanofibers. These peptide-gold one-dimensional composite nanostructures showed well defined conductivity properties.

By chemically functionalization specially designed peptides, it is possible to obtain well defined one-dimensional morphologies. These well defined inorganic nanostructures could be used as organic templates for mineralization by self-assembly as exactly nature does.

Herein, we demonstrated a new bottom-up approach for formation of titania nanostructures by mimicking the biomineralization process with synthetic peptide based nanostructures. The self-assembly process was used to form the template and

the mineralization process revealed the controlled formation of inorganic nanostructures.

Chapter 8

References

8. References

[1] Toksöz, S. and M.O. Guler, "Self-assembled peptidic nanostructures", *Nano Today*, 4(6),p.,458-469, 2009.

[2] Hwang, J.J., S.N. Iyer, L.-S. Li, R. Claussen, D.A. Harrington, and S.I. Stupp, "Self-assembling biomaterials: Liquid crystal phases of cholesteryl oligo(l-lactic acid) and their interactions with cells", *Proceedings of the National Academy of Sciences of the United States of America*, 99(15),p.,9662-9667, 2002.

[3] Silva, G.A., C. Czeisler, K.L. Niece, E. Beniash, D.A. Harrington, J.A. Kessler, and S.I. Stupp, "Selective Differentiation of Neural Progenitor Cells by High-Epitope Density Nanofibers", *Science*, 303(5662),p.,1352-1355, 2004.

[4] Mark Metzke, N.O.C., Soumen Maiti, Edward Nelson, Zhibin Guan,, "Saccharide-Peptide Hybrid Copolymers as Biomaterials13", *Angewandte Chemie International Edition*, 44(40),p.,6529-6533, 2005.

[5] Lee, K.Y., E. Alsberg, S. Hsiong, W. Comisar, J. Linderman, R. Ziff, and D. Mooney, "Nanoscale Adhesion Ligand Organization Regulates Osteoblast Proliferation and Differentiation", *Nano Letters*, 4(8),p.,1501-1506, 2004.

[6] Jin, Y., N. Friedman, M. Sheves, T. He, and D. Cahen, "Bacteriorhodopsin (bR) as an electronic conduction medium: Current transport through bR-containing monolayers", *Proceedings of the National Academy of Sciences*, 103(23),p.,8601-8606, 2006.

[7] Nguyen, S.T., D.L. Gin, J.T. Hupp, and X. Zhang, "Supramolecular chemistry: Functional structures on the mesoscale", *Proceedings of the National Academy of Sciences of the United States of America*, 98(21),p.,11849-11850, 2001.

[8] Scheibel, T., R. Parthasarathy, G. Sawicki, X.-M. Lin, H. Jaeger, and S.L. Lindquist, "Conducting nanowires built by controlled self-assembly of amyloid fibers and selective metal deposition", *Proceedings of the National Academy of Sciences of the United States of America*, 100(8),p.,4527-4532, 2003.

[9] Yang, F., M. Shtein, and S.R. Forrest, "Controlled growth of a molecular bulk heterojunction photovoltaic cell", *Nat Mater*, 4(1),p.,37-41, 2005.

[10] Sveinbjörnsson, B.R., R.A. Weitekamp, G.M. Miyake, Y. Xia, H.A. Atwater, and R.H. Grubbs, "Rapid self-assembly of brush block copolymers to photonic crystals", *Proceedings of the National Academy of Sciences*, 109(36),p.,14332-14336, 2012.

[11] Wang, L., J. Zheng, X.-t. Tao, and Z. Liu, "One-dimensional self-assembly of π-conjugated fluorophore as pH probe highlight", *Synthetic Metals*, 162(23),p.,2033-2038, 2012.

[12] Matsui, H., S. Pan, B. Gologan, and S.H. Jonas, "Bolaamphiphile Nanotube-Templated Metallized Wires", *The Journal of Physical Chemistry B*, 104(41),p.,9576-9579, 2000.

[13] Banerjee, I.A., L. Yu, and H. Matsui, "Cu nanocrystal growth on peptide nanotubes by biomineralization: Size control of Cu nanocrystals by tuning peptide conformation", *Proceedings of the National Academy of Sciences of the United States of America*, 100(25),p.,14678-14682, 2003.

[14] Song, Y.J., S.R. Challa, C.J. Medforth, Y. Qiu, R.K. Watt, D. Pena, J.E. Miller, F. van Swol, and J.A. Shelnutt, "Synthesis of peptide-nanotube platinum-nanoparticle composites", *Chemical Communications*, (9),p.,1044-1045, 2004.

[15] Ji, Q.M. and T. Shimizu, "Chemical synthesis of transition metal oxide nanotubes in water using an iced lipid nanotube as a template", *Chemical Communications*, (35),p.,4411-4413, 2005.

[16] Djalali, R., Y.-f. Chen, and H. Matsui, "Au Nanowire Fabrication from Sequenced Histidine-Rich Peptide", *Journal of the American Chemical Society*, 124(46),p.,13660-13661, 2002.

[17] Zhao, Z., I.A. Banerjee, and H. Matsui, "Simultaneous Targeted Immobilization of Anti-Human IgG-Coated Nanotubes and Anti-Mouse IgG-Coated Nanotubes on the Complementary Antigen-Patterned Surfaces via Biological Molecular Recognition", *Journal of the American Chemical Society*, 127(25),p.,8930-8931, 2005.

[18] Klem, M.T., M. Young, and T. Douglas, "Biomimetic magnetic nanoparticles", *Materials Today*, 8(9),p.,28-37, 2005.

[19] Jung, J.H., J.A. Rim, S.J. Lee, and S.S. Lee, "Spatial organization and patterning of palladium nanoparticles on a self-assembled helical ribbon lipid", *Chemical Communications*, (4),p.,468-470, 2005.

[20] Klem, M.T., D.A. Resnick, K. Gilmore, M. Young, Y.U. Idzerda, and T. Douglas, "Synthetic Control over Magnetic Moment and Exchange Bias in All-Oxide Materials Encapsulated within a Spherical Protein Cage", *Journal of the American Chemical Society*, 129(1),p.,197-201, 2007.

[21] Banerjee, I.A., L. Yu, and H. Matsui, "Room-Temperature Wurtzite ZnS Nanocrystal Growth on Zn Finger-like Peptide Nanotubes by Controlling Their Unfolding Peptide Structures", *Journal of the American Chemical Society*, 127(46),p.,16002-16003, 2005.

[22] Mizeikis, V., S. Juodkazis, A. Marcinkevicius, S. Matsuo, and H. Misawa, "Tailoring and characterization of photonic crystals", *Journal of Photochemistry and Photobiology C: Photochemistry Reviews*, 2(1),p.,35-69, 2001.

[23] Toprak, M.S., B.J. McKenna, M. Mikhaylova, J.H. Waite, and G.D. Stucky, "Spontaneous Assembly of Magnetic Microspheres", *Advanced Materials*, 19(10),p.,1362-1368, 2007.

[24] Hu, J., T.W. Odom, and C.M. Lieber, "Chemistry and Physics in One Dimension: Synthesis and Properties of Nanowires and Nanotubes", *Accounts of Chemical Research*, 32(5),p.,435-445, 1999.

[25] Xia, Y., P. Yang, Y. Sun, Y. Wu, B. Mayers, B. Gates, Y. Yin, F. Kim, and H. Yan, "One-Dimensional Nanostructures: Synthesis, Characterization, and Applications", *Advanced Materials*, 15(5),p.,353-389, 2003.

[26] Kuchibhatla, S.V.N.T., A.S. Karakoti, D. Bera, and S. Seal, "One dimensional nanostructured materials", *Progress in Materials Science*, 52(5),p.,699-913, 2007.

[27] Rodriguez, O., A. Schaefer, C. Mandato, P. Forscher, W. Bement, and C. Waterman-Storer, "Conserved microtubule-actin interactions in cell movement and morphogenesis", *Nature cell biology*, 5(7),p.,599-610, 2003.

[28] Kol, N., L. Adler-Abramovich, D. Barlam, R.Z. Shneck, E. Gazit, and I. Rousso, "Self-Assembled Peptide Nanotubes Are Uniquely Rigid Bioinspired Supramolecular Structures", *Nano Letters*, 5(7),p.,1343-1346, 2005.

[29] Fischer, E. and E. Fourneau, "Ueber einige Derivate des Glykocolls", *Berichte der deutschen chemischen Gesellschaft*, 34(2),p.,2868-2877, 1901.

[30] Merrifield, R.B., "Solid Phase Peptide Synthesis. I. The Synthesis of a Tetrapeptide", *J. Am. Chem. Soc.*, 85(14),p.,2149-2154, 1963.

[31] Ceylan, H., S. Kocabey, A.B. Tekinay, and M.O. Guler, "Surface-adhesive and osteogenic self-assembled peptide nanofibers for bioinspired functionalization of titanium surfaces", *Soft Matter*, 8(14),p.,3929-3937, 2012.

[32] Ceylan, H., A.B. Tekinay, and M.O. Guler, "Selective adhesion and growth of vascular endothelial cells on bioactive peptide nanofiber functionalized stainless steel surface", *Biomaterials*, 32(34),p.,8797-8805, 2011.

[33] Bulut, S., T.S. Erkal, S. Toksoz, A.B. Tekinay, T. Tekinay, and M.O. Guler, "Slow Release and Delivery of Antisense Oligonucleotide Drug by Self-Assembled Peptide Amphiphile Nanofibers", *Biomacromolecules*, 12(8),p.,3007-3014, 2011.

[34] Garifullin, R., T.S. Erkal, S. Tekin, B. Ortac, A.G. Gurek, V. Ahsen, H.G. Yaglioglu, A. Elmali, and M.O. Guler, "Encapsulation of a zinc phthalocyanine derivative in self-assembled peptide nanofibers", *Journal of Materials Chemistry*, 22(6),p.,2553-2559, 2012.

[35] Acar, H., R. Genc, M. Urel, T.S. Erkal, A. Dana, and M.O. Guler, "Self-Assembled Peptide Nanofiber Templated One-Dimensional Gold Nanostructures Exhibiting Resistive Switching", *Langmuir*, 2012.

[36] Khalily, M.A., O. Ustahuseyin, R. Garifullin, R. Genc, and M.O. Guler, "A supramolecular peptide nanofiber templated Pd nanocatalyst for efficient Suzuki coupling reactions under aqueous conditions", *Chemical Communications*, 48(92),p.,11358-11360, 2012.

[37] Cinar, G., H. Ceylan, M. Urel, T.S. Erkal, E. Deniz Tekin, A.B. Tekinay, A. Dâna, and M.O. Guler, "Amyloid Inspired Self-Assembled Peptide Nanofibers", *Biomacromolecules*, 13(10),p.,3377-3387, 2012.

[38] Ceylan, H., M. Urel, T.S. Erkal, A.B. Tekinay, A. Dana, and M.O. Guler, "Mussel Inspired Dynamic Cross-Linking of Self-Healing Peptide Nanofiber Network", *Advanced Functional Materials*,p.,n/a-n/a, 2012.

[39] Pearson, R.G., "Hard and Soft Acids and Bases", *Journal of the American Chemical Society*, 85(22),p.,3533-3539, 1963.

[40] Steed, J.W., "Supramolecular chemistry", ed. J.L. Atwood. Chichester ;: Wiley.2000.

[41] Demir, M. and M.H.B. Stowell, "A chemoselective biomolecular template for assembling diverse nanotubular materials", *Nanotechnology*, 13(4),p.,541, 2002.

[42] Li, Z., S.-W. Chung, J.-M. Nam, D.S. Ginger, and C.A. Mirkin, "Living Templates for the Hierarchical Assembly of Gold Nanoparticles", *Angewandte Chemie*, 115(20),p.,2408-2411, 2003.

[43] Knez, M., A.M. Bittner, F. Boes, C. Wege, H. Jeske, E. Mai, and K. Kern, "Biotemplate Synthesis of 3-nm Nickel and Cobalt Nanowires", *Nano Letters*, 3(8),p.,1079-1082, 2003.

[44] Mao, C., D.J. Solis, B.D. Reiss, S.T. Kottmann, R.Y. Sweeney, A. Hayhurst, G. Georgiou, B. Iverson, and A.M. Belcher, "Virus-Based Toolkit for the Directed Synthesis of Magnetic and Semiconducting Nanowires", *Science*, 303(5655),p.,213-217, 2004.

[45] Lehn, J.M., "Supramolecular Chemistry: Concept and Perspectives", 1995.

[46] Hartgerink, J.D., E.R. Zubarev, and S.I. Stupp, "Supramolecular one-dimensional objects", *Current Opinion in Solid State and Materials Science,* 5(4),p.,355-361, 2001.

[47] Faul, C.F.J. and M. Antonietti, "Ionic Self-Assembly: Facile Synthesis of Supramolecular Materials", *Advanced Materials,* 15(9),p.,673-683, 2003.

[48] Baars, M. and E. Meijer, "Host-Guest Chemistry of Dendritic Molecules". p. 131-182, 2000.

[49] Yokoi, H., T. Kinoshita, and S. Zhang, "Dynamic reassembly of peptide RADA16 nanofiber scaffold", *Proceedings of the National Academy of Sciences of the United States of America,* 102(24),p.,8414-8419, 2005.

[50] Holmes, T.C., S. de Lacalle, X. Su, G. Liu, A. Rich, and S. Zhang, "Extensive neurite outgrowth and active synapse formation on self-assembling peptide scaffolds", *Proceedings of the National Academy of Sciences of the United States of America,* 97(12),p.,6728-6733, 2000.

[51] Gelain, F., D. Bottai, A. Vescovi, and S. Zhang, "Designer Self-Assembling Peptide Nanofiber Scaffolds for Adult Mouse Neural Stem Cell 3-Dimensional Cultures", *PLoS ONE,* 1(1),p.,e119, 2006.

[52] Sieminski, A.L., C.E. Semino, H. Gong, and R.D. Kamm, "Primary sequence of ionic self-assembling peptide gels affects endothelial cell adhesion and capillary morphogenesis", *Journal of Biomedical Materials Research Part A,* 87A(2),p.,494-504, 2008.

[53] Hartgerink, J.D., E. Beniash, and S.I. Stupp, "Self-Assembly and Mineralization of Peptide-Amphiphile Nanofibers", *Science*, 294(5547),p.,1684-1688, 2001.

[54] Stendahl, J.C., M.S. Rao, M.O. Guler, and S.I. Stupp, "Intermolecular Forces in the Self-Assembly of Peptide Amphiphile Nanofibers", *Advanced Functional Materials*, 16(4),p.,499-508, 2006.

[55] Niece, K.L., J.D. Hartgerink, J.J.J.M. Donners, and S.I. Stupp, "Self-Assembly Combining Two Bioactive Peptide-Amphiphile Molecules into Nanofibers by Electrostatic Attraction", *Journal of the American Chemical Society*, 125(24),p.,7146-7147, 2003.

[56] Rajangam, K., H.A. Behanna, M.J. Hui, X. Han, J.F. Hulvat, J.W. Lomasney, and S.I. Stupp, "Heparin Binding Nanostructures to Promote Growth of Blood Vessels", *Nano Letters*, 6(9),p.,2086-2090, 2006.

[57] Guler, M.O., L. Hsu, S. Soukasene, D.A. Harrington, J.F. Hulvat, and S.I. Stupp, "Presentation of RGDS Epitopes on Self-Assembled Nanofibers of Branched Peptide Amphiphiles", *Biomacromolecules*, 7(6),p.,1855-1863, 2006.

[58] Wang, Z., C.J. Medforth, and J.A. Shelnutt, "Porphyrin Nanotubes by Ionic Self-Assembly", *Journal of the American Chemical Society*, 126(49),p.,15954-15955, 2004.

[59] McKeogh, I., J.P. Hill, E.S. Collins, T. McCabe, A.K. Powell, and W. Schmitt, "Self-assembly of FeIII complexes via hydrogen bonded water

molecules into supramolecular coordination networks", *New Journal of Chemistry*, 31(11),p.,1882-1886, 2007.

[60] Judas, N. and B. Kaitner, "One-dimensional self-assembly of bis(3-benzylpentane-2,4-dionato)copper(II) in the solid state, mediated by weak C-H...O hydrogen bonding", *Acta Crystallographica Section E*, 62(1),p.,m163-m165, 2006.

[61] Liu, C.-S., L.-M. Zhou, L.-Q. Guo, S.-T. Ma, and S.-M. Fang, "catena-Poly[[dichloridomercury(II)]-[mu]-1-(2-pyridylmethyl)-1H-benzotriazole]: the effect of different metal centers on the self-assembly of coordination complexes", *Acta Crystallographica Section C*, 64(12),p.,m394-m397, 2008.

[62] Collins, S.N., J.A. Krause, M. Regis, P.J. Ball, and W.B. Connick, "Self-assembly of a one-dimensional iron(II) coordination polymer with p-phenylenebis(picolinaldimine)", *Acta Crystallographica Section C*, 63(11),p.,m528-m530, 2007.

[63] Sabina Burazerovic, J.G.J.P.Thomas R.W., "Hierarchical Self-Assembly of One-Dimensional Streptavidin Bundles as a Collagen Mimetic for the Biomineralization of Calcite13", *Angewandte Chemie International Edition*, 46(29),p.,5510-5514, 2007.

[64] Ye, B.-H., M.-L. Tong, and X.-M. Chen, "Metal-organic molecular architectures with 2,2'-bipyridyl-like and carboxylate ligands", *Coordination Chemistry Reviews*, 249(5-6),p.,545-565, 2005.

[65] Burazerovic, S., J. Gradinaru, J. Pierron, and Thomas R. Ward, "Hierarchical Self-Assembly of One-Dimensional Streptavidin Bundles as a Collagen Mimetic for the Biomineralization of Calcite13", *Angewandte Chemie*, 119(29),p.,5606-5610, 2007.

[66] Dublin, S.N. and V.P. Conticello, "Design of a Selective Metal Ion Switch for Self-Assembly of Peptide-Based Fibrils", *Journal of the American Chemical Society*, 130(1),p.,49-51, 2008.

[67] Dong, J., J.E. Shokes, R.A. Scott, and D.G. Lynn, "Modulating Amyloid Self-Assembly and Fibril Morphology with Zn(II)", *Journal of the American Chemical Society*, 128(11),p.,3540-3542, 2006.

[68] Dong, H., S.E. Paramonov, and J.D. Hartgerink, "Self-Assembly of α-Helical Coiled Coil Nanofibers", *Journal of the American Chemical Society*, 130(41),p.,13691-13695, 2008.

[69] Zimenkov, Y., S.N. Dublin, R. Ni, R.S. Tu, V. Breedveld, R.P. Apkarian, and V.P. Conticello, "Rational Design of a Reversible pH-Responsive Switch for Peptide Self-Assembly", *Journal of the American Chemical Society*, 128(21),p.,6770-6771, 2006.

[70] Kong, L.-Y., X.-H. Lu, Y.-Q. Huang, H. Kawaguchi, Q. Chu, H.-F. Zhu, and W.-Y. Sun, "Unusual one-dimensional branched-chain structures assembled by a novel imidazole-containing tripodal ligand with cadmium(II) salts and their fluorescent property", *Journal of Solid State Chemistry*, 180(1),p.,331-338, 2007.

[71] Sone, E.D., E.R. Zubarev, and S.I. Stupp, "Semiconductor Nanohelices Templated by Supramolecular Ribbons", *Angewandte Chemie International Edition,* 41(10),p.,1705-1709, 2002.

[72] Sone, Eli D., Eugene R. Zubarev, and Samuel I. Stupp, "Supramolecular Templating of Single and Double Nanohelices of Cadmium Sulfide", *Small,* 1(7),p.,694-697, 2005.

[73] Adler-Abramovich, L., D. Aronov, P. Beker, M. Yevnin, S. Stempler, L. Buzhansky, G. Rosenman, and E. Gazit, "Self-assembled arrays of peptide nanotubes by vapour deposition", *Nature nanotechnology,* 4(12),p.,849-54, 2009.

[74] Fenniri, H., P. Mathivanan, K. Vidale, D. Sherman, K. Hallenga, K. Wood, and J. Stowell, "Helical rosette nanotubes: design, self-assembly, and characterization", *J Am Chem Soc,* 123,p.,3854 - 3855, 2001.

[75] Conn, M.M. and J. Rebek, "Self-Assembling Capsules", *Chemical Reviews,* 97(5),p.,1647-1668, 1997.

[76] Scanlon, S. and A. Aggeli, "Self-assembling peptide nanotubes", *Nano Today,* 3(3-4),p.,22-30.

[77] Hartgerink, J.D., J.R. Granja, R.A. Milligan, and M.R. Ghadiri, "Self-Assembling Peptide Nanotubes", *Journal of the American Chemical Society,* 118(1),p.,43-50, 1996.

[78] Clark, T.D., L.K. Buehler, and M.R. Ghadiri, "Self-Assembling Cyclic β3-Peptide Nanotubes as Artificial Transmembrane Ion Channels", *Journal of the American Chemical Society*, 120(4),p.,651-656, 1998.

[79] Velichko, Y.S., S.I. Stupp, and M.O. de la Cruz, "Molecular Simulation Study of Peptide Amphiphile Self-Assembly", *The Journal of Physical Chemistry B*, 112(8),p.,2326-2334, 2008.

[80] Paramonov, S.E., H.-W. Jun, and J.D. Hartgerink, "Self-Assembly of Peptide−Amphiphile Nanofibers: The Roles of Hydrogen Bonding and Amphiphilic Packing", *Journal of the American Chemical Society*, 128(22),p.,7291-7298, 2006.

[81] Guler, M.O., J.K. Pokorski, D.H. Appella, and S.I. Stupp, "Enhanced Oligonucleotide Binding to Self-Assembled Nanofibers", *Bioconjugate Chemistry*, 16(3),p.,501-503, 2005.

[82] Reches, M. and E. Gazit, "Casting Metal Nanowires Within Discrete Self-Assembled Peptide Nanotubes", *Science*, 300(5619),p.,625-627, 2003.

[83] Carny, O., D.E. Shalev, and E. Gazit, "Fabrication of Coaxial Metal Nanocables Using a Self-Assembled Peptide Nanotube Scaffold", *Nano Letters*, 6(8),p.,1594-1597, 2006.

[84] Hong, B.H., S.C. Bae, C.-W. Lee, S. Jeong, and K.S. Kim, "Ultrathin Single-Crystalline Silver Nanowire Arrays Formed in an Ambient Solution Phase", *Science*, 294(5541),p.,348-351, 2001.

[85] Hong, B.H., J.Y. Lee, C.-W. Lee, J.C. Kim, S.C. Bae, and K.S. Kim, "Self-Assembled Arrays of Organic Nanotubes with Infinitely Long One-Dimensional H-Bond Chains", *Journal of the American Chemical Society*, 123(43),p.,10748-10749, 2001.

[86] Emrick*, T. and J.M.J. Fréchet, "Self-assembly of dendritic structures", *Current Opinion in Colloid & Interface Science*, 4(1),p.,15-23, 1999.

[87] Percec, V., A.E. Dulcey, V.S.K. Balagurusamy, Y. Miura, J. Smidrkal, M. Peterca, S. Nummelin, U. Edlund, S.D. Hudson, P.A. Heiney, H. Duan, S.N. Magonov, and S.A. Vinogradov, "Self-assembly of amphiphilic dendritic dipeptides into helical pores", *Nature*, 430(7001),p.,764-768, 2004.

[88] Zubarev, E.R., M.U. Pralle, E.D. Sone, and S.I. Stupp, "Self-Assembly of Dendron Rodcoil Molecules into Nanoribbons", *Journal of the American Chemical Society*, 123(17),p.,4105-4106, 2001.

[89] Messmore, B.W., J.F. Hulvat, E.D. Sone, and S.I. Stupp, "Synthesis, Self-Assembly, and Characterization of Supramolecular Polymers from Electroactive Dendron Rodcoil Molecules", *Journal of the American Chemical Society*, 126(44),p.,14452-14458, 2004.

[90] Zubarev, E.R., M.U. Pralle, E.D. Sone, and S.I. Stupp, "Scaffolding of Polymers by Supramolecular Nanoribbons", *Advanced Materials*, 14(3),p.,198-203, 2002.

[91] Frusawa, H., A. Fukagawa, Y. Ikeda, J. Araki, K. Ito, G. John, and T. Shimizu, "Aligning a Single-Lipid Nanotube with Moderate Stiffness13", *Angewandte Chemie International Edition*, 42(1),p.,72-74, 2003.

[92] Shimizu, T., "Self-assembled lipid nanotube hosts: The dimension control for encapsulation of nanometer-scale guest substances", *Journal of Polymer Science Part A: Polymer Chemistry*, 44(17),p.,5137-5152, 2006.

[93] Balbo Block, M.A., C. Kaiser, A. Khan, and S. Hecht, "Discrete Organic Nanotubes Based on a Combination of Covalent and Non-Covalent Approaches", Springer Berlin / Heidelberg. p. 89-150, 2005.

[94] Kameta, N., M. Masuda, H. Minamikawa, Y. Mishima, I. Yamashita, and T. Shimizu, "Functionalizable Organic Nanochannels Based on Lipid Nanotubes: Encapsulation and Nanofluidic Behavior of Biomacromolecules", *Chemistry of Materials*, 19(14),p.,3553-3560, 2007.

[95] Grimme, S., "Do Special Noncovalent pi-pi Stacking Interactions Really Exist?13", *Angewandte Chemie International Edition*, 47(18),p.,3430-3434, 2008.

[96] Moore, J.S., "Shape-Persistent Molecular Architectures of Nanoscale Dimension", *Accounts of Chemical Research*, 30(10),p.,402-413, 1997.

[97] Höger, S., "Highly efficient methods for the preparation of shape-persistent macrocyclics", *Journal of Polymer Science Part A: Polymer Chemistry*, 37(15),p.,2685-2698, 1999.

[98] Pasini, D. and M. Ricci, "Macrocycles as Precursors for Organic Nanotubes", *Current Organic Synthesis*, 4,p.,59-80, 2007.

[99] Zhao, D. and J.S. Moore, "Shape-persistent arylene ethynylene macrocycles: syntheses and supramolecular chemistry", *Chemical Communications*, (7),p.,807-818, 2003.

[100] Ni, B.-B., Q. Yan, Y. Ma, and D. Zhao, "Recent advances in arylene ethynylene folding systems: Toward functioning", *Coordination Chemistry Reviews*, 254(9-10),p.,954-971, 2010.

[101] Zang, L., Y. Che, and J.S. Moore, "One-Dimensional Self-Assembly of Planar π-Conjugated Molecules: Adaptable Building Blocks for Organic Nanodevices", *Accounts of Chemical Research*, 41(12),p.,1596-1608, 2008.

[102] Balakrishnan, K., A. Datar, W. Zhang, X. Yang, T. Naddo, J. Huang, J. Zuo, M. Yen, J.S. Moore, and L. Zang, "Nanofibril Self-Assembly of an Arylene Ethynylene Macrocycle", *Journal of the American Chemical Society*, 128(20),p.,6576-6577, 2006.

[103] Gong, B., A. Sanford, and J. Ferguson, "Enforced Folding of Unnatural Oligomers: Creating Hollow Helices with Nanosized Pores". p. 1-29, 2007.

[104] Helsel, A.J., A.L. Brown, K. Yamato, W. Feng, L. Yuan, A.J. Clements, S.V. Harding, G. Szabo, Z. Shao, and B. Gong, "Highly Conducting Transmembrane Pores Formed by Aromatic Oligoamide Macrocycles", *Journal of the American Chemical Society*, 130(47),p.,15784-15785, 2008.

[105] Engelkamp, H., S. Middelbeek, and R.J.M. Nolte, "Self-Assembly of Disk-Shaped Molecules to Coiled-Coil Aggregates with Tunable Helicity", *Science*, 284(5415),p.,785-788, 1999.

[106] Curtis, M.D., J. Cao, and J.W. Kampf, "Solid-State Packing of Conjugated Oligomers: From Ï€-Stacks to the Herringbone Structure", *Journal of the American Chemical Society*, 126(13),p.,4318-4328, 2004.

[107] Cornil, J., D. Beljonne, J.-P. Calbert, and J.-L. Brédas, "Interchain Interactions in Organic &pgr;-Conjugated Materials: Impact on Electronic Structure, Optical Response, and Charge Transport", *Advanced Materials*, 13(14),p.,1053-1067, 2001.

[108] Briseno, A.L., S.C.B. Mannsfeld, S.A. Jenekhe, Z. Bao, and Y. Xia, "Introducing organic nanowire transistors", *Materials Today*, 11(4),p.,38-47, 2008.

[109] Fages, F., J.A. Wytko, and J. Weiss, "Minireview: From molecular nanowires to molecular nanocables: Synthetic strategies and conducting properties", *Comptes Rendus Chimie*, 11(10),p.,1241-1253, 2008.

[110] Schenning, A.P.H.J. and E.W. Meijer, "Supramolecular electronics; nanowires from self-assembled [small pi]-conjugated systems", *Chemical Communications*, (26),p.,3245-3258, 2005.

[111] Xiao, S., J. Tang, T. Beetz, X. Guo, N. Tremblay, T. Siegrist, Y. Zhu, M. Steigerwald, and C. Nuckolls, "Transferring Self-Assembled, Nanoscale

Cables into Electrical Devices", *Journal of the American Chemical Society*, 128(33),p.,10700-10701, 2006.

[112] Hill, J.P., W. Jin, A. Kosaka, T. Fukushima, H. Ichihara, T. Shimomura, K. Ito, T. Hashizume, N. Ishii, and T. Aida, "Self-Assembled Hexa-peri-hexabenzocoronene Graphitic Nanotube", *Science*, 304(5676),p.,1481-1483, 2004.

[113] Bushey, M.L., T.-Q. Nguyen, and C. Nuckolls, "Synthesis, Self-Assembly, and Switching of One-Dimensional Nanostructures from New Crowded Aromatics", *Journal of the American Chemical Society*, 125(27),p.,8264-8269, 2003.

[114] Wang, C., Z. Wang, and X. Zhang, "Amphiphilic Building Blocks for Self-Assembly: From Amphiphiles to Supra-amphiphiles", *Accounts of Chemical Research*, 45(4),p.,608-618, 2012.

[115] Rodnikova, M.N., "A new approach to the mechanism of solvophobic interactions", *Journal of Molecular Liquids*, 136(3),p.,211-213, 2007.

[116] Hartgerink, J.D., E. Beniash, and S.I. Stupp, "Peptide-amphiphile nanofibers: A versatile scaffold for the preparation of self-assembling materials", *Proceedings of the National Academy of Sciences of the United States of America*, 99(8),p.,5133-5138, 2002.

[117] Xu, H., J. Wang, S. Han, J. Wang, D. Yu, H. Zhang, D. Xia, X. Zhao, T.A. Waigh, and J.R. Lu, "Hydrophobic-Region-Induced Transitions in Self-Assembled Peptide Nanostructuresâ€ ", *Langmuir*, 25(7),p.,4115-4123, 2008.

[118] Cavalli, S. and A. Kros, "Scope and Applications of Amphiphilic Alkyl- and Lipopeptides", *Advanced Materials*, 20(3),p.,627-631, 2008.

[119] Meijer, J.T., M. Roeters, V. Viola, D.W.P.M. Löwik, G. Vriend, and J.C.M. van Hest, "Stabilization of Peptide Fibrils by Hydrophobic Interaction", *Langmuir*, 23(4),p.,2058-2063, 2006.

[120] Kokkoli, E., A. Mardilovich, A. Wedekind, E.L. Rexeisen, A. Garg, and J.A. Craig, "Self-assembly and applications of biomimetic and bioactive peptide-amphiphiles", *Soft Matter*, 2(12),p.,1015-1024, 2006.

[121] Cui, H., M.J. Webber, and S.I. Stupp, "Self-assembly of peptide amphiphiles: From molecules to nanostructures to biomaterials", *Peptide Science*, 94(1),p.,1-18, 2010.

[122] Won, Y.-Y., H.T. Davis, and F.S. Bates, "Giant Wormlike Rubber Micelles", *Science*, 283(5404),p.,960-963, 1999.

[123] Elgersma, R.C., T. Meijneke, G. Posthuma, D.T.S. Rijkers, and R.M.J. Liskamp, "Self-Assembly of Amylin(20-29) Amide-Bond Derivatives into Helical Ribbons and Peptide Nanotubes rather than Fibrils", *Chemistry - A European Journal*, 12(14),p.,3714-3725, 2006.

[124] Hoppener, J.W.M., B. Ahren, and C.J.M. Lips, "Islet Amyloid and Type 2 Diabetes Mellitus", *N Engl J Med*, 343(6),p.,411-419, 2000.

[125] Westermark, P., U. Engström, K.H. Johnson, G.T. Westermark, and C. Betsholtz, "Islet amyloid polypeptide: pinpointing amino acid residues linked

to amyloid fibril formation", *Proceedings of the National Academy of Sciences of the United States of America*, 87(13),p.,5036-5040, 1990.

[126] Zhang, J., H. Liu, Z. Wang, and N. Ming, "Synthesis of high purity Au nanobelts via the one-dimensional self-assembly of triangular Au nanoplates", *Applied Physics Letters*, 91(13),p.,133112-3, 2007.

[127] Nicolosi, V., P.D. Nellist, S. Sanvito, E.C. Cosgriff, S. Krishnamurthy, W.J. Blau, M.L.H. Green, D. Vengust, D. Dvorsek, D. Mihailovic, G. Compagnini, J. Sloan, V. Stolojan, J.D. Carey, S.J. Pennycook, and J.N. Coleman, "Observation of van der Waals Driven Self-Assembly of MoSI Nanowires into a Low-Symmetry Structure Using Aberration-Corrected Electron Microscopy", *Advanced Materials*, 19(4),p.,543-547, 2007.

[128] MacPhee, C.E. and D.N. Woolfson, "Engineered and designed peptide-based fibrous biomaterials", *Current Opinion in Solid State and Materials Science*, 8(2),p.,141-149, 2004.

[129] Zhao, Y.S., H. Fu, A. Peng, Y. Ma, D. Xiao, and J. Yao, "Low-Dimensional Nanomaterials Based on Small Organic Molecules: Preparation and Optoelectronic Properties", *Advanced Materials*, 20(15),p.,2859-2876, 2008.

[130] Banerjee, P., I. Perez, L. Henn-Lecordier, S.B. Lee, and G.W. Rubloff, "Nanotubular metal-insulator-metal capacitor arrays for energy storage", *Nat Nano*, 4(5),p.,292-296, 2009.

[131] Wang, C.-J. and L. Lin, "Nanoscale waveguiding methods", *Nanoscale Research Letters*, 2(5),p.,219-229, 2007.

[132] Gazit, E., "Self Assembly of Short Aromatic Peptides into Amyloid Fibrils and Related Nanostructures", *Prion*, 1(1),p.,32-35, 2007.

[133] Gilead, S. and E. Gazit, "Self-organization of short peptide fragments: From amyloid fibrils to nanoscale supramolecular assemblies", *Supramolecular Chemistry*, 17(1-2),p.,87-92, 2005.

[134] Harper, J.D. and P.T. Lansbury, "Models of amyloid seeding in Alzheimer's disease and scrapie: mechanistic truths and physiological consequences of the time-dependent solubility of amyloid proteins", *Annual review of biochemistry*, 66,p.,385-407, 1997.

[135] Gazit, E., "A possible role for pi-stacking in the self-assembly of amyloid fibrils", *FASEB journal : official publication of the Federation of American Societies for Experimental Biology*, 16(1),p.,77-83, 2002.

[136] Parkin, I.P., "Supramolecular chemistry. J.W. Steed and J.L. Atwood. John Wiley & Sons Ltd, Chichester, 2000. xxvii + 745 pages. £29.95 (paperback). ISBN 0-471-98791-3", *Applied Organometallic Chemistry*, 15(3),p.,236, 2001.

[137] Mazor, Y., S. Gilead, I. Benhar, and E. Gazit, "Identification and Characterization of a Novel Molecular-recognition and Self-assembly Domain within the Islet Amyloid Polypeptide", *Journal of Molecular Biology*, 322(5),p.,1013-1024, 2002.

[138] Gazit, E., "A possible role for {pi}-stacking in the self-assembly of amyloid fibrils", *FASEB J.*, 16(1),p.,77-83, 2002.

[139] Xu, X.-D., C.-S. Chen, B. Lu, S.-X. Cheng, X.-Z. Zhang, and R.-X. Zhuo, "Coassembly of Oppositely Charged Short Peptides into Well-Defined Supramolecular Hydrogels", *The Journal of Physical Chemistry B*, 114(7),p.,2365-2372, 2010.

[140] Kubelka, J. and T.A. Keiderling, "Differentiation of β-Sheet-Forming Structures: Ab Initio-Based Simulations of IR Absorption and Vibrational CD for Model Peptide and Protein β-Sheets", *Journal of the American Chemical Society*, 123(48),p.,12048-12058, 2001.

[141] Pashuck, E.T., H. Cui, and S.I. Stupp, "Tuning Supramolecular Rigidity of Peptide Fibers through Molecular Structure", *Journal of the American Chemical Society*, 132(17),p.,6041-6046, 2010.

[142] Ding, L., K. Chen, P.A. Santini, Z. Shi, and N.R. Kallenbach, "The Pentapeptide GGAGG Has PII Conformation", *Journal of the American Chemical Society*, 125(27),p.,8092-8093, 2003.

[143] Liu, Z., K. Chen, A. Ng, Z. Shi, R.W. Woody, and N.R. Kallenbach, "Solvent Dependence of PII Conformation in Model Alanine Peptides", *Journal of the American Chemical Society*, 126(46),p.,15141-15150, 2004.

[144] bagi, K., nacute, ska, J. Makowska, Wies, Lstrok, a. Wiczk, F. Kasprzykowski, L. Chmurzy, and SKI, "Conformational studies of alanine-rich peptide using CD and FTIR spectroscopy", *Journal of Peptide Science*, 14(3),p.,283-289, 2008.

[145] Shi, Z., C.A. Olson, G.D. Rose, R.L. Baldwin, and N.R. Kallenbach, "Polyproline II structure in a sequence of seven alanine residues", *Proceedings of the National Academy of Sciences of the United States of America*, 99(14),p.,9190-9195, 2002.

[146] Spek, E.J., C.A. Olson, Z. Shi, and N.R. Kallenbach, "Alanine Is an Intrinsic α-Helix Stabilizing Amino Acid", *Journal of the American Chemical Society*, 121(23),p.,5571-5572, 1999.

[147] Han, T.H., J. Kim, J.S. Park, C.B. Park, H. Ihee, and S.O. Kim, "Liquid Crystalline Peptide Nanowires", *Advanced Materials*, 19(22),p.,3924-3927, 2007.

[148] Borner, H.G., B.M. Smarsly, J. Hentschel, A. Rank, R. Schubert, Y. Geng, D.E. Discher, T. Hellweg, and A. Brandt, "Organization of Self-Assembled Peptide−Polymer Nanofibers in Solution", *Macromolecules*, 41(4),p.,1430-1437, 2008.

[149] Pomerantz, William C., Virany M. Yuwono, Claire L. Pizzey, Jeffery D. Hartgerink, Nicholas L. Abbott, and Samuel H. Gellman, "Nanofibers and Lyotropic Liquid Crystals from a Class of Self-Assembling beta-Peptides13", *Angewandte Chemie International Edition*, 47(7),p.,1241-1244, 2008.

[150] Hamley, I.W., "Liquid crystal phase formation by biopolymers", *Soft Matter*, 6(9),p.,1863-1863, 2010.

[151] Krimm, S. and J. Bandekar, "Advances in Protein Chemistry. Vol. 38", *Academic Press, Orlando, FL*,p.,181, 1986.

[152] Chirgadze, Y.N., E. Brazhnikov, and N. Nevskaya, "Intramolecular distortion of the α-helical structure of polypeptides", *Journal of Molecular Biology*, 102(4),p.,781-792, 1976.

[153] Doyle, B.B., E.G. Bendit, and E.R. Blout, "Infrared spectroscopy of collagen and collagen-like polypeptides", *Biopolymers*, 14(5),p.,937-957, 1975.

[154] Chang, M.C. and J. Tanaka, "FT-IR study for hydroxyapatite/collagen nanocomposite cross-linked by glutaraldehyde", *Biomaterials*, 23(24),p.,4811-4818, 2002.

[155] Haris, P.I. and F. Severcan, "FTIR spectroscopic characterization of protein structure in aqueous and non-aqueous media", *Journal of Molecular Catalysis B: Enzymatic*, 7(1-4),p.,207-221, 1999.

[156] Barth, A., "The infrared absorption of amino acid side chains", *Progress in Biophysics and Molecular Biology*, 74(3-5),p.,141-173, 2000.

[157] Murphy, K.P., ed. "Protein structure, stability, and folding". Methods in molecular biology, ed. J.M. Walker, Humana Press: Totowa, New Jersey, 2001.

[158] Krysmann, M.J., V. Castelletto, A. Kelarakis, I.W. Hamley, R.A. Hule, and D.J. Pochan, "Self-Assembly and Hydrogelation of an Amyloid Peptide Fragment", *Biochemistry*, 47(16),p.,4597-4605, 2008.

[159] Krysmann, M.J., V. Castelletto, J.E. McKendrick, L.A. Clifton, I.W. Hamley, P.J.F. Harris, and S.M. King, "Self-Assembly of Peptide Nanotubes in an Organic Solvent", *Langmuir*, 24(15),p.,8158-8162, 2008.

[160] Yoo, H., J. Yang, A. Yousef, M.R. Wasielewski, and D. Kim, "Excimer Formation Dynamics of Intramolecular π-Stacked Perylenediimides Probed by Single-Molecule Fluorescence Spectroscopy", *Journal of the American Chemical Society*, 132(11),p.,3939-3944, 2010.

[161] Yang, X., H. Tang, K. Cao, H. Song, W. Sheng, and Q. Wu, "Templated-assisted one-dimensional silica nanotubes: synthesis and applications", *Journal of Materials Chemistry*, 21(17),p.,6122-6135, 2011.

[162] Fan, R., Y. Wu, D. Li, M. Yue, A. Majumdar, and P. Yang, "Fabrication of Silica Nanotube Arrays from Vertical Silicon Nanowire Templates", *Journal of the American Chemical Society*, 125(18),p.,5254-5255, 2003.

[163] Piao, Y., A. Burns, J. Kim, U. Wiesner, and T. Hyeon, "Inside Front Cover: Designed Fabrication of Silica-Based Nanostructured Particle Systems for Nanomedicine Applications (Adv. Funct. Mater. 23/2008)", *Advanced Functional Materials*, 18(23),p.,n/a-n/a, 2008.

[164] Rao, C.N.R. and A. Govindaraj, "Synthesis of Inorganic Nanotubes", *Advanced Materials*, 21(42),p.,4208-4233, 2009.

[165] Liu, Y.-H., Y.-Y. Tsai, H.-J. Chien, C.-Y. Chen, Y.-F. Huang, J.-S. Chen, Y.-C. Wu, and C.-C. Chen, "Quantum-dot-embedded silica nanotubes as nanoprobes for simple and sensitive DNA detection", *Nanotechnology*, 22(15),p.,155102-155108, 2011.

[166] Yu, J., X. Bai, J. Suh, S.B. Lee, and S.J. Son, "Mechanical Capping of Silica Nanotubes for Encapsulation of Molecules", *Journal of the American Chemical Society*, 131(43),p.,15574-15575, 2009.

[167] Kim, M., J. Hong, J. Lee, C.K. Hong, and S.E. Shim, "Fabrication of silica nanotubes using silica coated multi-walled carbon nanotubes as the template", *Journal of Colloid and Interface Science*, 322(1),p.,321-326, 2008.

[168] Tsung-Wu, L. and S. Hsin-Hui, "The synthesis of silica nanotubes through chlorosilanization of single wall carbon nanotubes", *Nanotechnology*, 21(36),p.,365604, 2010.

[169] Chen, Y.J., X.Y. Xue, and T.H. Wang, "Large-scale controlled synthesis of silica nanotubes using zinc oxide nanowires as templates", *Nanotechnology*, 16(9),p.,1978-1982, 2005.

[170] Zhu, J., H. Peng, S.T. Connor, and Y. Cui, "Three-Dimensional Interconnected Silica Nanotubes Templated from Hyperbranched Nanowires", *Small*, 5(4),p.,437-439, 2009.

[171] Obare, S.O., N.R. Jana, and C.J. Murphy, "Preparation of Polystyrene- and Silica-Coated Gold Nanorods and Their Use as Templates for the Synthesis of Hollow Nanotubes", *Nano Letters*, 1(11),p.,601-603, 2001.

[172] Adachi, M., T. Harada, and M. Harada, "Formation of Huge Length Silica Nanotubes by a Templating Mechanism in the Laurylamine/Tetraethoxysilane System", *Langmuir*, 15(21),p.,7097-7100, 1999.

[173] Adachi, M., T. Harada, and M. Harada, "Formation Processes of Silica Nanotubes through a Surfactant-Assisted Templating Mechanism in Laurylamine Hydrochloride/Tetraethoxysilane System", *Langmuir*, 16(5),p.,2376-2384, 2000.

[174] Yuwono, V.M. and J.D. Hartgerink, "Peptide Amphiphile Nanofibers Template and Catalyze Silica Nanotube Formation", *Langmuir*, 23(9),p.,5033-5038, 2007.

[175] Jung, J.H., S. Shinkai, and T. Shimizu, "Preparation of Mesoscale and Macroscale Silica Nanotubes Using a Sugar-Appended Azonaphthol Gelator Assembly", *Nano Letters*, 2(1),p.,17-20, 2002.

[176] Yamanaka, M., Y. Miyake, S. Akita, and K. Nakano, "Sol–Gel Transcription of Semi-Fluorinated Organogel Fiber into Fluorocarbon-Functionalized Silica Nanotubes", *Chemistry of Materials*, 20(6),p.,2072-2074, 2008.

[177] Xie, C., B. Liu, Z. Wang, D. Gao, G. Guan, and Z. Zhang, "Molecular Imprinting at Walls of Silica Nanotubes for TNT Recognition", *Analytical Chemistry*, 80(2),p.,437-443, 2007.

[178] Pearson, R.G., "Hard and soft acids and bases, HSAB, part 1: Fundamental principles", *Journal of Chemical Education*, 45(9),p.,581, 1968.

[179] Acar, H., R. Garifullin, and M.O. Guler, "Self-Assembled Template-Directed Synthesis of One-Dimensional Silica and Titania Nanostructures", *Langmuir*, 27(3),p.,1079-1084, 2011.

[180] McQuade, D.T., A.E. Pullen, and T.M. Swager, "Conjugated Polymer-Based Chemical Sensors", *Chemical Reviews*, 100(7),p.,2537-2574, 2000.

[181] Nie, H., Y. Zhao, M. Zhang, Y. Ma, M. Baumgarten, and K. Mullen, "Detection of TNT explosives with a new fluorescent conjugated polycarbazole polymer", *Chemical Communications*, 47(4),p.,1234-1236, 2011.

[182] Rose, A., Z. Zhu, C.F. Madigan, T.M. Swager, and V. Bulovic, "Sensitivity gains in chemosensing by lasing action in organic polymers", *Nature*, 434(7035),p.,876-879, 2005.

[183] Toal, S.J. and W.C. Trogler, "Polymer sensors for nitroaromatic explosives detection", *Journal of Materials Chemistry*, 16(28),p.,2871-2883, 2006.

[184] Yang, Y., H. Wang, K. Su, Y. Long, Z. Peng, N. Li, and F. Liu, "A facile and sensitive fluorescent sensor using electrospun nanofibrous film for nitroaromatic explosive detection", *Journal of Materials Chemistry*, 21(32),p.,11895-11900, 2011.

[185] Naddo, T., Y. Che, W. Zhang, K. Balakrishnan, X. Yang, M. Yen, J. Zhao, J.S. Moore, and L. Zang, "Detection of Explosives with a Fluorescent Nanofibril Film", *Journal of the American Chemical Society*, 129(22),p.,6978-6979, 2007.

[186] Zhang, C., Y. Che, X. Yang, B.R. Bunes, and L. Zang, "Organic nanofibrils based on linear carbazole trimer for explosive sensing", *Chemical Communications*, 46(30),p.,5560-5562, 2010.

[187] Tao, S., G. Li, and H. Zhu, "Metalloporphyrins as sensing elements for the rapid detection of trace TNT vapor", *Journal of Materials Chemistry*, 16(46),p.,4521-4521, 2006.

[188] Tao, S., Z. Shi, G. Li, and P. Li, "Hierarchically Structured Nanocomposite Films as Highly Sensitive Chemosensory Materials for TNT Detection", *ChemPhysChem*, 7(9),p.,1902-1905, 2006.

[189] Yildirim, A., H. Budunoglu, H. Deniz, M. O. Guler, and M. Bayindir, "Template-Free Synthesis of Organically Modified Silica Mesoporous Thin Films for TNT Sensing", *ACS Applied Materials & Interfaces*, 2(10),p.,2892-2897, 2010.

[190] Fang, Q., J. Geng, B. Liu, D. Gao, F. Li, Z. Wang, G. Guan, and Z. Zhang, "Inverted Opal Fluorescent Film Chemosensor for the Detection of Explosive Nitroaromatic Vapors through Fluorescence Resonance Energy Transfer", *Chemistry – A European Journal*, 15(43),p.,11507-11514, 2009.

[191] Gao, D., Z. Wang, B. Liu, L. Ni, M. Wu, and Z. Zhang, "Resonance energy transfer-amplifying fluorescence quenching at the surface of silica nanoparticles toward ultrasensitive detection of TNT", *Analytical chemistry*, 80(22),p.,8545-53, 2008.

[192] Stöber, W., A. Fink, and E. Bohn, "Controlled growth of monodisperse silica spheres in the micron size range", *Journal of Colloid and Interface Science*, 26(1),p.,62-69, 1968.

[193] Venkateswara Rao, A. and S.D. Bhagat, "Synthesis and physical properties of TEOS-based silica aerogels prepared by two step (acid-base) sol-gel process", *Solid State Sciences*, 6(9),p.,945-952, 2004.

[194] Kang, S., S.I. Hong, C.R. Choe, M. Park, S. Rim, and J. Kim, "Preparation and characterization of epoxy composites filled with functionalized nanosilica particles obtained via sol-gel process", *Polymer*, 42(3),p.,879-887, 2001.

[195] Finsy, R., "On the Critical Radius in Ostwald Ripening", *Langmuir*, 20(7),p.,2975-2976, 2004.

[196] Wilson, G.J., A.S. Matijasevich, D.R.G. Mitchell, J.C. Schulz, and G.D. Will, "Modification of TiO2 for Enhanced Surface Properties: Finite Ostwald Ripening by a Microwave Hydrothermal Process", *Langmuir*, 22(5),p.,2016-2027, 2006.

[197] Ratke, L. and P.W. Voorhees, "Growth and Coarsening Ostwald Ripening in Material Processing", 2002.

[198] Tsantilis, S., H. Briesen, and S.E. Pratsinis, "Sintering Time for Silica Particle Growth", *Aerosol Science and Technology*, 34(3),p.,237 - 246, 2001.

[199] Xiong, Y., M. Kamal Akhtar, and S.E. Pratsinis, "Formation of agglomerate particles by coagulation and sintering--Part II. The evolution of the morphology of aerosol-made titania, silica and silica-doped titania powders", *Journal of Aerosol Science*, 24(3),p.,301-313, 1993.

[200] Yang, J.-S. and T.M. Swager, "Fluorescent Porous Polymer Films as TNT Chemosensors: Electronic and Structural Effects", *Journal of the American Chemical Society*, 120(46),p.,11864-11873, 1998.

[201] Kageyama, K., J.-i. Tamazawa, and T. Aida, "Extrusion Polymerization: Catalyzed Synthesis of Crystalline Linear Polyethylene Nanofibers Within a Mesoporous Silica", *Science*, 285(5436),p.,2113-2115, 1999.

[202] Mitchell, D.T., S.B. Lee, L.c.m. Trofin, N. Li, T.K. Nevanen, H. Soderlund, and C.R. Martin, "Smart Nanotubes for Bioseparations and Biocatalysis", *Journal of the American Chemical Society*, 124(40),p.,11864-11865, 2002.

[203] Guler, M.O., H. Acar, R. Genc, T.S. Erkal, M. Urel, and A. Dana, "Self-Assembled Peptide Nanofiber Templated One-Dimensional Gold Nanostructures Exhibiting Resistive Switching", *Langmuir*, 2012.

[204] Acar, H., R. Garifullin, and M.O. Guler, "Self-assembled template-directed synthesis of one-dimensional silica and titania nanostructures", *Langmuir*, 27(3),p.,1079-84, 2011.

[205] Tamamis, P., L. Adler-Abramovich, M. Reches, K. Marshall, P. Sikorski, L. Serpell, E. Gazit, and G. Archontis, "Self-assembly of phenylalanine oligopeptides: insights from experiments and simulations", *Biophys J*, 96(12),p.,5020-9, 2009.

[206] Yildirim, A., H. Acar, T.S. Erkal, M. Bayindir, and M.O. Guler, "Template-directed synthesis of silica nanotubes for explosive detection", *ACS applied materials & interfaces*, 3(10),p.,4159-64, 2011.

[207] Bolisetty, S., J. Adamcik, J. Heier, and R. Mezzenga, "Amyloid Directed Synthesis of Titanium Dioxide Nanowires and Their Applications in Hybrid Photovoltaic Devices", *Advanced Functional Materials*, 22(16),p.,3424-3428, 2012.

[208] Chen, X. and S.S. Mao, "Titanium Dioxide Nanomaterials:Synthesis, Properties, Modifications, and Applications", *Chemical Reviews*, 107(7),p.,2891-2959, 2007.

[209] Hardin, B.E., H.J. Snaith, and M.D. McGehee, "The renaissance of dye-sensitized solar cells", *Nature Photonics*, 6(3),p.,162-169, 2012.

[210] Karthikeyan, C., M. Thelakkat, and M. Willert-Porada, "Different mesoporous titania films for solid-state dye sensitised solar cells", *Thin Solid Films*, 511,p.,187-194, 2006.

[211] Kim, Y.J., M.H. Lee, H.J. Kim, G. Lim, Y.S. Choi, N.-G. Park, K. Kim, and W.I. Lee, "Formation of Highly Efficient Dye-Sensitized Solar Cells by Hierarchical Pore Generation with Nanoporous TiO 2 Spheres", *Advanced Materials*, 21(36),p.,3668-3673, 2009.

[212] Schlichthörl, G., S. Huang, J. Sprague, and A. Frank, "Band edge movement and recombination kinetics in dye-sensitized nanocrystalline TiO2 solar cells: a study by intensity modulated photovoltage spectroscopy", *The Journal of Physical Chemistry B*, 101(41),p.,8141-8155, 1997.

[213] Son, H.-J., X. Wang, C. Prasittichai, N.C. Jeong, T. Aaltonen, R.G. Gordon, and J.T. Hupp, "Glass-Encapsulated Light Harvesters: More Efficient Dye-

Sensitized Solar Cells by Deposition of Self-Aligned, Conformal, and Self-Limited Silica Layers", *Journal of the American Chemical Society,* 134(23),p.,9537-9540, 2012.

[214] Grätzel, M., "Recent advances in sensitized mesoscopic solar cells", *Accounts of chemical research,* 42(11),p.,1788-98, 2009.

[215] Feng, X., K. Shankar, M. Paulose, and C.A. Grimes, "Tantalum-Doped Titanium Dioxide Nanowire Arrays for Dye-Sensitized Solar Cells with High Open-Circuit Voltage", *Angewandte Chemie,* 121(43),p.,8239-8242, 2009.

[216] Liu, B. and E.S. Aydil, "Growth of oriented single-crystalline rutile TiO(2) nanorods on transparent conducting substrates for dye-sensitized solar cells", *Journal of the American Chemical Society,* 131(11),p.,3985-90, 2009.

[217] Zhu, K., N.R. Neale, A. Miedaner, and A.J. Frank, "Enhanced charge-collection efficiencies and light scattering in dye-sensitized solar cells using oriented TiO2 nanotubes arrays", *Nano letters,* 7(1),p.,69-74, 2007.

[218] Varghese, O.K., M. Paulose, and C.a. Grimes, "Long vertically aligned titania nanotubes on transparent conducting oxide for highly efficient solar cells", *Nature nanotechnology,* 4(9),p.,592-7, 2009.

[219] Rurack, K. and R. Martínez-Máñez, "The Supramolecular Chemistry of Organic-Inorganic Hybrid Materials": Wiley.2010.

[220] Wang, Z.-S., H. Kawauchi, T. Kashima, and H. Arakawa, "Significant influence of TiO2 photoelectrode morphology on the energy conversion

efficiency of N719 dye-sensitized solar cell", *Coordination Chemistry Reviews*, 248(13-14),p.,1381-1389, 2004.

[221] Hočevar, M., M. Berginc, M. Topič, and U.O. Krašovec, "Sponge-like TiO2 layers for dye-sensitized solar cells", *Journal of SolGel Science and Technology*, 53(3),p.,647-654, 2010.

[222] González-García, L., I. González-Valls, M. Lira-Cantu, A. Barranco, and A.R. González-Elipe, "Aligned TiO2 nanocolumnar layers prepared by PVD-GLAD for transparent dye sensitized solar cells", *Energy Environmental Science*, 2011.

[223] Zhang, Y. and L. Jiang, "Easily preparation of high yield anatase TiO 2 crystals by adding a wonderful additive", *Journal of Physics: Conference Series*, 188(1),p.,012004, 2009.

[224] Djerdj, I. and A.M. Tonejc, "Structural investigations of nanocrystalline TiO2 samples", *Journal of Alloys and Compounds*, 413(1-2),p.,159-174, 2006.

[225] Zhang, J., M. Li, Z. Feng, J. Chen, and C. Li, "UV Raman Spectroscopic Study on TiO2. I. Phase Transformation at the Surface and in the Bulk", *The Journal of Physical Chemistry B*, 110(2),p.,927-935, 2005.

[226] Zhang, J., Q. Xu, M. Li, Z. Feng, and C. Li, "UV Raman Spectroscopic Study on TiO2. II. Effect of Nanoparticle Size on the Outer/Inner Phase Transformations", *The Journal of Physical Chemistry C*, 113(5),p.,1698-1704, 2009.

[227] O'Regan, B. and M. Grätzel, "A low-cost, high-efficiency solar cell based on dye-sensitized colloidal TiO2 films", *Nature*, 353(6346),p.,737-740, 1991.

[228] Katoh, R., K. Yaguchi, and A. Furube, "Effect of dye concentration on electron injection efficiency in nanocrystalline TiO2 films sensitized with N719 dye", *Chemical Physics Letters*, 511(4–6),p.,336-339, 2011.

[229] Wenger, B., M. Grätzel, and J.-E. Moser, "Rationale for Kinetic Heterogeneity of Ultrafast Light-Induced Electron Transfer from Ru(II) Complex Sensitizers to Nanocrystalline TiO2", *Journal of the American Chemical Society*, 127(35),p.,12150-12151, 2005.

[230] Nazeeruddin, M.K., R. Humphry-Baker, P. Liska, and M. Grätzel, "Investigation of Sensitizer Adsorption and the Influence of Protons on Current and Voltage of a Dye-Sensitized Nanocrystalline TiO2 Solar Cell", *The Journal of Physical Chemistry B*, 107(34),p.,8981-8987, 2003.

[231] Ghadiri, E., N. Taghavinia, S.M. Zakeeruddin, M. Gra¨tzel¸ and J.-E. Moser, "Enhanced Electron Collection Efficiency in Dye-Sensitized Solar Cells Based on Nanostructured TiO2 Hollow Fibers", *Nano Letters*, 10(5),p.,1632-1638, 2010.

[232] Eustis, S. and M.A. el-Sayed, "Why gold nanoparticles are more precious than pretty gold: noble metal surface plasmon resonance and its enhancement of the radiative and nonradiative properties of nanocrystals of different shapes", *Chemical Society reviews*, 35(3),p.,209-17, 2006.

[233] Correa-Duarte, M.A. and L.M. Liz-Marzán, "Carbon nanotubes as templates for one-dimensional nanoparticle assemblies", *Journal of Materials Chemistry*, 16(1),p.,22-25, 2006.

[234] Yuwono, V.M. and J.D. Hartgerink, "Peptide amphiphile nanofibers template and catalyze silica nanotube formation", *Langmuir : the ACS journal of surfaces and colloids*, 23(9),p.,5033-8, 2007.

[235] Mirkin, C.A., R.L. Letsinger, R.C. Mucic, and J.J. Storhoff, "A DNA-based method for rationally assembling nanoparticles into macroscopic materials", *Nature*, 382(6592),p.,607-9, 1996.

[236] Toksoz, S., H. Acar, and M.O. Guler, "Self-assembled one-dimensional soft nanostructures", *Soft Matter*, 6(23),p.,5839-5849, 2010.

[237] Mack, C., B. Wilhelmi, J.R. Duncan, and J.E. Burgess, "Biosorption of precious metals", *Biotechnology advances*, 25(3),p.,264-71, 2007.

[238] Wilms, M., J. Conrad, K. Vasilev, M. Kreiter, and G. Wegner, "Manipulation and conductivity measurements of gold nanowires", *Applied Surface Science*, 238(1-4),p.,490-494, 2004.

[239] Gole, A. and C.J. Murphy, "Seed-Mediated Synthesis of Gold Nanorods: Role of the Size and Nature of the Seed", *Chemistry of Materials*, 16(19),p.,3633-3640, 2004.

[240] Chen, W., H.-H. Deng, L. Hong, Z.-Q. Wu, S. Wang, A.-L. Liu, X.-H. Lin, and X.-H. Xia, "Bare gold nanoparticles as facile and sensitive colorimetric probe for melamine detection", *Analyst*, 2012.

[241] Joshi, H., P.S. Shirude, V. Bansal, K.N. Ganesh, and M. Sastry, "Isothermal Titration Calorimetry Studies on the Binding of Amino Acids to Gold Nanoparticles", *The Journal of Physical Chemistry B*, 108(31),p.,11535-11540, 2004.

[242] Lotfi Zadeh Zhad, H.R., F. Aboufazeli, O. Sadeghi, V. Amani, E. Najafi, and N. Tavassoli, "Tris(2-Aminoethyl)Amine-Functionalized Fe3O4 Magnetic Nanoparticles as a Selective Sorbent for Separation of Silver and Gold Ions in Different pHs", *Journal of Chemistry*, 2013,p.,7, 2013.

[243] Ayyappan, S., R.S. Gopalan, G.N. Subbanna, and C.N.R. Rao, "Nanoparticles of Ag, Au, Pd, and Cu produced by alcohol reduction of the salts", *Journal of Materials Research*, 12(02),p.,398-401, 1997.

[244] Liao, J., "Linear aggregation of gold nanoparticles in ethanol", *Colloids and Surfaces A: Physicochemical and Engineering Aspects*, 223(1-3),p.,177-183, 2003.

[245] Tanahashi, I. and T. Tohda, "Photoinduced Formation of Small Gold Particles in Silica Gels", *Journal of the American Ceramic Society*, 79(3),p.,796-798, 2005.

[246] Lin, S., M. Li, E. Dujardin, C. Girard, and S. Mann, "One-Dimensional Plasmon Coupling by Facile Self-Assembly of Gold Nanoparticles into Branched Chain Networks", *Advanced Materials*, 17(21),p.,2553-2559, 2005.

[247] Gray, H.B. and C.J. Ballhausen, "A Molecular Orbital Theory for Square Planar Metal Complexes", *Journal of the American Chemical Society*, 85(3),p.,260-265, 1963.

[248] Jana, N.R., L. Gearheart, and C.J. Murphy, "Evidence for Seed-Mediated Nucleation in the Chemical Reduction of Gold Salts to Gold Nanoparticles", *Chemistry of Materials*, 13(7),p.,2313-2322, 2001.

[249] Jana, N.R., L. Gearheart, and C.J. Murphy, "Wet Chemical Synthesis of High Aspect Ratio Cylindrical Gold Nanorods", *The Journal of Physical Chemistry B*, 105(19),p.,4065-4067, 2001.

[250] Jana, N.R., L. Gearheart, and C.J. Murphy, "Seeding Growth for Size Control of 5–40 nm Diameter Gold Nanoparticles", *Langmuir*, 17(22),p.,6782-6786, 2001.

[251] Kaufman, L.J., C.P. Brangwynne, K.E. Kasza, E. Filippidi, V.D. Gordon, T.S. Deisboeck, and D.A. Weitz, "Glioma expansion in collagen I matrices: analyzing collagen concentration-dependent growth and motility patterns", *Biophysical journal*, 89(1),p.,635-50, 2005.

[252] Branco, M.C., D.J. Pochan, N.J. Wagner, and J.P. Schneider, "Macromolecular diffusion and release from self-assembled beta-hairpin peptide hydrogels", *Biomaterials*, 30(7),p.,1339-1347, 2009.

[253] Yang, Y.-L., L.M. Leone, and L.J. Kaufman, "Elastic moduli of collagen gels can be predicted from two-dimensional confocal microscopy", *Biophysical journal*, 97(7),p.,2051-60, 2009.

[254] Sinha, A.K., M. Basu, S. Sarkar, M. Pradhan, and T. Pal, "Electrostatic field force directed gold nanowires from anion exchange resin", *Langmuir : the ACS journal of surfaces and colloids,* 26(22),p.,17419-26, 2010.

[255] Zhang, T., W. Wang, D. Zhang, X. Zhang, Y. Ma, Y. Zhou, and L. Qi, "Biotemplated Synthesis of Gold Nanoparticle-Bacteria Cellulose Nanofiber Nanocomposites and Their Application in Biosensing", *Advanced Functional Materials,* 20(7),p.,1152-1160, 2010.

[256] Bromley, K.M., A.J. Patil, A.W. Perriman, G. Stubbs, and S. Mann, "Preparation of high quality nanowires by tobacco mosaic virus templating of gold nanoparticles", *Journal of Materials Chemistry,* 18(40),p.,4796-4801, 2008.

[257] Zhang, G., B. Keita, R.N. Biboum, F. Miserque, P. Berthet, A. Dolbecq, P. Mialane, L. Catala, and L. Nadjo, "Synthesis of various crystalline gold nanostructures in water: The polyoxometalate [small beta]-[H4PMo12O40]3- as the reducing and stabilizing agent", *Journal of Materials Chemistry,* 19(45),p.,8639-8644, 2009.

[258] Borsook, H., H.W. Davenport, C.E.P. Jeffreys, and R.C. Warner. American Society of Biological Chemists, 1937.

[259] Zhong, Z., S. Patskovskyy, P. Bouvrette, J.H.T. Luong, and A. Gedanken, "The Surface Chemistry of Au Colloids and Their Interactions with Functional Amino Acids", *The Journal of Physical Chemistry B,* 108(13),p.,4046-4052, 2004.

[260] Borsook, H. and G. Keighley, "Oxidation-Reduction Potential of Ascorbic Acid (Vitamin C)", *Proceedings of the National Academy of Sciences of the United States of America*, 19(9),p.,875-8, 1933.

[261] Qin, Y., X. Ji, J. Jing, H. Liu, H. Wu, and W. Yang, "Size control over spherical silver nanoparticles by ascorbic acid reduction", *Colloids and Surfaces A: Physicochemical and Engineering Aspects*, 372(1-3),p.,172-176, 2010.

[262] Huang, C.-C., Z. Yang, and H.-T. Chang, "Synthesis of dumbbell-shaped Au-Ag core-shell nanorods by seed-mediated growth under alkaline conditions", *Langmuir : the ACS journal of surfaces and colloids*, 20(15),p.,6089-92, 2004.

[263] Reed, M.A., C. Zhou, C.J. Muller, T.P. Burgin, and J.M. Tour, "Conductance of a Molecular Junction", *Science*, 278(5336),p.,252-254, 1997.

[264] Lee, P., J. Lee, H. Lee, J. Yeo, S. Hong, K.H. Nam, D. Lee, S.S. Lee, and S.H. Ko, "Highly Stretchable and Highly Conductive Metal Electrode by Very Long Metal Nanowire Percolation Network", *Advanced Materials*, 24(25),p.,3326-3332, 2012.

[265] White, S.I., R.M. Mutiso, P.M. Vora, D. Jahnke, S. Hsu, J.M. Kikkawa, J. Li, J.E. Fischer, and K.I. Winey, "Electrical Percolation Behavior in Silver Nanowire–Polystyrene Composites: Simulation and Experiment", *Advanced Functional Materials*, 20(16),p.,2709-2716, 2010.

[266] Hicks, J., A. Behnam, and A. Ural, "Resistivity in percolation networks of one-dimensional elements with a length distribution", *Physical Review E*, 79(1),p.,012102, 2009.

[267] Moniruzzaman, M. and K.I. Winey, "Polymer Nanocomposites Containing Carbon Nanotubes", *Macromolecules*, 39(16),p.,5194-5205, 2006.

[268] Bostanci, U., M.K. Abak, O. Aktas, and A. Dana, "Nanoscale charging hysteresis measurement by multifrequency electrostatic force spectroscopy", *Applied Physics Letters*, 92(9),p.,093108-3, 2008.

[269] Trouwborst, M.L., C.A. Martin, R.H.M. Smit, C.M. Guédon, T.A. Baart, S.J. van der Molen, and J.M. van Ruitenbeek, "Transition Voltage Spectroscopy and the Nature of Vacuum Tunneling", *Nano Letters*, 11(2),p.,614-617, 2011.

[270] Huisman, E.H., C.M. Guédon, B.J. van Wees, and S.J. van der Molen, "Interpretation of transition voltage spectroscopy", *Nano letters*, 9(11),p.,3909-13, 2009.